# DEVELOPMENT AND VALIDATION OF ANALYTICAL EQUATIONS FOR PREDICTING LOCAL WIND SETUP FOR BAYS, ESTUARIES, AND LAKES

By

JACOB MCBEE

A THESIS PRESENTED TO THE GRADUATE SCHOOL
OF THE UNIVERSITY OF FLORIDA IN PARTIAL FULFILLMENT
OF THE REQUIREMENTS FOR THE DEGREE OF
MASTER OF SCIENCE

UNIVERSITY OF FLORIDA

2010

To mom and dad, without you this would not be possible

ACKNOWLEDGMENTS

I would like to thank my committee (Dr. Robert Thieke and my advisor Dr. D. Max Sheppard) for their advice, and imparting of their extensive knowledge in the fields of coastal and civil engineering during my undergraduate and graduate career at the University of Florida. I would like to thank Dr. Mark Gosselin and Mr. Philip Dompe for their mentoring over the past few years on coastal engineering projects. I would like to thank the rest of the OEA family for contributing to an interesting and collaborative work environment. I would like to thank all of the outstanding professors and teachers that I have had the privilege of learning from throughout the years. I would like to thank Ms. Katie Wilson for her encouragement to surmount the insurmountable and for her patience while during the thesis process. Finally, I would like to thank my parents and brother for their unceasing support of my goals and ambitions.

TABLE OF CONTENTS

page

LIST OF TABLES

LIST OF FIGURES

Abstract of Thesis Presented to the Graduate School
of the University of Florida in Partial Fulfillment of the
Requirements for the Degree of Master of Science

DEVELOPMENT AND VALIDATION OF WIND SET-UP EQUATIONS AND METHODOLOGIES FOR BAYS, ESTUARIES, AND LAKES

By

Jacob McBee

December 2010

Chair: D. Max Sheppard
Major: Coastal and Oceanographic Engineering

Analytic equations and methodologies for predicting local wind set-up were developed based upon the equilibrium of hydrostatic forces acting on an element of a water body. Results obtained using these equations showed excellent agreement with those obtained with a 3D computer model. The equations and methodology were also tested using measured field data. The paths of Hurricanes Frances and Jeanne passed near Lake Okeechobee in central Florida. Water elevation measurements made during these storms provided the field data for evaluating the analytic equations. Surprisingly good agreement between prediction and measurement was achieved. The good agreement between the analytic and the 3D computer model results and the field data show that these models can be used for situations where cost and time constraints prevent the use of more sophisticated methods such as 2 and 3D hydraulic models.

# CHAPTER 1
# INTRODUCTION

## Motivation for Research

Hurricane Ivan made landfall near Pensacola, Florida in 2004. In doing so it increased the water level in Escambia Bay (via storm surge and local wind set-up) and generated waves large enough to remove several spans of the I-10 Escambia Bay Bridge and deposit them into the bay. Traffic utilizing I-10 was rerouted for almost a year while the replacement bridge was designed and constructed at a tremendous cost due to the size of the bridge and the tight timeline for construction. The failure of the I-10 Bridge motivated the Florida Department of Transportation (FDOT) to initiate research at the University of Florida on the topic of predicting surge/wave loading on bridge superstructures. This work resulted in predictive equations that require design water elevation, wave height and length, and bridge superstructure shape, dimensions and elevation as input parameters. A parametric form of these equations were included in an AASHTO specification, “Guide Specifications for Bridges Vulnerable to Coastal Storms” along with guidelines for obtaining design water elevations and wave parameters (i.e. met/ocean conditions). Three levels of analysis are outlined in the AASHTO spec with both the effort required and the accuracy of the results increasing with level. Levels I and II rely heavily on existing met/ocean information and analytical equations for computing wave heights and lengths, local wind setup/set-down etc. FEMA or other government predicted storm surge elevations are used in these analyses. The level of analysis to be used depends on many factors including the importance (criticality) of the bridge, the number of bridges in the same water body, available funds for analysis, etc.

In locations subject to tropical storms and hurricanes, design water levels in coastal bays and waterways are usually due to storm surge and local wind setup/set-down. Storm surge is a long wave that is generated offshore and propagates into the coastal waters through tidal inlets and, in some cases, over barrier islands. Local wind setup/set-down refers to the movement of water in the bay due to stresses on the water surface induced by local winds. The predictive equation for local wind setup/set-down in the AASHTO specs is intended for use on the open coast and thus often yields overly conservative elevations when used in bays and coastal waterways. The objective of this research is to provide improved analytic tools for estimating local wind setup in typical coastal waters. Even the improved analytic model predictions will produce conservative results due to the assumptions that have to be made regarding the phasing of storm surge and local wind setup/set-down. This, however, is appropriate since the accuracy of the input parameters for a Level I analysis is less than that for a Level III.

A Level III analysis utilizes computer models for storm surge, local wind setup and waves and thus the analytic expressions developed in this study are not needed in this case. There are, however, situations, where a Level III analysis cannot be justified due to economic or time constraints and either a Level I or II must be used.

The analytic equations developed in this study are transcendental in form and thus require iterative solutions. Most computer spreadsheets are, however, capable of solving these types of equations.

## Problem Statement

During wind events of significant magnitude gusting over a water body, the water surface responds with a local increase in elevation above the mean water level at the downwind end of the water body known as local wind set-up, and a decrease in the

water surface elevation from the mean water level occurs at the upwind end of the water body known as local wind set-down. Typically, the consequences of local wind set-up pose far greater risks to lives and property than the effects of local wind set-down. Not only does wind set-up increase potential flood inundation, but it also allows for greater wave heights to be generated. This, in turn, increases the potential hydraulic loads on coastal structures including bridge piers and superstructures. Failure to consider the appropriate local water level in the bridge superstructure wave force analysis could be the difference between a bridge surviving a hurricane impact and it being destroyed. In the Gulf of Mexico and Atlantic coastal states, tropical cyclones produce wind fields capable of inducing significant wind set-up in lakes, bays, and other basins. In previous research on the topic of wind set-up, researchers determined that wind set-up is a function of wind shear stress applied to the water surface, bathymetry, wind fetch length, bed shear-stress, water body boundaries, and water properties. Earlier pertinent research, including: formulations of wind shear stress, the relationship between wind shear stress and bed shear stress, and existing methodologies for computing wind set-up are contained in Chapter 2. The analytical models are developed in Chapter 3. Chapter 4 compares the analytical model predictions with 3D computer model results for a variety of idealized water body geometries and bathymetries and one actual complex lake system during two actual hurricanes. Finally, Chapter 5 summarizes the results and conclusions of this and makes recommendations for future research on this topic.

# CHAPTER 2
# LITERATURE REVIEW

## Introduction to Wind Set-Up as a Component of Storm Surge

In the 1950s and 1960s the U.S. Commerce Department Weather Bureau took interest in hurricane storm surge, and in 1963, it published Technical Paper No. 48: Characteristics of the Hurricane Storm Surge authored by D. Lee Harris. In this report, Harris identifies the five components of storm surge: pressure set-up, direct wind effect, the effect of the earth's rotation, the effect of waves, and the rainfall effect. The direct wind effect, the effect of the earth's rotation, and the effect of waves are now more commonly referred to as wind set-up, the Coriolis Effect, and wave set-up. Further, Harris concluded that though storm surge may propagate into a bay or estuary, local wind set-up within that bay or estuary is largely independent of the wind set-up component of the storm surge propagating into the tidally connected bay or estuary from the open coast. Harris notes that wind shear stress on a water surface is a function of the wind velocity, and the roughness of the surface also varies due to the wave climate (also a function of the wind velocity). Even today, 47-years after the publication of Technical Paper No. 48, a plethora of formulations for application of wind shear stress at the water surface exist, with no formula clearly superior to its peers.

## Wind Shear Stress

Every reasonable wind shear stress formulation is dependent upon wind velocity, which is customarily measured at a height of 10 meters above ground level (or water level). If the wind speed is sufficient to produce even a moderate wind set-up, the associated surface waves typically produce an aerodynamically rough boundary. For

the vast majority of coastal water bodies the spatial scale is such that Coriolis forces can be neglected. For these situations the wind velocity profile can be described by:

$$\frac{\bar{u}}{u_*} = \frac{1}{k}\ln\left(\frac{z}{z_0}\right),$$

where:

k = von Karman's constant = 0.4,
$\bar{u}$ = wind velocity at height z above the reference level,
$u_*$ = friction velocity,
$z$ = height above reference level, and
$z_0$ = aerodynamic roughness length.

Furthermore, Dattatri et al. confirmed through laboratory experiments and field measurements that the aforementioned logarithmic velocity profile describes the atmospheric boundary layer satisfactorily over water, even when a substantial wave climate has been generated. Their paper notes that the boundary layer wind action over water differs from the action over land in that the boundary presented by the water surface is in motion rather than stationary, the stresses imposed on the water surface induce currents and wave generation, and the generated waves interact with the atmospheric boundary layer potentially altering the boundary layer wind velocity profile. Dattatri et al. concluded that laboratory data and field measurements showed correlation of wind velocity profiles, and for high wind velocities, the flow may be treated as turbulent flow over a completely rough boundary. Dattatri et al. slightly modified the previous logarithmic wind velocity profile with the roughness length corresponding to the significant wave height. This equation fits the data contained in Dattatri et al. 1977 well and is presented below:

$$\frac{\bar{u}}{u_*} = 2.5\ln\left(\frac{z}{z_0}\right) + 8.5,$$

where:

$\bar{u}$ = wind velocity at height z above the reference level,
$u_*$ = friction velocity,
$z$ = height above reference level, and
$z_0$ = aerodynamic roughness length, the significant wave height in this case (fully turbulent flow over a rough surface).

It should be noted that von Karman's constant is included in the factor in front of the natural logarithm term. Since the objective of this work is to produce improved local wind setup/set-down analytical models for design purposes it is assumed that the wind speeds will be sufficient to produce an aerodynamically rough boundary. This simplifies the selection of a wind stress equation.

Jones and Toba (2001) give the following relationship for drag coefficient ($C_D$) for use in the wind stress equation:

$$\sqrt{C_D} = \frac{u_*}{\bar{u}},$$

or

$$C_D = \left[\frac{1}{2.5 \ln \frac{z}{z_0} + 8.5}\right]^2.$$

Several other formulations of $z_0$ are summarized in Jones and Toba (2001), for completeness, all are contained in Table 2-1 below. Each is defined by the wave-dependent non-dimensional roughness length $z^*_0$ ($z_0^* = \frac{g z_0}{u_*^2}$). Once the drag coefficient ($C_D$) is determined, the wind shear stress may then be calculated with the following equation:

$$\tau_w = \rho C_D \overline{u^2},$$

where:

$\rho$ = air density,
$C_D$ = drag coefficient, and
$\bar{u}$ = wind velocity.

## Relationship between Wind Shear Stress and Bed Shear Stress

Once the local wind setup/set-down has reached equilibrium the sum of bed shear stress and wind stress are balanced by the hydrostatic pressure gradient as shown in Figure 2-1. Bed shear stress is a function of bed roughness and flow velocity near the bed. The velocity near the bed is directly related to that near the surface as shown in Figure 2-2 which shows a typical flow velocity profile in the center of a closed basin with a wind-driven current. For this reason some of the earlier work on this problem expressed the bed shear stress in terms of the wind stress. Since the bed shear stress depends on bed roughness, this must be taken into consideration in this relationship. Some guidance regarding the magnitude of the coefficient in this relationship based on bed roughness is presented in this document. These recommendations are the result of information produced by 3D hydraulic computer model simulations and not actual laboratory or field experiments.

## ADCIRC Model

One method of calibrating and testing the analytical models for wind set-up developed in this study is to setup and run 3D hydrodynamic models for the same conditions as analyzed with the analytical models and compare the results. The Advanced Circulation model (ADCIRC) was used for this purpose. ADCIRC was created by Professor Rick Luettich of the University of North Carolina at Chapel Hill along with Professor Joannes Westerink at the University of Notre Dame and others. ADCIRC has evolved over many versions and solves the equations of motion for a fluid with a free surface. The equations use traditional hydrostatic pressure and Boussinesq approximations and are discretized spatially by the finite element method and temporally with the finite difference method. ADCIRC is capable of two-dimensional

depth integrated model runs as well as three-dimensional model runs. The water surface elevation is determined via the Generalized Wave Continuity Equation (GWCE) and the flow velocities are established with either the two-dimensional depth integrated or three-dimensional momentum equations, both of which include non-linear terms. (Luettich and Westerink, 2010) Other model capabilities include:

- Ability to run in a Cartesian or spherical coordinate system
- Multiple approaches for implementing bottom friction (quadratic, linear, or hybrid),
- Application spatially and temporally varying bottom friction factors,
- User control of element wetting and drying parameters, and
- User control of eddy viscosity (including vertical eddy viscosity in 3-d mode).

Furthermore, several types of model boundary conditions may be employed to drive a hydrodynamic simulation, these include:

- Tidal potential,
- Water surface elevation,
- Normal flow,
- Earth load/self-attraction tide, and
- Surface stress (such as wind stress).

Each of these boundary conditions may vary with model time. The wind stress boundary condition may be applied as a wind stress and atmospheric pressure at each individual model node or ADCIRC also allows the input of wind velocity fields. If the user chooses to input a wind velocity field, ADCIRC employs the Garrett formulation of wind stress to develop the surface wind stresses applied during the model simulation. Garrett's formulations reside in the following equations:

$$\tau_w = 0.001293 C_D \vec{U} |U|,$$

where:

$C_D = 0.001(0.75 + 0.067|U|)$ unless $C_D > 0.003$ then, $C_D = 0.003$,
$\vec{U} =$ wind velocity (m/s), and
$|U| =$ wind velocity magnitude (m/s).

Note that ADCIRC requires wind velocities to be input in meters per second (m/s), and the wind velocity ($\vec{U}$) is at an elevation of 10 meters above the vertical datum (mean sea level in a typical ADCIRC model). Also, the ADCIRC program restricts the aerodynamic drag coefficient to a maximum of 0.003.

## Tidal Inlets

Tidal inlets are the primary source of storm surge in the coastal water system. State and/or Federal Agencies have computed 100-year storm surge elevations for most, if not all, coastal waters in the United States. Thus this information is available for use with Levels I and II met/ocean analyses. However, many of these storm surge analyses did not include local wind setup/set-down. It is for this reason that more accurate setup/set-down predictive equations are needed. The presence of tidal inlets increases the complexity of computing local wind setup/set-down. Water entering or leaving the coastal system through the inlet as a result of local wind setup/set-down can impact the setup/set-down. A method for estimating the quantity of water that enters or leaves the coastal system due to the setup/set-down during the setup/set-down process and its effect on setup/set-down is included in the analytical model development.

## Characterization of Estuarine and Bay Tidal Entrances

O'Brien first developed a relation between tidal entrance area and the tidal prism of the coastal water system. His relation is:

$$A = 1000V^{0.85},$$

where:

$A =$ entrance cross sectional area below the mean water level in ft$^2$, and
$V =$ tidal volume in miles$^2$-ft (between MLLW and MHHW).

The USACE Coastal Engineering Manual (CEM) tabulates the bay or estuary surface areas, bay or estuary tidal range, the tidal range at the ocean near the inlet, and the mean tidal prism for selected bays and estuaries connected to the Gulf of Mexico or the Atlantic Ocean via a tidal inlet. These values are tabulated in Table 2-2.

The USACE CEM attributes the recognition of a relationship between minimum inlet cross-sectional area and the tidal prism to O'Brien, but noted that the equation O'Brien developed was better suited to Pacific coast inlets where a mixed tidal pattern is prevalent. Subsequent work was performed by Jarrett whom performed a regression analysis on inlets from different coastal regions and developed minimum inlet cross-sectional area equations for inlets on the Atlantic Coast, the Gulf Coast, and the Pacific Coast dependent on tidal prism volumes. Furthermore, he recommended O'Brien's relationship for dual jettied inlets. (USACE, 2002) Table 2-3 summarizes Jarrett's regression equations for minimum inlet cross-sectional area ($A_c$) as a function of tidal prism (P). If the flow that enters or leaves the bay through the inlet due to setup or set-down is to be considered, then this information will be useful.

**Previous Research on Local Wind Set-up**

Ippen (1966) summarizes early formulations for wind set-up in enclosed lakes and reservoirs, offshore, on the open-coast, behind the open-coast, and in open bays or estuaries. Ippen recognized that lakes and reservoirs may have irregular shapes and varying depth, and as such suggests employing mean depth as the depth, and if necessary segmenting the lake or reservoir to obtain a solution. The equation Ippen suggests for wind set-up within an enclosed lake is:

$$\frac{dS}{dx} = \frac{(\tau_w + \tau_b)}{\rho g(h+S)},$$

where:

$S$ = wind set-up height,
$\frac{dS}{dx}$ = slope of water surface,
$h$ = water depth,
$\tau_w$ = surface wind shear stress,
$\tau_b$ = bed shear stress,
$\rho$ = density of water, and
$g$ = gravitational constant.

Ippen also recommends that if a wind field with variable velocities is encountered over the water body of interest, calculations should be performed along the streamlines of the wind field while employing variable wind stress and segmenting the equations appropriately. Since this report focuses on storm surge within enclosed basins, bays and estuaries, for brevity, Ippen's solutions for wind set-up offshore and on the open-coast are not included. Computing water surface elevations within a bay or estuary during a tropical cyclone event is complex due to the combination of discharge into the bay from rainfall runoff, storm surge propagation into the bay via the tidal inlet, and local wind set-up/set-down from wind stress applied to the water surface. The geometry of the bay or estuary may add to the complexity as large bays and estuaries require a significant amount of time for the surge to fully propagate to the extents of the water body. Ippen states the discharge through the tidal entrance is quantified through the following equation:

$$Q = C_2 A_c \sqrt{2g|h_0 - h_1|},$$

where:
$Q$ = discharge through the tidal entrance (inflow when $h_0 - h_1 > 0$ and outflow when $h_0 - h_1 < 0$),
$C_2$ = discharge coefficient determined from past conditions or assumed 0.6 if conditions are unknown,
$A_c$ = cross-sectional area of the tidal entrance (varies with time),
$h_0$ = offshore water level, and
$h_1$ = bay or estuary level (near tidal entrance).

Ippen also states that an alternative approach to computing discharge through a inlet due to storm surge is to use a modified form of Manning's equation:

$$Q\Delta t = \frac{1.49}{n\sqrt{l}} \frac{AR^{2/3}}{\left[1 + \left(\frac{1.49}{n\sqrt{l}} AR^{2/3}\right)^2 \frac{K_1 + K_2}{2gA^2}\right]^{1/2}} \sqrt{\Delta H}\Delta t,$$

where:
$Q$ =discharge (ft$^3$/s),
$\Delta t$ = time of inflow (s),
$n$ = Manning's friction factor,
$A$ = tidal entrance area,
$R$ = hydraulic radius (ft),
$l$ = effective channel length (ft),
$K_1$ = coefficient of entrance loss,
$K_2$ = coefficient of exit loss, and
$\Delta H$ = differential head between entrance and exit. (Ippen, 1966)

The Manning's friction factor is a function of the bed composition. The USACE published a coastal engineering technical note concerning the 1-dimensional modeling of inlets, and it stated the range of Manning's friction factor (n) for inlets typically ranges from 0.025 to 0.050. (Seaburgh and Kraus, 1997) Dean and Dalrymple (2002) suggest that the entrance loss coefficient ($K_1$) is between 0.1 and 0.3 for a tidal inlet and the exit loss coefficient ($K_2$) is approximately 1.0 for a tidal inlet.

The USACE Shore Protection Manual (SPM) (1977) contains an expression for calculating wind set-up within its section detailing storm surge. The SPM splits the set-up computations into onshore and longshore components. Since the assumption that flows induced by processes other than surface wind shear stress are negligible, the longshore component of the SPM wind set-up equation when comparing the SPM equation to the analytic equations developed in this report. The USACE SPM wind set-up equation is presented below, the fV term is the longshore component and the $kW^2\cos\theta$ term is the onshore component,

$$S = \frac{(fV + kW^2 cos\theta)x}{gD},$$

where:

$S =$ wind set-up,
$W =$ wind velocity,
$D =$ water depth,
$V =$ longshore volume transport of water,
$k =$ wind stress coefficient (SPM suggests Van Dorn, which is 3.6 x $10^{-6}$ for wind speeds over 14 knots),
$\theta =$ angle between x-axis and local wind vector,
$x =$ fetch length or length of water body along axis of interest, whichever is less, and
$f =$ Darcy-Weisbach friction factor.

Dean and Dalrymple (2002) developed an analytical expression for wind set-up based on the hydrostatic force balance acting on a vertical element of the water column. Their equation assumes a flat bottom profile, and provides a basis for further analytical wind set-up analyses for sloping bottoms, wind set-up within enclosed water bodies, wind set-up in bays and estuaries, and wind setup in irregularly shaped water bodies. Figure 2-3 illustrates the hydrostatic force balance acting on an element of the water column similar to the schematic presented in Dean and Dalrymple (2002).

The equilibrium equation corresponding to the diagram above is:

$$\frac{1}{2}\rho g(h + \eta(x))^2 - \frac{1}{2}\rho g\big(h + \eta(x + \Delta x)\big)^2 + \tau_w \Delta x - \tau_b \Delta x = 0,$$

where:

$\eta(x + \Delta x) = \eta(x) + \frac{\Delta \eta}{\Delta x}\Delta x.$

Rearranging the equation to solve for $\frac{\Delta \eta(x)}{\Delta x}$ and then multiplying both sides by $\Delta x$ and integrating both sides of the resulting equation gives a formulation for $\eta(x)$,

$$\eta(x) = h\left(\sqrt{1 + \frac{A_s x}{l}} - 1\right),$$

where:

$A_s = \frac{2n\tau_s l}{\rho g h^2}$, and $n = 1 - \frac{\tau_b}{\tau_s}$, typically n resides between 1.15 and 1.3 (Dean and Dalrymple, 2002).

By the definition in Figure 2-1, the bed shear stress is directed in the direction opposite of the surface wind shear stress. However, when the value of n is greater than one, the bed shear stress must act in a direction opposite of the direction indicated in Figure 2-1. Dean and Dalrymple (2002) recommends n be set between 1.15 and 1.3.

Subsequent chapters will build upon past research and present a methodology for estimating wind set-up in closed basins and coastal bays with small tidal inlets.

Table 2-1. Summary of non-dimensional roughness lengths ($z_0^*$) and roughness height ($z_0$) divided by significant wave height ($z_0/H_s$) [Jones and Toba (2001)]

| Author | $z_0^* = \frac{g z_0}{u_*^2}$ | $\frac{z_0}{H_s}$ |
|---|---|---|
| Charnock (1995) | $z_0^* = \beta_*$<br>$\beta_* = 0.0185$ ($Wu$ 1980)<br>0.035 (Kitaigorodskii and Volkov 1965)<br>0.0144 (Garratt 1977)<br>0.0192 (Geernaert et al. 1986) | $\frac{z_0}{H_s} = 1.10\beta_* \left(\frac{u_*}{c_p}\right)^{3/2}$ |
| Kitaigorodskii (1968) | $z_0^2 = A^2 \int_0^\infty F(k) e^{\left(\frac{-2\kappa c}{u_*}\right)} dk$<br>$c = c(k)$<br>$z_0^* = 0.012\phi(\mathrm{x}_0)$ | |
| Kitaigorodskii with $F(w) = \beta g^2 \omega^{-5}$<br>$\beta = 0.012$ | $\phi(\mathrm{x}_0) = \left[1 - e^{-x_0}\left(1 + \mathrm{x}_0 + \frac{{\mathrm{x}_0}^2}{2} + \frac{{\mathrm{x}_0}^3}{6}\right)\right]^{1/2}$<br>$\mathrm{x}_0 = 2\kappa c_p u_*$<br>$z_0^* = 0.014\phi(\mathrm{x}_0)$ | $\frac{z_0}{H_s} = 0.013 \left(\frac{u_*}{c_p}\right)^{3/2} \phi(\mathrm{x}_0)$ |
| Kitaigorodskii with $F(w) = \alpha_s g u_* \omega^{-4}$<br>$\alpha_s = 0.062$ | $\phi(\mathrm{x}_0) = \left[1 - e^{-x_0}\left(1 + \mathrm{x}_0 + \frac{{\mathrm{x}_0}^2}{2} + \frac{{\mathrm{x}_0}^3}{6}\right)\right]^{1/2}$<br>$\mathrm{x}_0 = 2\kappa c_p u_*$ | $\frac{z_0}{H_s} = 0.015 \left(\frac{u_*}{c_p}\right)^{3/2} \phi(\mathrm{x}_0)$ |
| Kitaigorodskii (1970) | $z_0^* = 0.068 \left(\frac{u_*}{c_p}\right)^{-3/2} e^{-\kappa \frac{c_p}{u_*}}$ | $\frac{z_0}{H_s} = 0.075 e^{-\kappa \frac{c_p}{u_*}}$ |
| Hsu (1974) | $z_0^* = 0.144 \left(\frac{u_*}{c_p}\right)^{1/2}$ | $\frac{z_0}{H_s} = 0.159 \left(\frac{u_*}{c_p}\right)^2 = \frac{1}{2\pi}\left(\frac{u_*}{c_p}\right)^2$ |
| Toba and Koga (1986) | $z_0^* = \Omega \left(\frac{u_*}{c_p}\right)^{-1}$<br>$\Omega = 0.025$ (Toba and Koga 1986)<br>$\Omega = 0.015$ (Toba et al. 1990) | $\frac{z_0}{H_s} = 1.1\Omega \left(\frac{u_*}{c_p}\right)^{1/2}$ |

Table 2-1. Continued

| Author | $z_0^* = \frac{g z_0}{u_*^2}$ | $\frac{z_0}{H_s}$ |
|---|---|---|
| Huang et al. (1986) | $z_0^* = 0.085\left(\frac{u_*}{c_p}\right)^{1/2}\phi(x_0)$<br>$\phi(x_0) = \left[1 - e^{-x_0}\left(1 + x_0 + \frac{{x_0}^2}{2} + \frac{{x_0}^3}{6}\right)\right]^{1/2}$<br>$x_0 = 2\kappa c_p/u_*$ | $\frac{z_0}{H_s} = 0.06{x_0}^{-2}\phi(x_0)$ |
| Geernaert, Larsen and Hansen (1987) | $z_0^* = \frac{10g}{u_*^2}e^{-3.65\left(\frac{u_*}{c_p}\right)^{1/3}}$<br>$C_D = 0.012\left(\frac{u_*}{c_p}\right)^{2/3}$ | |
| Masuda and Kusaba (1987) | $z_0^* = 0.129\left(\frac{u_*}{c_p}\right)^{1.10}$ | $\frac{z_0}{H_s} = 0.0142\left(\frac{u_*}{c_p}\right)^{2.60}$ |
| Donelan (1990) Field | $z_0^* = 0.42\left(\frac{u_*}{c_p}\right)^{1.03}$ | $\frac{z_0}{H_s} = 0.46\left(\frac{u_*}{c_p}\right)^{2.53}$ |
| Donelan (1990) Lab | $z_0^* = 0.047\left(\frac{u_*}{c_p}\right)^{0.68}$ | $\frac{z_0}{H_s} = 0.051\left(\frac{u_*}{c_p}\right)^{2.18}$ |
| Toba et al. (1990) [TIKEJ] | $z_0^* = 0.020\left(\frac{u_*}{c_p}\right)^{1/2}$ | $\frac{z_0}{H_s} = 0.022\left(\frac{u_*}{c_p}\right)$ |
| Mast, Kraan and Oost (1991) | $z_0^* = 0.8\left(\frac{u_*}{c_p}\right)$ | $\frac{z_0}{H_s} = 0.88\left(\frac{u_*}{c_p}\right)^{5/2}$ |
| Nordeng (1991) | $z_0^* = 0.11\left(\frac{u_*}{c_p}\right)^{3/4}\phi(x_0)$<br>$\phi(x_0) = \left[1 - e^{-x_0}\left(1 + x_0 + \frac{{x_0}^2}{2} + \frac{{x_0}^3}{6}\right)\right]^{1/2}$<br>$x_0 = 2\kappa c_p/u_*$ | $\frac{z_0}{H_s} = 0.073{x_0}^{-9/4}\phi(x_0)$ |
| Smith et al. (1992) | $z_0^* = 0.48\left(\frac{u_*}{c_p}\right)$ | $\frac{z_0}{H_s} = 0.53\left(\frac{u_*}{c_p}\right)^{5/2}$ |

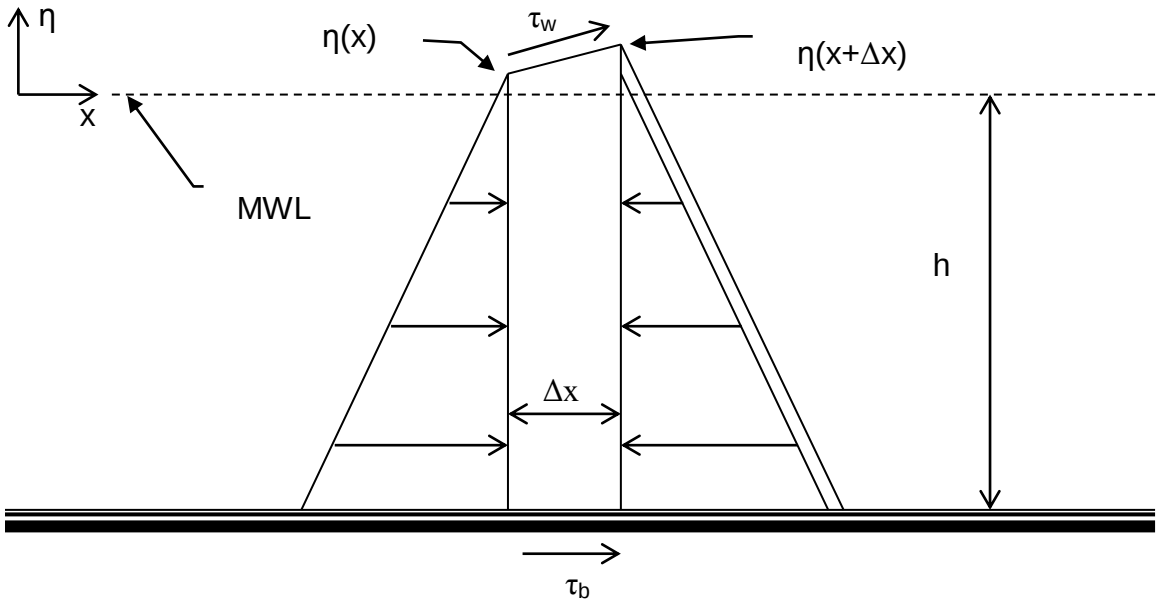


Figure 2-1. Hydrostatic force balance

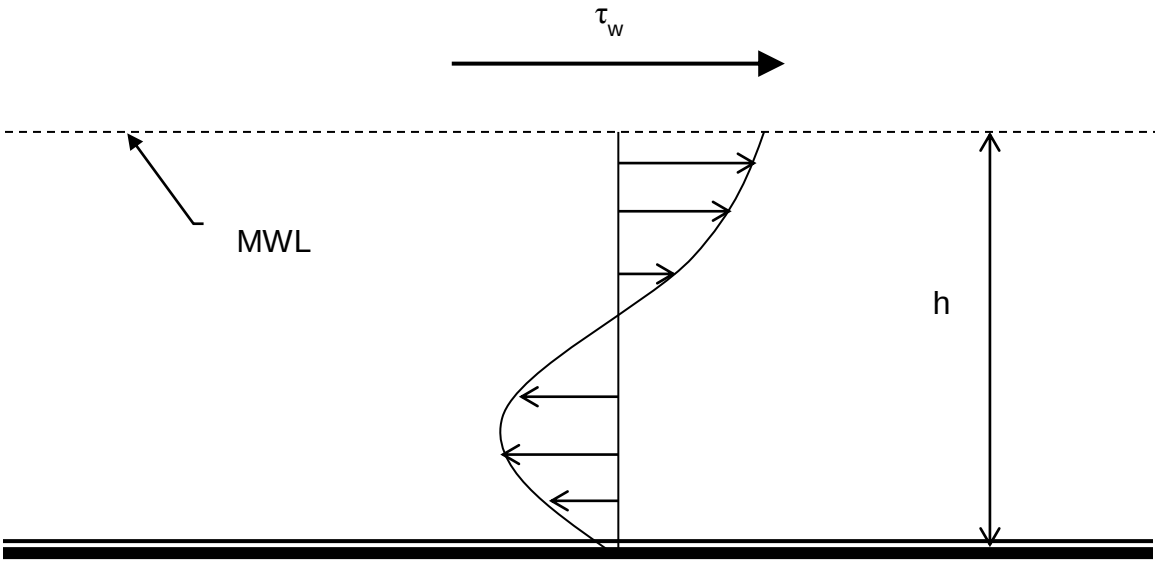


Figure 2-2. Flow velocity profile for a closed basin with a wind surface shear stress

Table 2-2. Tidal inlet parameters for the Atlantic and Gulf coasts [USACE (2002)]

| Atlantic Coast | | | | |
|---|---|---|---|---|
| Inlet | Mean Tidal Prism ($ft^3$) | Area of Bay ($A_b$) ($ft^2$) | Bay Tidal Range ($2a_b$) (ft) | Ocean Tidal Range ($2a_o$) (ft) |
| Shinnecock | 1.82E+08 | 3.65E+08 | 0.5 | 2.9 |
| Fire Island | 1.59E+09 | 2.69E+09 | 0.59 | 4.1 |
| Jones | 7.89E+08 | 4.48E+08 | 1.76 | 4.5 |
| East Rockaway | 4.03E+08 | 1.06E+08 | 3.8 | 4.5 |
| Rockaway | 2.24E+09 | 4.64E+08 | 4.83 | 4.7 |
| Manasquan | 1.40E+08 | 4.91E+07 | 2.85 | 4.3 |
| Barmegat | 4.91E+08 | 1.34E+09 | 0.37 | 4.2 |
| Indian River | 4.00E+08 | 4.20E+08 | 1.02 | 4.1 |
| Beaufort | 4.20E+08 | 2.56E+09 | 1.64 | 3.6 |
| New River | 1.59E+08 | 5.31E+08 | 0.3 | 3.6 |
| Winyah Bay | 2.47E+09 | 9.14E+08 | 2.7 | 4.6 |
| Port Royal | 1.25E+10 | 2.40E+09 | 5.22 | 6.6 |
| Calibogue Sd | 3.05E+09 | 5.28E+08 | 5.78 | 6.6 |
| Wassaw Sd | 3.34E+09 | 5.84E+08 | 5.72 | 6.9 |
| Ossabaw Sd | 5.82E+09 | 1.17E+09 | 4.98 | 7.2 |
| Sapelo Sd | 6.36E+09 | 9.66E+08 | 6.59 | 6.9 |
| St Catherines | 5.94E+09 | 1.04E+09 | 5.73 | 7.1 |
| Doboy Sd | 3.43E+09 | 5.19E+09 | 6.62 | 6.8 |
| Altamaha Sd | 2.45E+09 | 5.01E+08 | 4.9 | 6.6 |
| St. Simon | 5.52E+09 | 8.51E+08 | 6.5 | 6.6 |
| St. Andrew Sd | 8.34E+09 | 1.41E+09 | 5.92 | 6.6 |
| St Marys | 4.11E+09 | 7.93E+08 | 5.19 | 5.8 |
| Nassau Sd | 1.87E+09 | 4.40E+08 | 4.25 | 5.7 |
| St. Johns | 1.50E+09 | 1.22E+09 | 1.23 | 5.2 |
| Ft. Pierce | 5.10E+08 | 1.10E+09 | 0.46 | 2.6 |
| Lake Worth | 7.00E+08 | 4.00E+08 | 1.75 | 2.6 |
| Gulf of Mexico Coast | | | | |
| Inlet | Mean Tidal Prism ($ft^3$) | Area of Bay ($A_b$) ($ft^2$) | Bay Tidal Range ($2a_b$) (ft) | Ocean Tidal Range ($2a_o$) (ft) |
| Venice | 8.50E+07 | 4.43E+07 | 1.92 | 2.6 |
| Midnight pass | 2.61E+08 | 1.29E+08 | 2.12 | 2.6 |
| Sarasota Bay | 2.46E+09 | 1.16E+09 | 2.12 | 2.6 |
| Tampa Bay | 1.95E+10 | 1.01E+10 | 1.95 | 2.6 |
| Pensacola Bay | 5.87E+09 | 4.65E+09 | 1.26 | 1.3 |
| Mobile Bay | 1.56E+10 | 1.20E+10 | 1.3 | 1.3 |
| Galveston Bay | 5.94E+09 | 8.36E+09 | 0.71 | 2.1 |

Table 2-3. Jarrett's tidal prism-minimum channel cross-sectional area relationships [USACE (2002)]

| Location | Metric | English Units |
|---|---|---|
| Atlantic Coast | $A_c = 3.039\ x\ 10^{-5} P^{1.05}$ | $A_c = 7.75\ x\ 10^{-6} P^{1.05}$ |
| Gulf Coast | $A_c = 9.311\ x\ 10^{-4} P^{0.84}$ | $A_c = 5.02\ x\ 10^{-4} P^{0.84}$ |
| Pacific Coast | $A_c = 2.833\ x\ 10^{-4} P^{0.91}$ | $A_c = 1.19\ x\ 10^{-4} P^{0.91}$ |
| Dual-Jettied Inlets (O'Brien) | $A_c = 7.489\ x\ 10^{-4} P^{0.86}$ | $A_c = 3.76\ x\ 10^{-4} P^{0.86}$ |

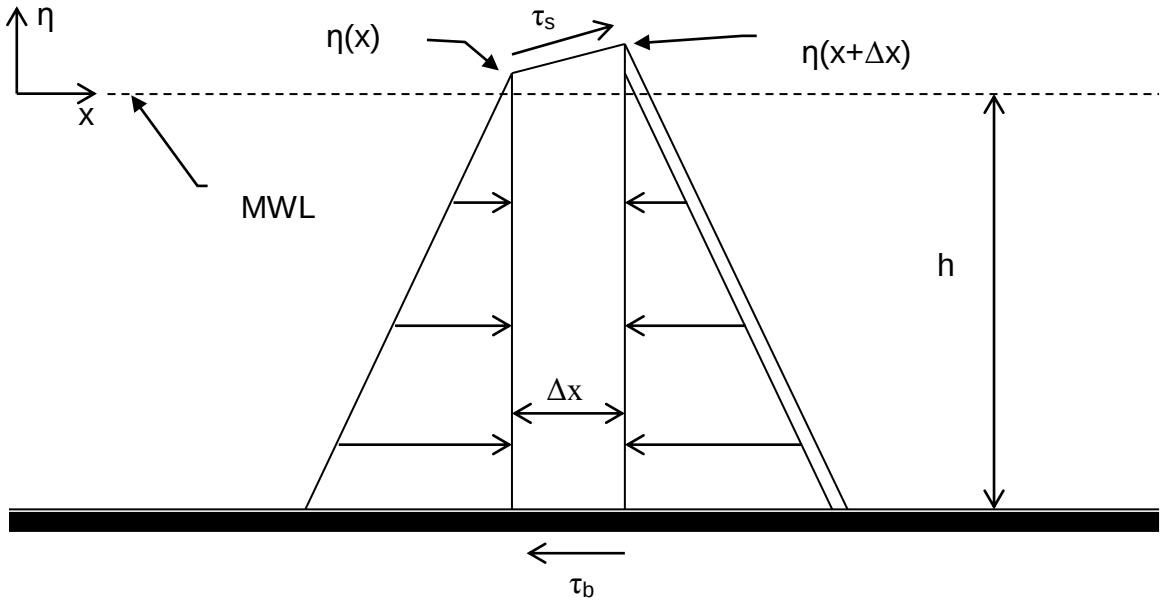


Figure 2-3. Hydrostatic force balance acting on an element in the water column

# CHAPTER 3
# METHODOLOGY AND DEVELOPMENT OF EQUATIONS

## Flat-Bottom Wind Set-Up Case

As mentioned in Chapter 2, the analytical equations are based on hydrostatic equilibrium of the water column in a formulation similar to Dean and Dalrymple (2002). This relies on the assumption that currents other than the wind induced currents are insignificant. In order to produce analytic expressions suitable for Levels I and II met/ocean analyses as discussed earlier in this only the steady-state case of wind set-up will be considered.

### Development of Equations

First, the wind set-up equation for a rectangular water body with a flat bottom will be derived. Figure 3-1 contains a definition sketch for this analysis. In Figure 3-1, the water surface elevation is denoted by η which is positive upward and is a function of x. The x-axis is the axis parallel to the wind direction (for purposes of this analysis the wind field is uniform in direction over the water body) with $x_0$ corresponding to the upwind shoreline (set to equal zero), and $x_L$ the value of x at the downwind shoreline. The depth is denoted with the variable h; while $\tau_w$ and $\tau_b$ are the surface and the bed shear stress respectively. Summing the forces in the x direction and setting equal to zero results in:

$$\tfrac{1}{2}\rho g\big(h+\eta(x)\big)^2-\tfrac{1}{2}\rho g\left(h+\eta(x)+\tfrac{\partial\eta}{\partial x}dx\right)^2+(\tau_w+\tau_b)dx=0.$$

Next, the terms are expanded and rearranged with like terms being combined.

$$\frac{2(\tau_w+\tau_b)}{\rho g}dx-2h\frac{\partial\eta}{\partial x}dx-2\eta(x)\frac{\partial\eta}{\partial x}dx-\left(\frac{\partial\eta}{\partial x}\right)^2dx^2=0.$$

Dividing both sides by dx the equation becomes:

$$\frac{2(\tau_w+\tau_b)}{\rho g}-2h\frac{\partial\eta}{\partial x}-2\eta(x)\frac{\partial\eta}{\partial x}-\left(\frac{\partial\eta}{\partial x}\right)^2dx=0.$$

Assuming that $\left(\frac{\partial \eta}{\partial x}\right)^2 dx$ is negligible compared to the other terms the equation becomes

$$\frac{(\tau_w + \tau_b)}{\rho g} - h\frac{\partial \eta}{\partial x} - \eta(x)\frac{\partial \eta}{\partial x} = 0.$$

This separable, non-linear, first-order differential equation can be written as:

$$\frac{d\eta}{dx}\big(h + \eta(x)\big) = \frac{(\tau_w + \tau_b)}{\rho g}.$$

Integrating the equation:

$$\int_{\eta_0}^{\eta(x)} \big(h + \eta(x)\big) d\eta = \int_{x_0}^{x} \frac{(\tau_w + \tau_b)}{\rho g} dx\,,$$

results in:

$$h\eta(x) - h\eta_0 + \frac{\eta(x)^2}{2} - \frac{\eta_0^2}{2} - \frac{(\tau_w + \tau_b)x}{\rho g} + \frac{(\tau_w + \tau_b)x_0}{\rho g} = 0.$$

Selecting the origin such that $x_0 = 0$ simplifies the equation to:

$$h\eta(x) - h\eta_0 + \frac{\eta(x)^2}{2} - \frac{\eta_0^2}{2} - \frac{(\tau_w + \tau_b)x}{\rho g} = 0.$$

Solving this quadratic equation for $\eta(x)$ results in:

$$\eta(x) = -h \pm \sqrt{h^2 + \eta_0^2 + 2h\eta_0 + 2\frac{(\tau_w + \tau_b)x}{\rho g}},$$

where:
$\eta(x)$ = water surface elevation,
$h$ = mean water depth,
$\eta_0$ = water surface elevation at x=0,
$\tau_w$ = wind shear stress applied at the water's free surface,
$\tau_b$ = bed shear stress, and
$x$ = distance from origin along the x-axis.

The negative square root solution in the solution is physically unrealistic and is disregarded, thus the solution is:

$$\eta(x) = -h + \sqrt{h^2 + \eta_0^2 + 2h\eta_0 + 2\frac{(\tau_w + \tau_b)x}{\rho g}}.$$

Note that this solution for the water surface elevation resulting from local wind stress is a function of $\eta$ at the origin, $\eta_0$, which at this point is unknown.

**Solving for $\eta_0$ in a Rectangular Basin with a Horizontal Bottom**

Even though local wind set-up/set-down will be occurring while other, elevation changing, mechanisms (such as storm surge) are in progress, the conservative

assumption that the maximum wind set-up occurs at the time of maximum elevation from the other mechanisms is made. For coastal waters on the Gulf of Mexico and Atlantic coasts this is typically the 100-year storm surge elevation. In general, these values can be obtained from FEMA or other government studies. In some cases local wind set-up has been included in these studies and thus there is no need for this analysis.

For a closed system the mass of water in the set-up must equal the mass of water depleted by the set-down. The value of $\eta_0$ can thus be obtained by the application of conservation of mass to the basin. Integrating ($\rho$ w η(x) dx) from $x_0$ to $x_m$ must equal the negative of the integral from $x_m$ to $x_L$ where $x_m$ is the point along the x-axis where η(x) is zero, $x_L$ is the length of the basin, w the width of the basin and $\rho$ the mass density of the water.

$$-\int_0^{x_m} \rho w \eta(x)\, dx = \int_{x_m}^{x_L} \rho w \eta(x) dx.$$

Figure 3-2 illustrates the conservation of mass (volume) by showing that $A_1$ must be equal to $A_2$.

The result of the integration is:

$$\frac{(h^2+\eta_0^2+2h\eta_0)^{\frac{3}{2}}}{3\left(\frac{\tau_w+\tau_b}{\rho g}\right)} = \frac{\left(h^2+\eta_0^2+2h\eta_0+2\left(\frac{\tau_w+\tau_b}{\rho g}\right)x_L\right)^{\frac{3}{2}}}{3\left(\frac{\tau_w+\tau_b}{\rho g}\right)} - hx_L.$$

The above equation is a transcendental equation for $\eta_0$ and must be solved iteratively. Many commercial spreadsheets and mathematics programs have built-in tools for solving such equations. Otherwise a simple computer program, using Newton-Raphson techniques can be written for this purpose. These programs require an initial estimate

for the root (i.e. a starting value for $\eta_0$ in the iteration). For most coastal water situations and design wind speeds setting $\eta_0$ = -h/2 is adequate. For deeper water (greater than ~5 m) and lower wind speeds a smaller negative value such as $\eta_0$ = -h/4 would be more appropriate.

**Linear Sloping Bottom Wind Set-Up Case for Beds with Small Slopes**

The next step is to add a sloping bottom to the analysis. In this case, m will define the bottom slope as the amount of vertical rise per one unit of horizontal run. Only very shallow slopes are considered (i.e. m < 1/5280). Figure 3-3 is a definition sketch for the wind set-up case with a sloping bottom.

The same logic for orientation of the x-axis, $x_0$, and $x_L$, is applied to the sloping bottom case as for the horizontal bottom case. For this case, $h_0$ is the still water depth at $x_0$. The hydrostatic equilibrium equation for the linear slope bottom wind set-up case is:

$$\frac{1}{2}\rho g(h_0 - mx + \eta(x))^2 - \frac{1}{2}\rho g\left(h_0 - m(x+dx) + \eta(x) + \frac{\partial \eta}{\partial x}dx\right)^2 + (\tau_w + \tau_b)dx = 0.$$

Expanding and rearranging the terms results in:

$$\frac{2(\tau_w + \tau_b)}{\rho g}dx + 2h_0 m dx - 2h_0\frac{\partial \eta}{\partial x}dx - 2m^2 x dx + 2mx\frac{\partial \eta}{\partial x}dx + 2m\eta(x)dx - 2\eta(x)\frac{\partial \eta}{\partial x}dx$$

$$-\left(m^2 - 2m\frac{\partial \eta}{\partial x} + \left(\frac{\partial \eta}{\partial x}\right)^2\right)dx^2 = 0.$$

After neglecting higher order terms, the equation becomes:

$$\frac{(\tau_w + \tau_b)}{\rho g} + h_0 m - h_0\frac{\partial \eta}{\partial x} - m^2 x + mx\frac{\partial \eta}{\partial x} + m\eta(x) - \eta(x)\frac{\partial \eta}{\partial x} = 0.$$

Rearranging the terms in this non-linear first-order differential equation and noting that h is only a function of x results in:

$$\frac{d\eta}{dx} = \frac{\frac{(\tau_w + \tau_b)}{\rho g} + h_0 m - m^2 x + m\eta(x)}{(h_0 + \eta(x) - mx)}.$$

The substitution of $z = \eta(x) - mx$ transforms the equation to one that is separable,

$$\frac{dz}{dx} + m = \frac{\frac{(\tau_w + \tau_b)}{\rho g} + h_0 m + mz}{h_0 + z},$$

or

$$\frac{dz}{dx} = \frac{\frac{(\tau_w + \tau_b)}{\rho g}}{h_0 + z}.$$

Separating the variables and integrating,

$$\int_{z_0}^{z_1} \frac{h_0 + z}{\frac{(\tau_w + \tau_b)}{\rho g}} dz = \int_{x_0}^{x_1} dx,$$

where:

$z_0 = \eta_0$,
$z_1 = \eta(x) - mx$,
$x_1 = x$, and
$x_0 = 0$,

results in:

$$2h_0\,(\eta(x) - mx - \eta_0) + (\eta(x) - mx)^2 - {\eta_0}^2 - 2x\frac{(\tau_w + \tau_b)}{\rho g} = 0.$$

This quadratic equation can be solved to yield the following solution for η(x):

$$\eta(x) = -h_0 + mx + \sqrt{{h_0}^2 + 2h_0\eta_0 + {\eta_0}^2 + 2x\frac{(\tau_w + \tau_b)}{\rho g}}.$$

This closed form solution does, however, significantly over-predict the values produced by the 3D version of the hydraulics model ADCIRC when applied to fetch lengths typically found in coastal waters and thus cannot be used. This the result of gravity not being taken into consideration in the analysis.

### Solving for $\eta_0$ in a Rectangular Basin with a Linearly-Sloping Bottom

Following the same procedure as in the case with a flat bottom the integral of $\eta(x)$over the length of the basin is zero or

$$-\int_0^{x_m} \rho w \eta(x) dx = \int_{x_m}^{x_L} \rho w \eta(x) dx.$$

The result of the integration is:

$$\frac{(h_0^2+\eta_0^2+2h\eta_0)^{\frac{3}{2}}}{3\left(\frac{\tau_w+\tau_b}{\rho g}\right)} = -h_0 x_L + \frac{m{x_L}^2}{2} + \frac{\left(h_0^2+\eta_0^2+2h\eta_0+2\left(\frac{\tau_w+\tau_b}{\rho g}\right)x_L\right)^{\frac{3}{2}}}{3\left(\frac{\tau_w+\tau_b}{\rho g}\right)}.$$

The above equation must be solved iteratively as in the case of the flat bottom. However, as stated above these equations produce large over predictions when compared to 3D computer model (ADCIRC) results.

## Steep Linearly Sloping Bottom Wind Set-up Case

### Development of Equations

In cases where the bottom may be approximated by a linearly sloping plane, the effects of gravity require consideration in the equilibrium force balance (Figure 3-4). In this system, the balanced force equation for the x'-direction is:

$$\frac{1}{2}\rho g\left(h'(x')+\eta'(x')\right)^2 cos\theta - \frac{1}{2}\rho g(h'(x')+\eta'(x')+d\eta')^2 cos\theta$$

$$-\rho g sin\theta\left(\left(h'(x')+\eta'(x')\right)+\frac{1}{2}d\eta'\right)dx' + (\tau_w+\tau_b)dx' = 0,$$

Combination of like terms results in:

$$-\left(2\eta'(x')d\eta' + 2h'(x')d\eta' + d\eta'^2\right)cos\theta dx' - 2sin\theta\left(\left(h'(x') + \eta'(x')\right) + \frac{1}{2}d\eta'\right)dx'$$

$$+\frac{2(\tau_w + \tau_b)dx'}{\rho g} = 0,$$

and after eliminating higher order terms the equation becomes:

$$-(2\eta'(x')d\eta' + 2h'(x')d\eta')cos\theta dx' - 2sin\theta\left(\left(h'(x') + \eta'(x')\right) + \frac{1}{2}d\eta'\right)dx'$$

$$+\frac{2(\tau_w + \tau_b)dx'}{\rho g} = 0,$$

Rearranging, the equation becomes:

$$\frac{2(\tau_w + \tau_b)}{\rho g} - 2sin\theta\left(h'(x') + \eta'(x')\right) = (sin\theta + 2\eta'(x')cos\theta + 2h'(x')cos\theta)d\eta',$$

or

$$\frac{\frac{2(\tau_w + \tau_b)}{\rho g} - 2sin\theta\left(h'(x') + \eta'(x')\right)}{(sin\theta + \eta'(x')cos\theta + 2h'(x')cos\theta)} = d\eta',$$

integrating both sides:

$$\int_{\eta_0}^{\eta'(x')} \frac{\frac{2(\tau_w + \tau_b)}{\rho g} - 2sin\theta\left(h'(x') + \eta'(x')\right)}{(sin\theta + \eta'(x')cos\theta + 2h'(x')cos\theta)}d\eta' = \int_0^{x'} dx'.$$

Once integrated, it results in a transcendental equation:

$$2\left(\frac{(\tau_w + \tau_b)}{\rho g cos\theta} + \frac{h'(x')tan\theta}{cos\theta} + sin^2\theta\right)ln\left(\left(2h'(x') + \eta'(x')\right)cos\theta + sin\theta\right) - \eta'(x')tan\theta$$

$$-2\left(\frac{(\tau_w + \tau_b)}{cos\theta\rho g} + \frac{h'_0 tan\theta}{cos\theta} + sin^2\theta\right)ln\left(\left(2h'_0 + \eta'_0\right)cos\theta + sin\theta\right) + \eta'_0 tan\theta$$

$$= x'.$$

When converted to the original coordinates, this equation becomes:

$$2\left(\sqrt{1+m}\frac{(\tau_w+\tau_b)}{\rho g}+m(h_0-mx)+\frac{m^2}{m+1}\right)\ln\left(\frac{2(h_0-mx)+\eta(x)}{m+1}+\frac{m}{\sqrt{m+1}}\right)$$
$$-\frac{m}{\sqrt{m+1}}\eta(x)$$
$$-2\left(\sqrt{1+m}\frac{(\tau_w+\tau_b)}{\rho g}+mh_0+\frac{m^2}{m+1}\right)\ln\left(\frac{2h_0+\eta_0}{m+1}+\frac{m}{\sqrt{m+1}}\right)$$
$$+\frac{m}{\sqrt{m+1}}\eta_0=\frac{x}{\sqrt{m+1}}.$$

Use of the equation above requires a numerical solver common in many spreadsheet and engineering analysis software packages. Additionally, $\eta_0$ must be iteratively adjusted, and the area under the curve numerically integrated to determine the value of $\eta_0$.

**Solving for $\eta_0$ in a Rectangular Basin with a Linearly-Sloping Bottom**

Applying the conservation of mass (volume) once again to the set-up/set-down problem results in

$$-\int_0^{x_m}\rho w\eta(x)dx=\int_{x_m}^{x_L}\rho w\eta(x)dx.$$

Since there is not an explicit expression for η, the above two equations must be solved simultaneously as outlined below:

1. Choose an initial value for $\eta_0$ and substitute it into the equation for η.
2. Solve the η equation for x ranging from 0 to $x_L$ in equal increments
3. Perform the numerical integration

$$\int_0^{x_m}\eta_i(x)dx+\int_{x_m}^{x_L}\eta_i(x)dx=\epsilon_i.$$

4. Increment the value of $\eta_0$ and repeat steps 2 and 3.

5. With two values of $\eta_0$ and corresponding values of $\epsilon_i$ a linear fit to this data can be obtained. Setting $\epsilon = 0$ and solving for $\eta_0$ yields the next value to be substituted into the η equation.

6. Repeat the procedure until $\epsilon_i$ is sufficiently small.

7. The resulting $\eta_0$ is the set-down at the up wind boundary (origin) and the numerical values of η for the discrete values of x from 0 to $x_L$ is the water surface elevation relative to the still water level for the specified conditions.

**Discrete Method of Analysis**

In cases with varying bathymetries along the long-axis profile, the equation for the horizontal bottom slope presented earlier in this chapter may be discretized into segments with the water depth (h) of each segment represented by mean water depth occurring in each segment. The water surface profile for the basin is then determined with a step-wise method. Figure 3-5 is an example of a variable bed profile split into discrete segments.

When computing wind set-up with this method, sharp variations in bathymetry should be smoothed in order to avoid errors in the analysis. Computation is performed for each segment from the upwind end to the downwind end. Similar to the previous method an initial value of $\eta_0$ is required. Using this $\eta_0$ the area under the curve is integrated for each segment and the total for the basin summed. A second value of $\eta_0$ is chosen and the process repeated. With two values of $\eta_0$ and the corresponding values the integrated areas the scheme outlined in the previous method can be used to obtain a better value of $\eta_0$. This process is repeated until the integrated area is sufficiently close to zero. The flat bottom wind set-up equation (repeated below) is used for computations at each segment. $\eta_0$ for all segments beyond the first segment is the value of η from the previous segment. The water depth (h) in the equation corresponds to the mean water depth for the individual segment. Finally, x is the length of the

segment being computed and it is not necessary for all segments be the same length. The stress terms are considered to be unchanged over the length of the basin.

$$\eta(x) = -h + \sqrt{h^2 + \eta_0^2 + 2h\eta_0 + 2\frac{(\tau_w + \tau_b)x}{\rho g}}.$$

This methodology is the recommended means of computing wind set-up for basins with varying bathymetry or for basins with a linearly sloping bottom. The maximum bottom slope recommended for use based upon sensitivity testing is 0.005.

**Analysis of Complex Basin Geometries**

For the purposes of this report, a complex basin is an irregularly shaped basin which has multiple segments as shown in Figure 3-6. Note that trapezoidal basins with sharply converging or diverging shorelines may induce two-dimensional effects into the wind set-up water surface profile. In the case of a trapezoidal basin shape with sharp converging or diverging sides, a hydrodynamic computer model should be used to determine the wind set-up/set-down Each segment of the complex basin has an associated width used during the integration of the basin to achieve conservation of mass. The procedure is similar to that for a uniform width basin except both the depth and width change at each section along the x-axis.

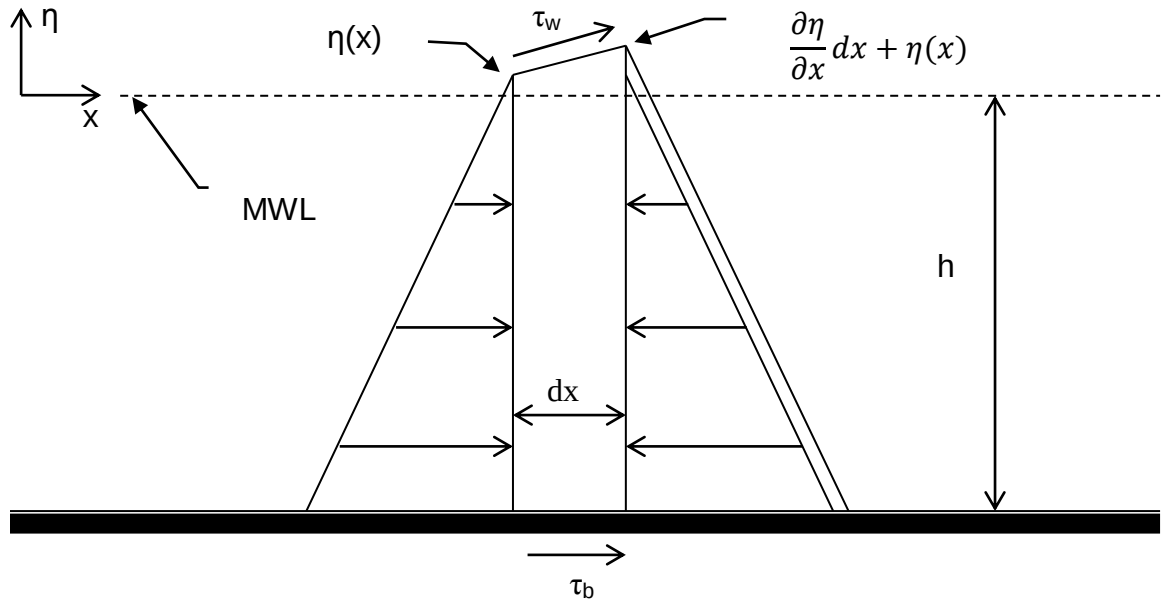


Figure 3-1. Definition sketch for wind set-up case with a horizontal bottom

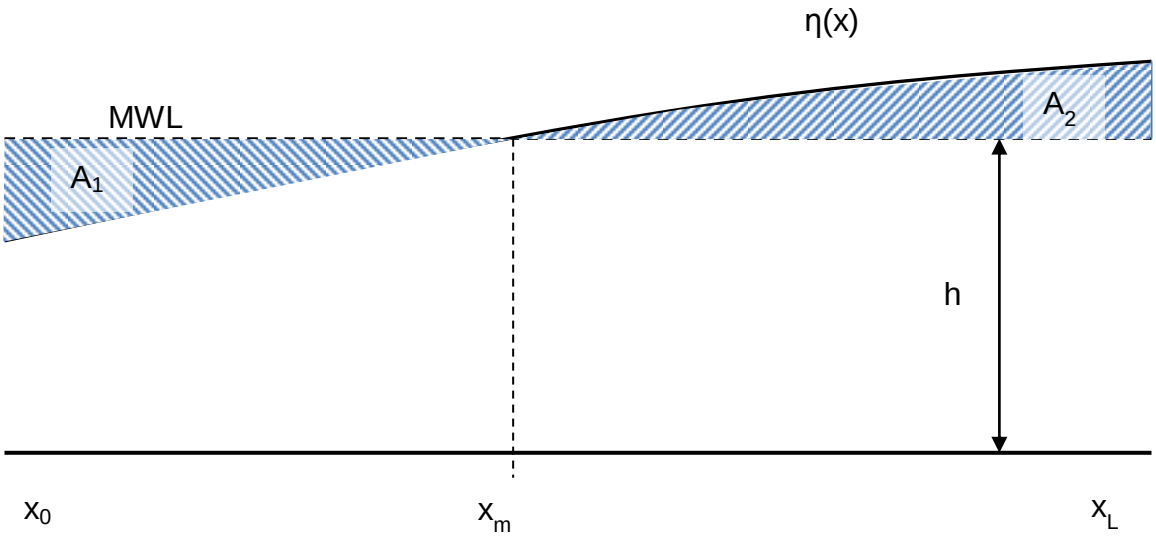


Figure 3-2. Diagram defining conservation of mass for a basin along its x-axis

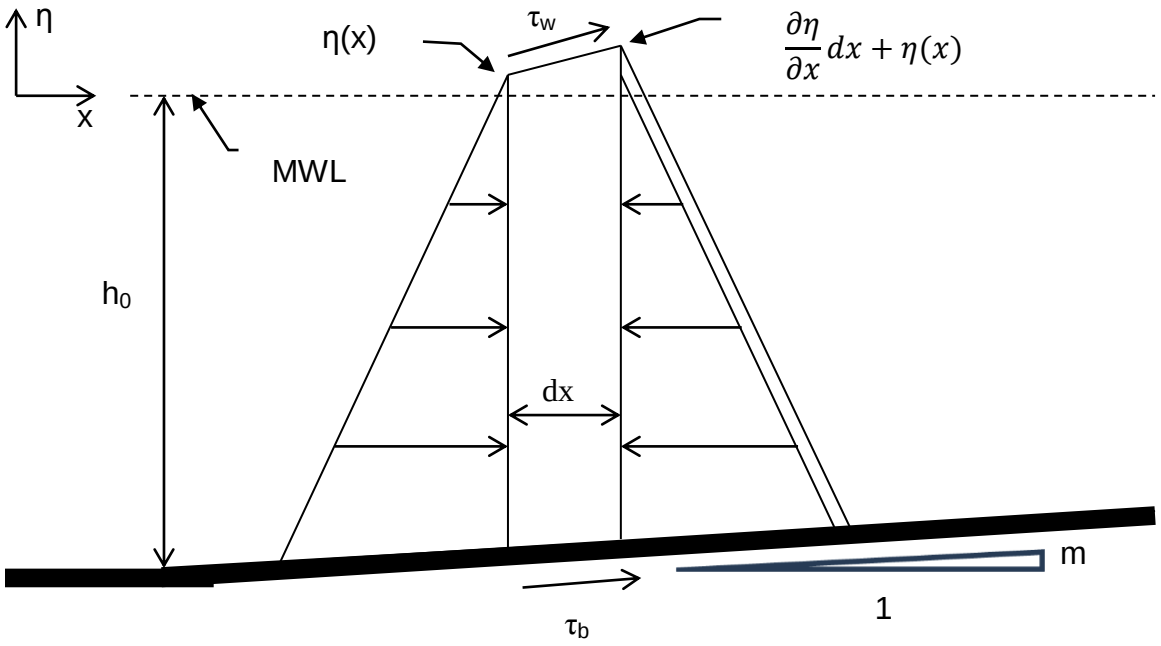


Figure 3-3. Definition sketch for the wind set-up case with a linearly sloping bottom

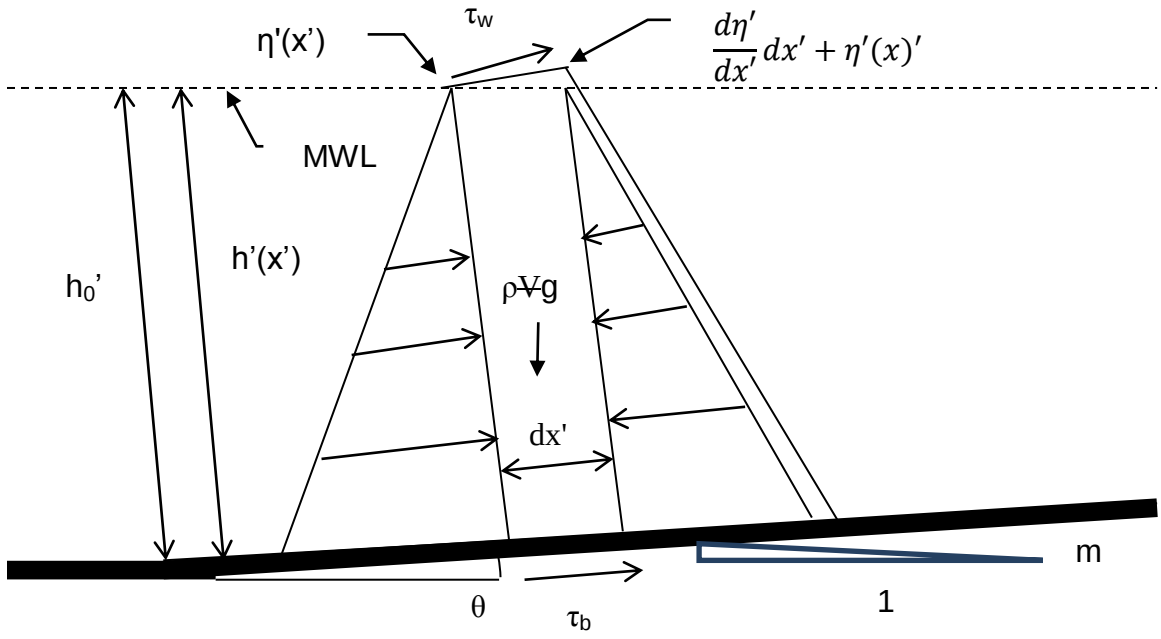


Figure 3-4. Equilibrium force balance diagram for the steep bottom slopes

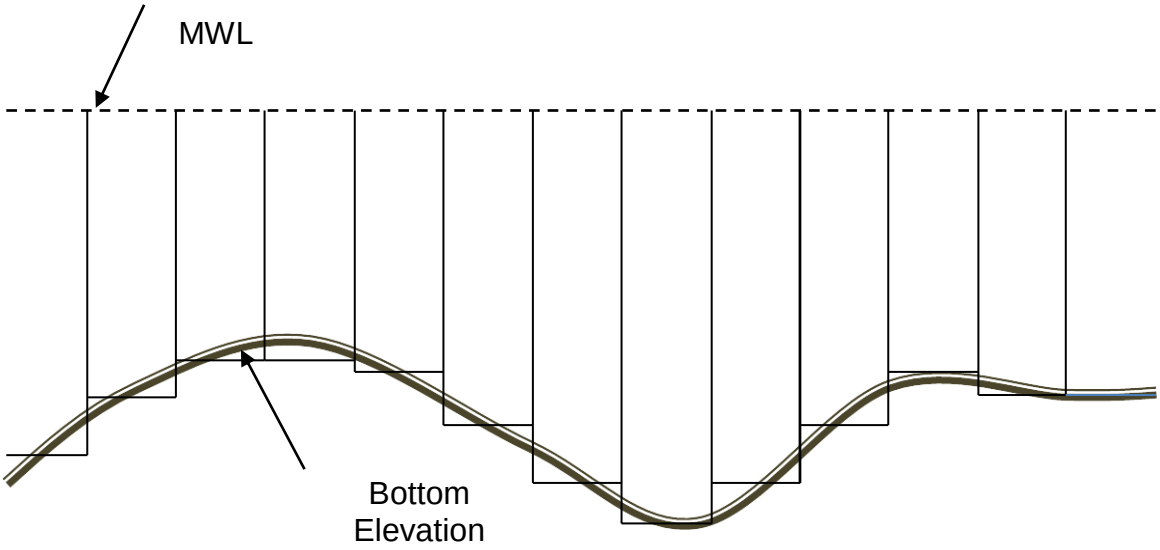


Figure 3-5. Example of profile discretization

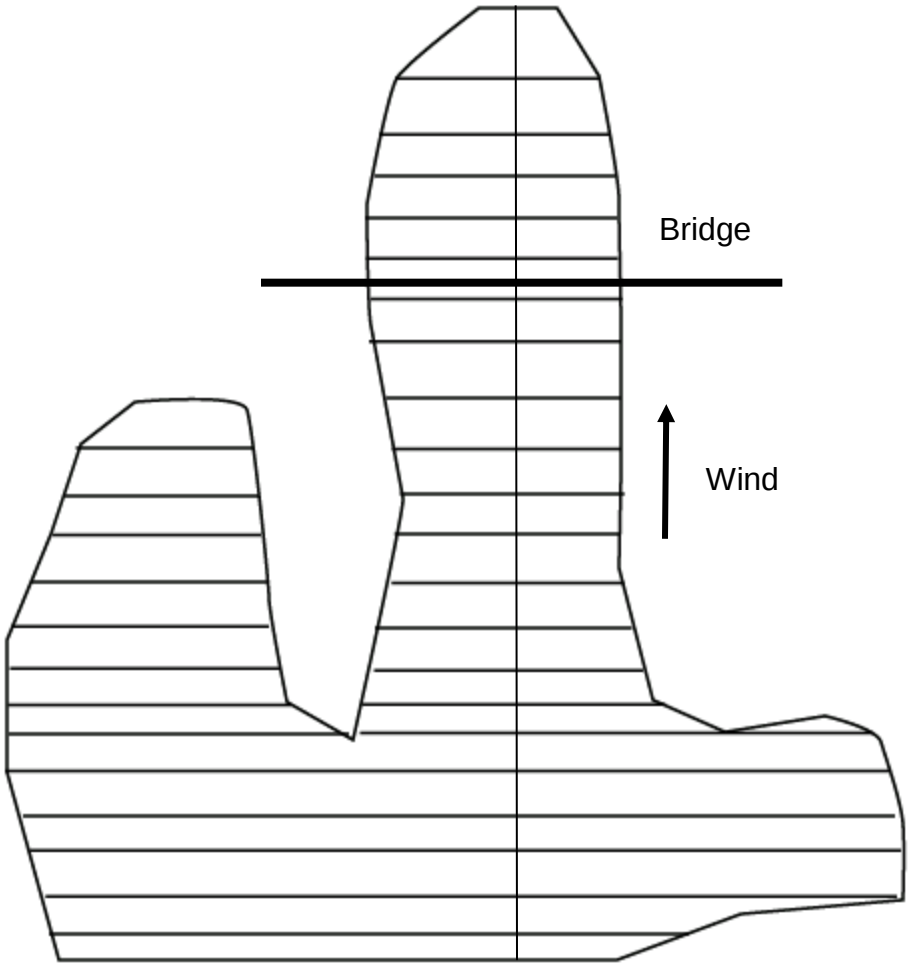


Figure 3-6. Example of a complex basin geometry

# CHAPTER 4
# VALIDATION OF EQUATIONS WITH ADCIRC MODEL

In this chapter, the equations developed in the previous chapter are compared with ADCIRC model results for idealized basins. Additionally, ADCIRC is employed to determine the best approach to modeling basins with varying bed slope, the validity of the equations for irregularly shaped basins, and to estimate the error in the equations. The results of these comparisons indicate that the equations developed in this study provide good approximations for local wind set-up/set-down for situations where the use of sophisticated 2D and 3D computer models cannot be justified.

## ADCIRC Model Configuration

Since the analytical models are being tested with 3D ADCIRC results, it is important to specify the parameters and settings used in the ADCIRC model. The model was set to run in the barotropic three-dimensional mode on a Cartesian coordinate system mesh. Coriolis forces were not included in the analysis since the basins considered are relatively small. The wind was blown at a constant velocity across all nodes of the model mesh in the direction used in the analytical equation analysis (i.e. the x-axis in the analytical models). Additionally, the boundary elements of the mesh were idealized as vertical walls allowing free tangential slip. Since ADCIRC is only capable of dynamic hydrodynamic simulations, the simulations were conducted for simulation durations such that the results for the final several hours of time step output remained unchanged. For completeness, Table 4-1 contains the pertinent parameters from the model parameter and periodic boundary condition file (fort.15 file).

## Basin Geometry

Several idealized basin geometries were developed for the comparison tests. The ADCIRC basins were constructed with the Surface Water Modeling System (SMS) 9.0. These idealized basin shapes were: 1) a rectangular basin, 2) a “T-shaped” basin, and 3) a basin with multiple legs as shown in Figure 4-1 through Figure 4-6. All of the basins were modeled with flat as well was linearly sloping beds (in the x-axis direction).

Comparisons of the equations and ADCIRC model results for the wind set-up/set-down were made for multiple depths, bottom slopes, and wind velocities. Since the primary focus of this study is wind set-up/set-down, only one wind stress model was used throughout the study. The default wind shear stress model in ADCIRC (Garrett’s formulation) was employed for both the ADCIRC modeling and the analytic equations. Wind velocity magnitudes employed for the comparisons are 30-, 40-, 50-, 60-, and 65-meters per second. These values encompass the range of tropical cyclone wind speeds of primary interest.

## Flat-Bottom Geometry Comparisons

First, the results of the simplest cases are compared. The first analysis is for a rectangular basin with a bottom elevation of -5 meters (Figure 4-1). The overall length of this particular basin is 8,000 meters. Figure 4-7 shows the water surface elevation contour plot for the rectangular basin with a 30 m/s wind directed upward across the basin. During the comparison process, it became apparent that the ratio of bed shear stress to surface wind shear stress ($\tau_b/\tau_w$) is a function of the magnitude of the applied wind shear stress. Hereafter the ratio, $\tau_b/\tau_w$ will be referred to as r. For each wind speed analyzed, the r-value will be modified to achieve the best fit to the ADCIRC results. This allowed the development of an equation for r as a function of wind shear stress. Figure

4-8 is a comparison of the ADCIRC model results with the equation results for a 30 m/s wind speed and r set equal to 0.1. Modification of the equations contained in Chapter 3 to accommodate r results in the following equations for a basin with a horizontal bottom:

$$\eta(x) = -h + \sqrt{h^2 + \eta_0^2 + 2h\eta_0 + 2\frac{\left(\tau_w(1+r)\right)x}{\rho g}}.$$

The equation for $\eta_0$ becomes:

$$\frac{(h^2 + \eta_0^2 + 2h\eta_0)^{\frac{3}{2}}}{3\left(\frac{\tau_w(1+r)}{\rho g}\right)} = \frac{\left(h^2 + \eta_0^2 + 2h\eta_0 + 2\left(\frac{\tau_w(1+r)}{\rho g}\right)x_L\right)^{\frac{3}{2}}}{3\left(\frac{\tau_w(1+r)}{\rho g}\right)} - hx_L.$$

Figure 4-9 compares the ADCIRC modeled results to that produced by the analytic model with r set equal to 0.3. These figures show that for these conditions, a ratio of wind shear stress to bed shear stress near the lower end of the range suggested by Dean and Dalrymple (2002) provides the better agreement between the models. Since r set equal to 0.1 and 0.3 both over-predicted the ADCIRC output water surface elevation, an additional plot with an r-value of 0.05 was produced that showed an extremely tight fit to the ADCIRC results (Figure 4-10).

The 40 m/s comparison plots contained in Figure 4-11 and Figure 4-12 further demonstrate that r is a function of wind speed. At the 40 m/s wind velocity magnitude, r set equal to 0.1 results in under-prediction of the ADCIRC results while r set equal to 0.3 slightly over-predicts the results. Equating r to 0.25 produced an acceptable fit (Figure 4-13).

At the 50 m/s wind speed, r equal to 0.1, caused the analytic equation to under-predict the ADCIRC values by 0.2 m at the downwind end of the basin (Figure 4-14). However, when r is set equal to 0.3, the result is an almost perfect fit (Figure 4-15).

Beginning at a wind speed of 60 m/s, an r-value equal to 0.3 results in a slight under-prediction of the water surface elevation at the downwind end of the basin by the analytic equation (0.07 m difference) over the length of the 8000 m rectangular basin (Figure 4-16). Given the magnitude of the difference, setting r equal to 0.3 is probably acceptable in most cases, however, setting r equal to 0.35 results in a nearly perfect fit (Figure 4-17). Figure 4-18 and Figure 4-19 show water surface profile plots for a 65-m/s wind speed with an r-value equal to 0.38 providing the best fit to the ADCIRC results.

### Summary of Comparisons between the Analytic and ADCIRC Models for a Basin with a Horizontal Bottom

The comparison plots show that if an appropriate relation between the surface wind shear stress and the bed shear stress (the r-value) is applied that the equation for analyzing the wind set-up in a basin with a horizontal bottom produces an extremely good fit to the 3D ADCIRC model results. The relationship between r and wind speed observed in the comparison tests was fit using a second-order polynomial. Recall that these tests were all performed with a single wind stress model (Garrett formulation) and thus the curve fit for velocity magnitude versus r may be different with other models. However, the curve fit for wind stress versus r will remain the same regardless of model. Curve fits for r-values for a basin with a horizontal bottom with a mean depth of 5 m are contained in Figure 4-20 and Figure 4-21.

It should be noted that the relations between r-value and wind shear stress were developed based on data for basins with a 5 meter deep horizontal bottom. It is likely that water depth, bottom slope, and bottom roughness also influence the r-value to some degree. In the next section, a comparison of the equation results with ADCIRC model results for horizontal bottom basins of different depths is presented. Additionally,

the relation of r-value to depth will be reevaluated to determine the effects of water depth on the r-value.

## Comparison of Equation Results to ADCIRC Model Results for Additional Basin Depths

The previous section demonstrated that with an appropriately selected r-value, the analytic equations compare well with ADCIRC results for simple basins with horizontal bottoms. In this section, comparisons show that the analytic equations reliably predict water surface profiles induced by surface wind stress for flat bottom basins of different water depths.

As in the previous section, the r-value employed in the equation was adjusted in order to produce the best fit for the ADCIRC model results for the water surface elevation across the profile. The objective of this process is to produce a surface fit for the r-value parameter as a function of water depth and wind stress. Having an equation or tables to determine the r-value allows the engineer to select an appropriate value. Since the previous section effectively demonstrates the effects of r-value adjustments, only comparison plots of the best fitting curve for each case are included in this section.

### 3.5-meter Water Depth Comparison

The shallowest depth compared is 3.5 meters; unfortunately, ADCIRC model instabilities limited analysis for shallower depths. Furthermore, the 3.5 m depth was limited to a maximum wind velocity magnitude of 50 m/s due to model instabilities at greater wind velocities. Figure 4-22 and Figure 4-23 contain comparison plots for the water surface elevation across the profile for 30 m/s and 40 m/s wind speeds, respectively.

Interestingly, the r-value for a 50 m/s wind blowing over a basin with a depth of 3.5 m is 0.36. This is larger than the r-value for the 50-m/s wind blowing over a 5-m deep basin. All of the other simulations indicate that the r-value increases with water depth and wind velocity, so the magnitude of this increase was unexpected. Perhaps the increase is due to increased water velocities occurring near the bottom of the basin forced by the shallow depth at the upwind end of the basin (1.5 m in this case). Figure 4-24 illustrates the 50-m/s wind over a 3.5-m deep basin.

**7.5-meter Water Depth Comparison**

For the 7.5 m water depth basin, simulations were conducted for 30 m/s, 40 m/s, 50 m/s, 60 m/s, and 65 m/s. The results of the simulation confirmed the trend of the r-value increasing with water depth. Figure 4-25 through Figure 4-29 contain the comparison plots of water surface elevation profiles for a 7.5-m deep rectangular basin for winds speeds of 30-, 40-, 50-, 60-, and 65-m/s with r-values equal to 0.063, 0.275, 0.355, 0.39, and 0.4025, respectively.

**10-meter Water Depth Comparison**

For the 10-m water depth basin, ADCIRC simulations with 30-, 40-, 50-, 60-, and 65-m/s wind velocity magnitude were performed. Close inspection of the ADCIRC model results reveals a slight increase in the slope of the water surface profile near the downwind end of the basin in the last 5 meters of the profile. This increase in slope is apparent in every simulation performed for the 10-m basin, and it is likely attributed to non-linear end effects occurring in basins with greater depths. Nonetheless, the increase is very minor due to the short distance over which it occurs, and the equation of Chapter 3 still performs extremely well as shown in Figure 4-30 through Figure 4-34.

Figure 4-30 through Figure 4-34 are comparisons of the ADCIRC model results with equation results for a 10-m basin with winds of 30-, 40-, 50-, 60-, and 65-m/s, respectively. The r-values resulting in the best equation fit are 0.09, 0.30, 0.36, 0.40, and 0.42, for the 30-, 40-, 50-, 60-, and 65-m/s wind speed cases, respectively.

**30-meter Water Depth Comparison**

As water depth increases, the effects of wind set-up diminish. This is verified by both the analytic and ADCIRC model results. For the 30-m basin, wind set-up was very minor when compared to the shallower basins previously discussed. Additionally, as the water depth increases, the effects of the non-linear terms become more pronounced. These terms are discounted in the equations presented in Chapter 3 in order to provide equations suitable for design codes. Furthermore, in shallow water, these terms are quite small when compared to the other terms in the equations. Additionally, the ADCIRC water surface profile results for the 30-m basin include some interesting features, such as a concave upward curve at the upwind end of the basin and instabilities at the downwind end of the basin. In order to develop the most comprehensive surface fit equations possible, the r-values are approximated for each still water depth and wind speed tested. However, in these cases of deep still water depths ($h > 10$ m), it is critical to recognize that the increased r may be compensating for the effects of non-linearity associated with deeper basins and not an increase in the proportion of bed shear stress to surface wind shear stress. Due to the lower confidence in the equation for deeper basins and the small magnitude of wind set-up for this situation, only three simulations were conducted for a 30-m basin. Figure 4-35 through Figure 4-37 compare ADCIRC modeled water surface elevation profiles to the profiles

developed with the Chapter 3 equations. The r-values of the best fitting equation results were 0.25, 0.51, and 0.51, for 30-, 50-, and 60-m/s wind speeds, respectively.

### Development of an Empirical Relation for r

Given the Chapter 3 equations dependency on the relation of bed shear stress to wind shear stress ($r = \tau_b/\tau_w$), it is critical to establish a method for the determination of r in order to arrive at reasonable results. The two previous sections have shown that r is dependent on both wind shear stress and water depth. A summary of r, water depth and wind shear stress based on the results of this study is presented in Table 4-2 below.

Since a simple relation is not apparent for r-value as a function of wind shear stress and depth, a polynomial surface fit of the data was performed. A third degree polynomial fit for both wind shear stress and basin depth provided the lowest root-mean square error (RMSE) for the data. The best-fit surface had an RMSE of 0.0115 for r when compared to the extracted values of r. Furthermore, the coefficient of determination for the fit ($R^2$) was 0.9962. The upper bound surface provides a measure of conservatism which may be useful in design applications. Figure 4-38 illustrates the best fit surface for r as a function of wind shear stress and water depth. The equation for the best fit surface (graphically illustrated in Figure 4-38) is presented below:

$$r = 0.003424 - 0.02119h + 0.04291\tau_w + 0.002211h^2 + 0.000136\tau_w h + 0.0005034{\tau_w}^2 - 4.622 \cdot 10^{-5}h^3 - 1.238 \cdot 10^{-5}h^2\tau_w + 1.410 \cdot 10^{-5}h{\tau_w}^2 - 9.828 \cdot 10^{-5}{\tau_w}^3,$$

where:

$\tau_w$ = wind shear stress ($N/m^2$), and
$h$ = water depth (m).

## Linearly-Sloping Bottom Comparisons

In this section, a rectangular basin with a linearly sloping bottom is analyzed to validate the discrete method developed in Chapter 3. The first basin analyzed has a mean depth of 5 m (shown in Figure 4-2), and the following basin has an identical horizontal geometry, however its mean depth is 7.5 m. For the initial comparison, both basins have an extremely mild bottom slope of 1:5280 (V:H). It was suspected that bottom slope may influence the r-value developed in the previous section. The transcendental equation developed in Chapter 3 for a steep sloping bottom was also plotted for comparison purposes for cases with steeper bottom slopes where numerical instabilities did not prevent calculation. Due to instabilities arising in cases of mild slope analysis with the transcendental equation, it is recommended that the discrete method be employed in practice for the analysis of linearly sloping bottoms.

### 5-meter Mean Depth with a 1:5280 Sloping Bottom Comparison

The equation for water surface profiles were developed by employing the equation for a linearly sloping bottom developed in Chapter 3, along with the selection of r by using the surface fit equation with the wind stress and mean depths as inputs to the fit function. The discrete method results fit the ADCIRC output very well. Figure 4-39 though Figure 4-42 display comparisons of the water surface profile for a basin with a 5-m mean depth and a 1:5280 (V:H) bottom slope for wind velocity magnitudes of 30-, 40-50-, and 60-m/s, respectively.

### 7.5-meter Mean Depth with a 1:5280 Sloping Bottom Comparison

A second basin with the same bottom slope as in the previous case was developed, but with a mean bottom depth of 7.5 m. Again, all values of r were

determined with the surface fit contained earlier in this chapter. Figure 4-43 through Figure 4-46 compare ADCIRC modeled water surface profiles with those output from the linear sloping discrete method of analysis contained in Chapter 3. The discrete method's output compares quite favorably with ADCIRC model output for basins with linearly sloping bottoms. The results also suggest that the mild bottom slope makes a very minor, if any, contribution to r.

### Determination of Maximum Allowable Slope for Discrete Method

Due to the assumptions made during the development of the analytic equations in Chapter 3 there is a limit to the bottom slope steepness where the equations are valid., Interestingly, the discrete method compared well to the steeply sloping bottom transcendental equation (also described in Chapter 3), as well as the ADCIRC results for steeper slopes. The maximum bottom slope for which ADCIRC was stable was m = 0.0011 with a mean still water depth of 4.65 meters. The comparison plot for that simulation is shown in Figure 4-49. The plots in Figure 4-47 through Figure 4-50 compare the results for bottom slopes between 0.0005 and 0.005. Figure 4-50 shows that the resulting increase in depth at the upwind end of a basin due to the steep slope diminishes the potential wind set-up at the downwind end of the basin.

## Validation of Equations for Complex Basin Geometries

A complex basin is defined as a basin that is split into segments in the x-axis direction as shown in Figure 3-6. It is important to note that in this analysis it is assumed that the set-up/set-down is not very sensitive to variations in depth in the direction normal to the x axis. Additionally, application of the analytic equations is limited to bottom slopes less than the maximum value discussed previously in this chapter.

The model mesh geometry for the first complex basin example is shown in Figure 4-51. The basin has a 5-m uniform bottom depth. The 50-m/s wind velocity was in the direction of the basin's long axis. Figure 4-52 compares the water surface profiles generated by ADCIRC and the equations and methods for complex geometry basins. The complex basin consists of a 500-m by 8000-m sub-basin and two 1500-m by 2000-m sub-basins attached at the upwind end as shown in Figure 4-51. The value of r was computed with the surface fit equation discussed earlier in this chapter.

The next comparison validates the complex basin approach by illustrating the one-dimensional nature of wind set-up for applications described in this study, as well as demonstrating the importance of the conservation of mass (volume) within the system. A two-leg complex basin with the sub-basins connected at the upwind end of the basin was chosen for this analysis (shown in Figure 4-6). The basin has a linearly sloping bottom with a slope of 1:5280, and the mean depth in the longest sub-basin (12000-m by 1500-m) is 5 m. The shorter of the two leg sub-basins is 6000-m by 1500-m, and the middle connecting sub-basin has dimensions of 1500-m by 3000 m. The bottom elevations are uniform in the y-direction (direction perpendicular to the wind direction). For the model simulation, the wind speed was 65 m/s in a direction parallel to the basin's long axis. Figure 4-53 contains plots of the water surface profiles for both the long sub-basin and the short sub-basin. There is good agreement between the analytic equation and the ADCIRC results. Figure 4-54 shows the water surface elevation contours for the ADCIRC simulation.

### Validation with Observed Field Data

In 2004, Hurricanes Frances and Jeanne made landfall in Florida, both impacting Lake Okeechobee as they passed over the state. Lake Okeechobee is the largest lake

in Florida with a surface area of 730 square miles and an average depth of only 9 ft. The combination of shallow depths and long fetches makes the lake vulnerable to wind set-up (and set-down) during severe wind events such as hurricanes. In this section, Imperial units were used as inputs and outputs to for consistency with comparison data acquired from South Florida Water Management District (SFWMD). Figure 4-55 shows the bathymetry of Lake Okeechobee; the mean water level of the lake is typically near +13 ft-NGVD29 under normal conditions.

Both of these hurricanes produced wind set-up/set-down within Lake Okeechobee, as measured by several gages deployed throughout the lake. Figure 4-56 is a location map of Lake Okeechobee showing the location of the water level measurement stations.

Time series plots of water level recorded at several gages throughout the lake during September 2004 are shown in Figure 4-57. Four of the stations were also equipped with meteorological instrumentation capable of measuring wind velocity. Figure 4-58 contains plots of wind speeds from these four stations from September 2004, when both Hurricane Frances and Hurricane Jeanne impacted the lake with low hurricane winds. Note that there is little variation in wind speed over the portion of the lake covered by the recording stations. . Figure 4-59 and Figure 4-60 show the wind speeds measured by the gages during Hurricane Frances and Jeanne respectively.

The wind direction is also critical for wind set-up as a uniform wind field along the basin’s long axis maximizes wind set-up. Figure 4-61 shows the wind direction during September 2004, while Figure 4-62 and Figure 4-63 detail the wind direction during Hurricane Frances and Jeanne, respectively.

The plots show that during Frances, the wind blew from approximately north (0,360 degrees) until the wind speeds began to subside. The wind component along the long axis of the lake was determined to be 0.81 times the wind velocity magnitude based on data from the four metrological stations averaged during the peak winds from 23:00 on September 4, 2004 to 02:45 on September 5, 2004. Thus, the maximum wind speed recorded was multiplied by this factor to arrive at the wind velocity component in the direction parallel to the profile. For Jeanne, the wind direction followed a similar pattern with the winds blowing from the north until the peak wind speed, and then they gradually shifted to the west then south. The plots show that during Frances and Jeanne, significant variations in wind direction were not observed between the stations.

Given this information, the peak wind velocity observed across all of the gages during each storm was employed for the model validation (71 mph for Frances and 79 mph for Jeanne). The fetch analyzed is shown in Figure 4-64.

**Hurricane Frances**

First, the horizontal bed equation developed in Chapter 3 is compared to the measured values during Hurricane Frances. The mean water depth across the profile is selected as the depth (using the +13.5 ft-NGVD29 water level shown on the gages prior to impact of the storm). This equation predicts that 4.3 miles of the upwind portion of the lake bottom will be dry, increasing the mean water depth of the wetted portion of the lake by 1.48 ft. The resulting water surface elevation at the downwind end of the basin is calculated to be +19.9 ft-NGVD which is above the measured elevation of +17.7 ft-NGVD at SFWMD observation station S-3_T. This station is located on the lake side of the control structure S-3 which is connected to the lake via a short canal running nearly

east-west. At the SFWMD station, LZ40, the model predicted water level was +16.0 ft-NGVD, while the maximum measured level was +15.7 ft-NGVD. At SFWMD gage L006, the maximum modeled water level was +17.7 ft-NGVD, and the maximum measured level was +16.9 ft-NGVD. Figure 4-65 shows the computed water surface profile developed with the horizontal bottom equation for a rectangular basin. Note that this analysis was for a simple rectangular basin with a horizontal bottom across the entire length of the basin. Possible reasons for this over prediction include: the short duration of the hurricane event did not allow the wind set-up to reach equilibrium levels at the south end of the lake. There may also be a local depression in the water surface elevation near the S-3 structure due to out-flow through the control structure, flooding of adjacent low lying areas, and/or over simplification of the basin shape.

Next, an analysis considering the basin as a rectangular basin with a bottom profile presented in Figure 4-66 is performed. This simulation shows 5.0 miles of the upwind end (north end) of the lake bed are exposed due to local wind set-down, which results in an increase of 1.35 ft in the mean water level. The resulting wind set-up at the downwind end of the lake is 5.25 ft above the mean water level which is equal to a water surface elevation of +20.1 ft-NGVD, while SFWMD gage S-3_T near this location registered a maximum water level of +17.7 ft-NGVD. This may be attributed to low lying land beyond the shoreline which may act as storage thus suppressing the maximum wind set-up at S-3_T or a local depression in the water level at S-3_T due to flow through the control structure. At SFWMD gage LZ40, the model predicted a maximum water surface elevation of +15.6 ft-NGVD, and the gage showed a maximum elevation of +15.7 ft-NGVD. At SFWMD gage L006, the model predicted a maximum water

surface elevation of +17.1 ft-NGVD, and the gage showed a maximum water surface elevation of +16.9 ft-NGVD. Figure 4-67 shows the water surface profile as computed by the discrete method. Again, the over-prediction of the local wind set-up at the end of the basin may be attributed to the same factors contributing to the differences as the horizontal bed basin mentioned previously.

Next, Lake Okeechobee is treated as a complex shaped basin, the basin widths were measured at points of marked shoreline change (Figure 4-68) for the complex basin analysis. The green lines in the figure outline the shoreline, while the red lines show the location of the measured basin widths. Additionally, the yellow line describes the fetch, and also corresponds to the transect from which the bottom profile was extracted.

First, the complex basin is analyzed with the horizontal bottom equation. The initial still water depth was again set to 8.6 ft. The surface wind stress caused 4.35 miles of the upwind end of the lake bottom to become exposed according to the analytical equation for a horizontal bottom. The mean water level was raised 1.27-ft due to the 4.3 miles of drying of the upwind end of the lake. At station LZ40, the analytical equation predicted a maximum water elevation of +16.2 ft-NGVD. At station L006, a maximum water elevation of +17.9 ft-NGVD was predicted by the discrete analytical model. At the south shoreline, the discrete analytical model predicted a water elevation of +20.1 ft-NGVD.

For the complex basin with a discrete stepwise bottom profile shown in Figure 4-66, the wind stress applied at the surface exposed 4.2 miles of the bottom in upwind end of the basin. The discrete analytical model predicted a water elevation of +15.8 ft-

NGVD at SFWMD station LZ40 (compared to a maximum elevation at the gage of +15.7 ft-NGVD). At station L006, the discrete analytical model predicted a maximum water elevation of +17.25 ft-NGVD while the gage recorded a maximum water elevation of +16.9 ft-NGVD. Finally, at the south shoreline, a maximum water elevation of +20.2 ft-NGVD was predicted, which was greater than the measured value of +17.7 at gage S3_T.Figure 4-69 shows the computed water surface profile for a complex basin with the discrete method for Hurricane Frances. Table 4-3 summarizes the modeled and measured values at each gage during Hurricane Frances. Figure 4-70 contains a time series plot of water level at seven gages within Lake Okeechobee during Hurricane Frances.

**Hurricane Jeanne**

From September 25, 2004, to September 26, 2004, Hurricane Jeanne impacted Lake Okeechobee. Analysis of Hurricane Jeanne was performed using the same methodology as that used for Hurricane Frances. Figure 4-60 and Figure 4-61 contain wind speed and wind direction plots recorded at four meteorological stations on Lake Okeechobee during Hurricane Jeanne. Like the wind fields for Hurricane Frances, the wind fields for Hurricane Jeanne showed similar wind speeds and wind directions at all four stations. The component of wind direction along the axis was averaged between all four stations between 18:45 September 25 and 0:00 September 26 to arrive at a factor of 0.63 of the wind velocity magnitude. The mean water elevation of the lake increased to +16.3 ft-NGVD prior to the landfall of Hurricane Jeanne due to the rainfall runoff inflows to Lake Okeechobee associated with Hurricane Frances.

First, the horizontal bottom analytical equation developed in Chapter 3 is compared to the measured values during Hurricane Jeanne. The mean depth across the profile is selected as the depth (using the +16.3 ft-NGVD29 water elevation shown on the gages prior to impact of the storm). The initial still water depth is 11.4-ft. This equation predicts no drying will occur along the length of the profile, and the water surface elevation at the downwind end of the basin is calculated to be +19.8-ft-NGVD which is above the measured elevation of +18.4 ft-NGVD at SFWMD observation station S-3_T. This station is located on the lake side of control structure S-3 which is connected to the lake via a short canal running nearly east-west. At SFWMD station LZ40, the model predicted water elevation was +17.3 ft-NGVD, while the maximum measured elevation was +17.2 ft-NGVD. At SFWMD gage L006, the maximum modeled water elevation was +18.4 ft-NGVD, and the maximum measured elevation was +18.2 ft-NGVD. Figure 4-71 shows the water surface profile computed with the horizontal bottom equation for a rectangular basin. Note that this analysis was for a simple rectangular basin with a horizontal bottom along the entire length of the basin.

Next, an analysis is performed considering the basin to be rectangular with the bottom profile presented in Figure 4-66. This simulation shows none of the lake bed is exposed due to local wind set-down. The modeled water surface elevation at the south end of the lake is +19.8 ft-NGVD, while the SFWMD gage S-3_T near this location registered a maximum water elevation of +18.4 ft-NGVD. This may be attributed to low lying land beyond the shoreline which may act as storage thus suppressing the maximum wind set-up at S-3_T or a local depression in the water level due to flow through the control structure. At SFWMD gage LZ40, the model predicted a maximum

water surface elevation of +17.3 ft-NGVD, and the gage showed a maximum elevation of +17.2 ft-NGVD. At SFWMD gage L006, the model predicted a maximum water surface elevation of +18.4 ft-NGVD, and the gage showed a maximum water surface elevation of +18.2 ft-NGVD. Figure 4-72 shows the water surface profile as calculated with the discrete method for a rectangular basin for Hurricane Jeanne. Again, the over-prediction of the local wind set-up at the end of the basin may be attributed to the same factors contributing to the differences as the horizontal bed basin mentioned previously.

Next, the complex basin is analyzed using the horizontal bottom equation. The mean water depth was again set to 11.4 ft. At station LZ40, the analytical equation for a horizontal bottom predicted a maximum water elevation of +17.2 ft-NGVD. At station L006, a maximum water elevation of +18.2 ft-NGVD was predicted by the analytical equation. At the south shoreline, the analytical equation predicted a water elevation of +19.7 ft-NGVD. Figure 4-73 contains the water surface profile computed with the horizontal bottom equation for a complex basin for Hurricane Jeanne.

Computations were performed for the complex basin with the discrete analytic model (bottom profile shown in Figure 4-66), using the same methods used for Hurricane Frances. The model predicted a water elevation of +17.0 ft-NGVD at SFWMD station LZ40 (compared to a maximum elevation at the gage of +17.2 ft-NGVD). At station L006, the model predicted a maximum water elevation of +17.9 ft-NGVD while the gage recorded a maximum water elevation of +18.2 ft-NGVD. Finally, at the south shoreline, a maximum water elevation of +19.9 ft-NGVD was predicted, which was greater than the measured elevation of +18.4 at gage S3_T. Table 4-4 summarizes the modeled and measured values at each gage during Hurricane Frances. Figure 4-74

presents the water surface profile as calculated using the discrete method for the complex basin for Hurricane Jeanne. Figure 4-75 contains a time series plot of water level at seven gages within Lake Okeechobee during Hurricane Jeanne. Some of the gages failed during the storm, as is apparent in the plot.

Table 4-1. ADCIRC model parameters

| Parameter Description | Setting Description (Setting Number) |
|---|---|
| ICS – Coordinate system option | Cartesian (1) |
| NOLIFA – Finite amplitude terms option | Finite amplitude terms are included, but wetting and drying of elements is disabled (1) |
| NOLICA – Convective acceleration terms | Terms are included (1) |
| NOLICAT – Option to consider time derivative of convective acceleration terms | Time derivative of convective acceleration terms is considered (1) |
| NWS – Wind stress and barometric pressure option | Wind velocity and barometric pressure are input at each mesh node (5) |
| G - Acceleration due to gravity | 9.80665 $m/s^2$ |
| Time Weighting factors in GWCE equation | 0.35, 0.30, 0.35 |
| EVM - Horizontal eddy viscosity for Momentum Equations | 2.0 |
| ITITER – Solver type | JCG iterative solver (1) |
| CONVCR – Absolute convergence criteria | $1.0 \times 10^{-5}$ |
| ITMAX – maximum number of iterations per time step | 50 |
| ISLIP – 3D bottom friction type | Quadratic slip boundary condition (2) |
| KP – 3D bottom friction coefficient | 0.01 |
| Z0S – Free surface roughness | 0.01 |
| Z0B – Bottom roughness | 0.1 |
| ALP1, ALP2, ALP3 – Time weighting coefficients for the 3D velocity solution | 0.5, 0.5, 0.5 |
| IGC – Vertical grid code | Uniform vertical grid generated (1) |
| NFEN – Number of vertical grid points | 12 |
| EVCON – Vertical eddy viscosity | 0.05 |

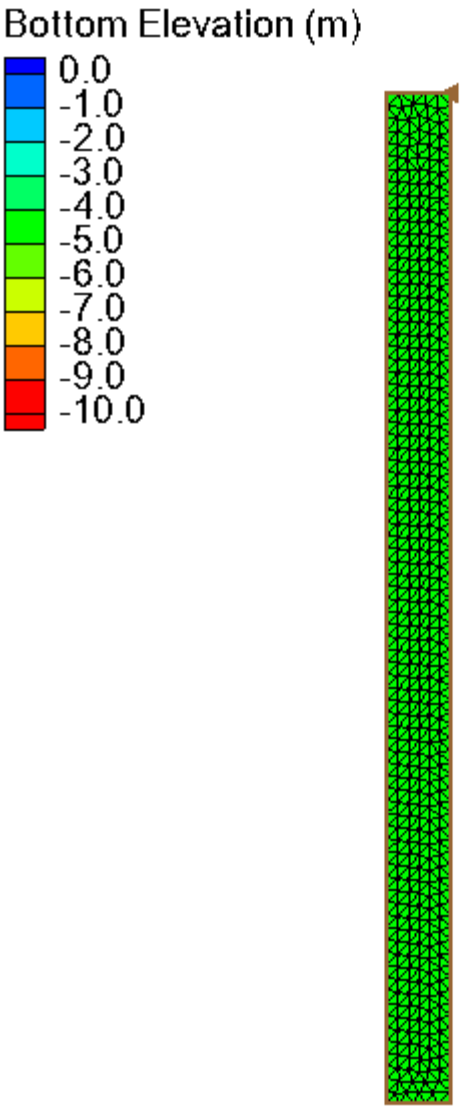


Figure 4-1. Rectangular basin mesh with a horizontal bottom

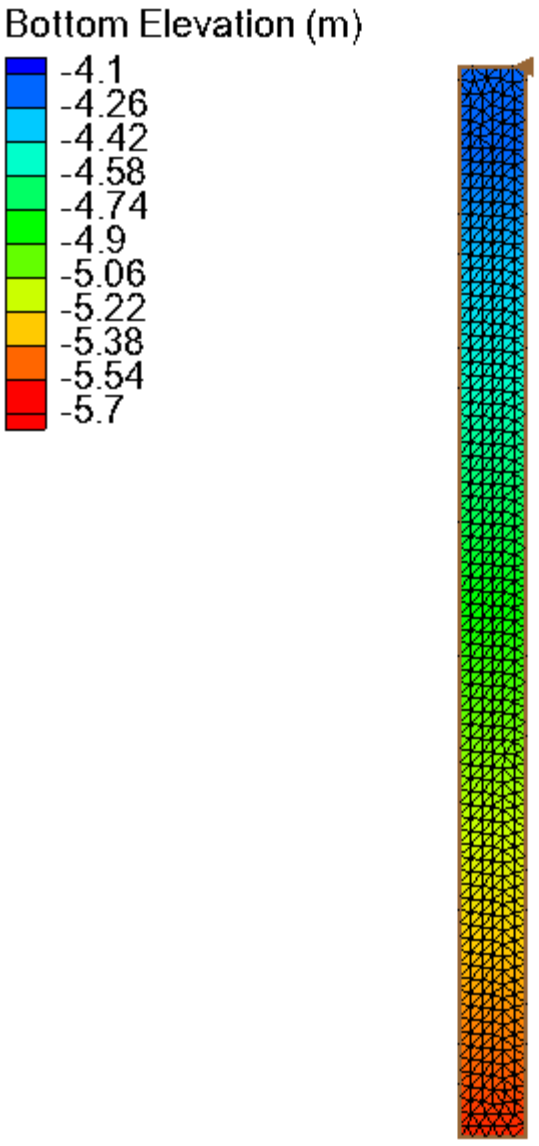


Figure 4-2. Rectangular basin mesh with a linearly sloping bottom

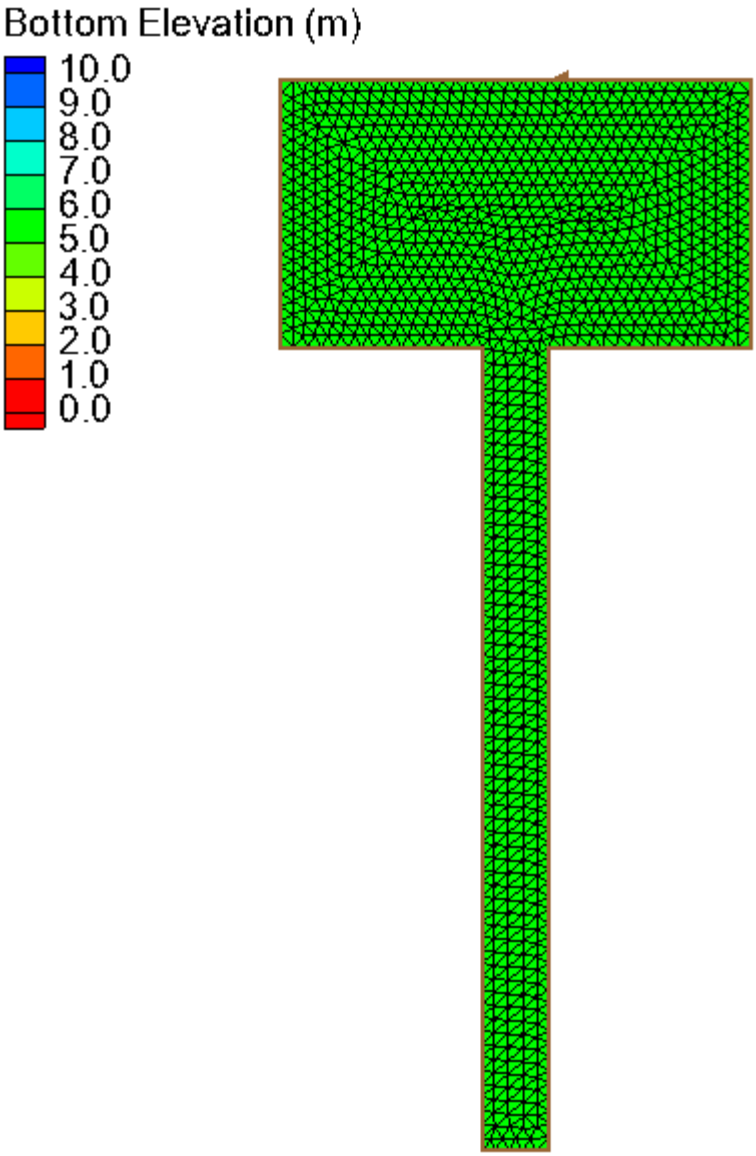


Figure 4-3. T-shaped basin mesh with a horizontal bottom

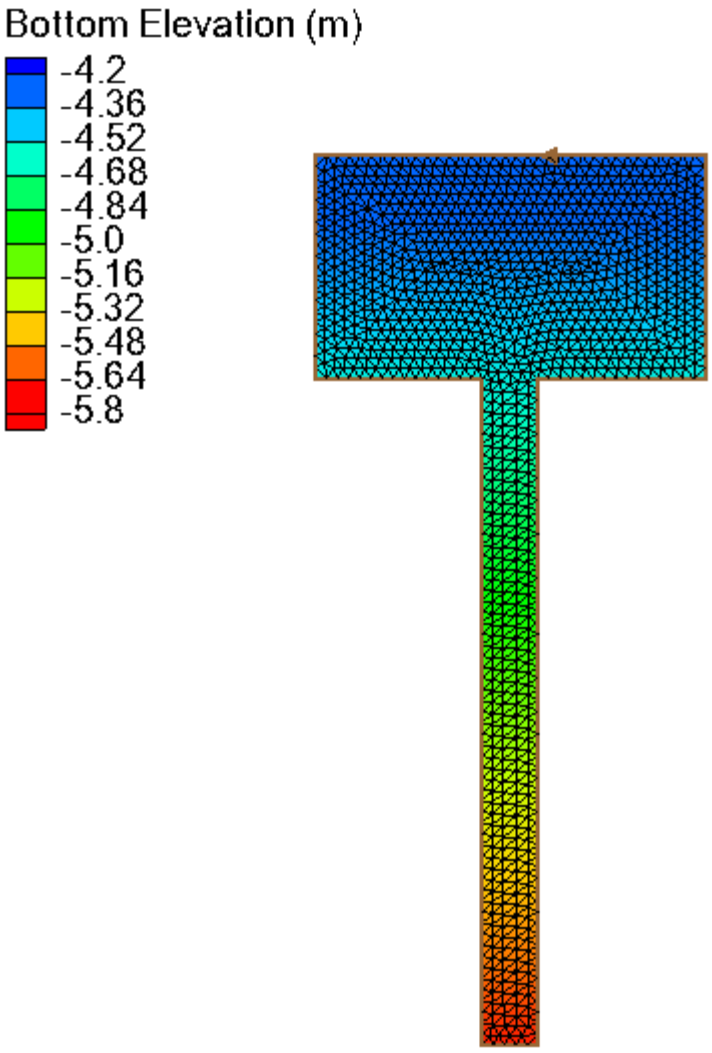


Figure 4-4. T-shaped basin mesh with linearly sloping bottom

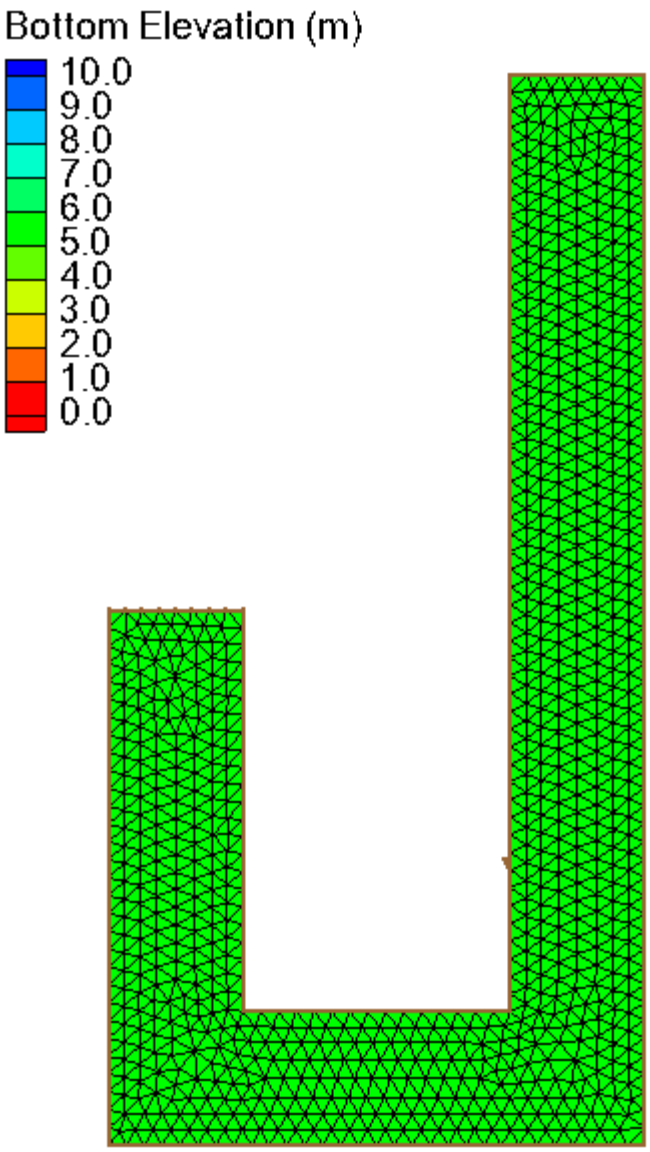


Figure 4-5. Multi-leg basin mesh with a horizontal bottom

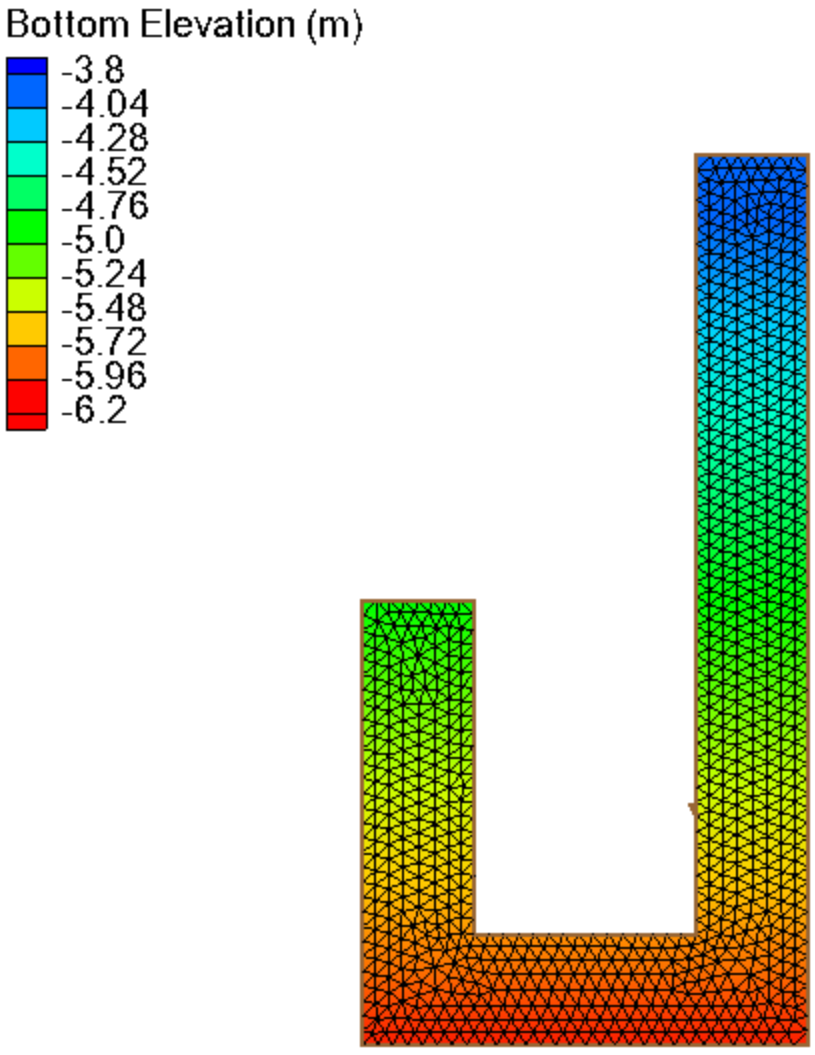


Figure 4-6. Multi-leg basin with a linearly sloping bottom

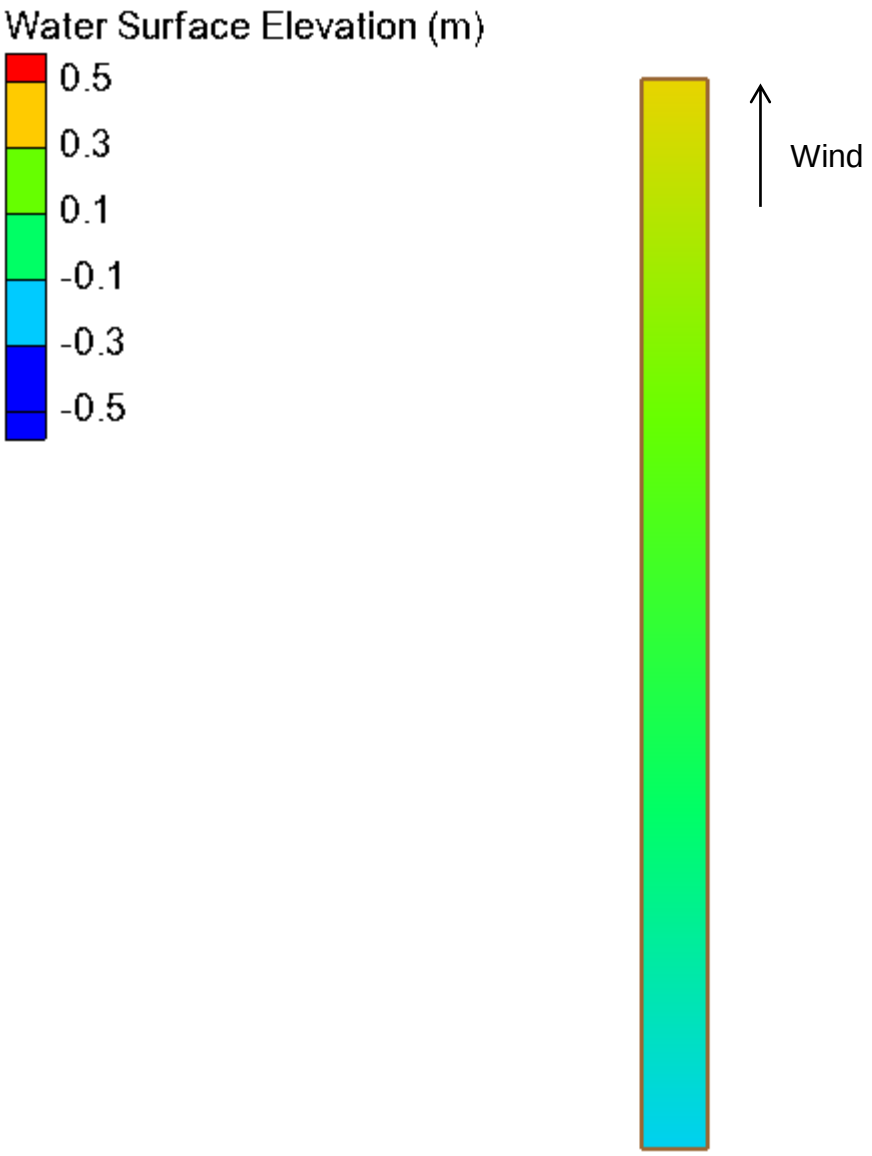


Figure 4-7. Water surface elevation contour plot for the 8000-m long by 500-m wide rectangular basin with a 30 m/s wind directed upward in the figure.

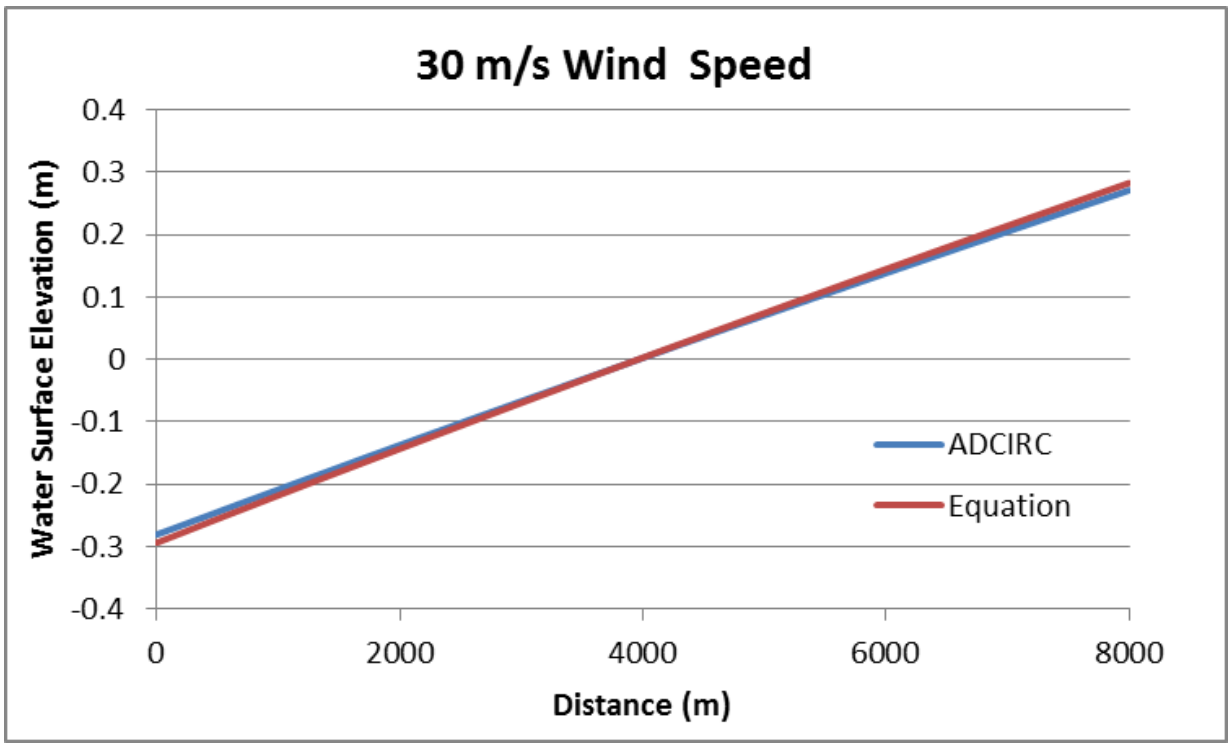


Figure 4-8. Water surface comparison plot for a rectangular basin with a 30 m/s wind speed and r = 0.1

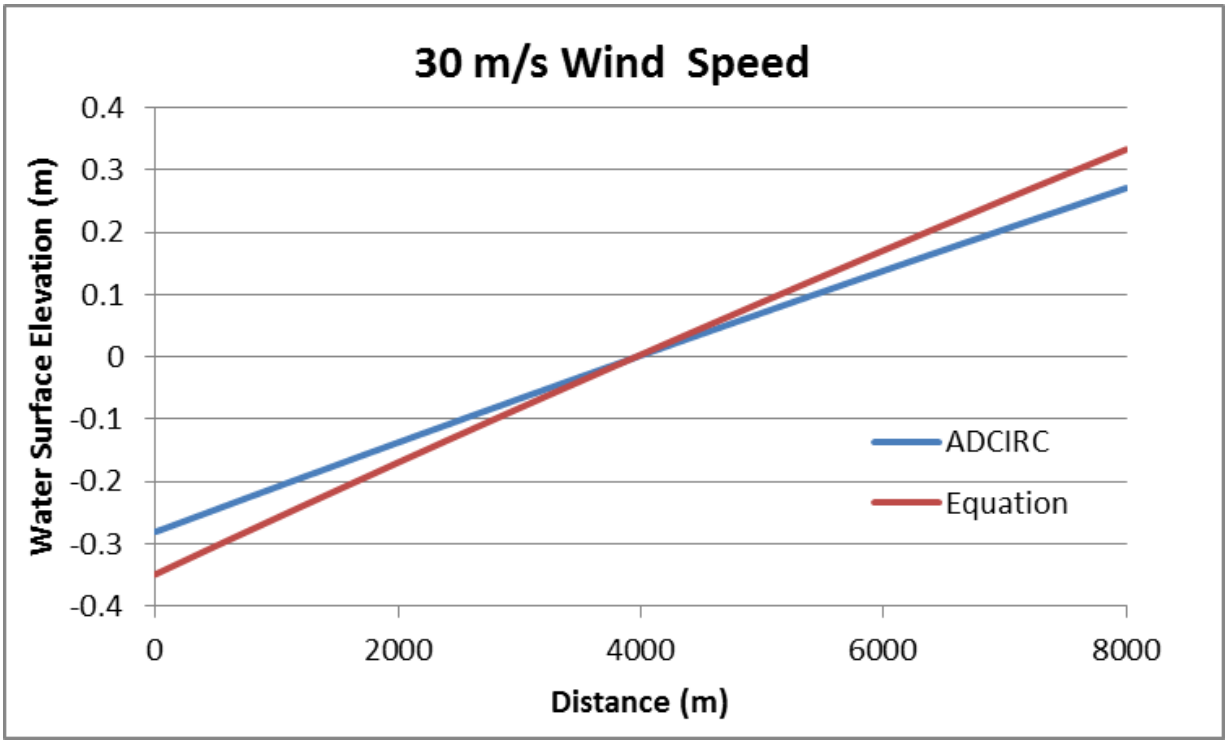


Figure 4-9. Water surface comparison plot for a rectangular basin with a 30 m/s wind speed and r = 0.3

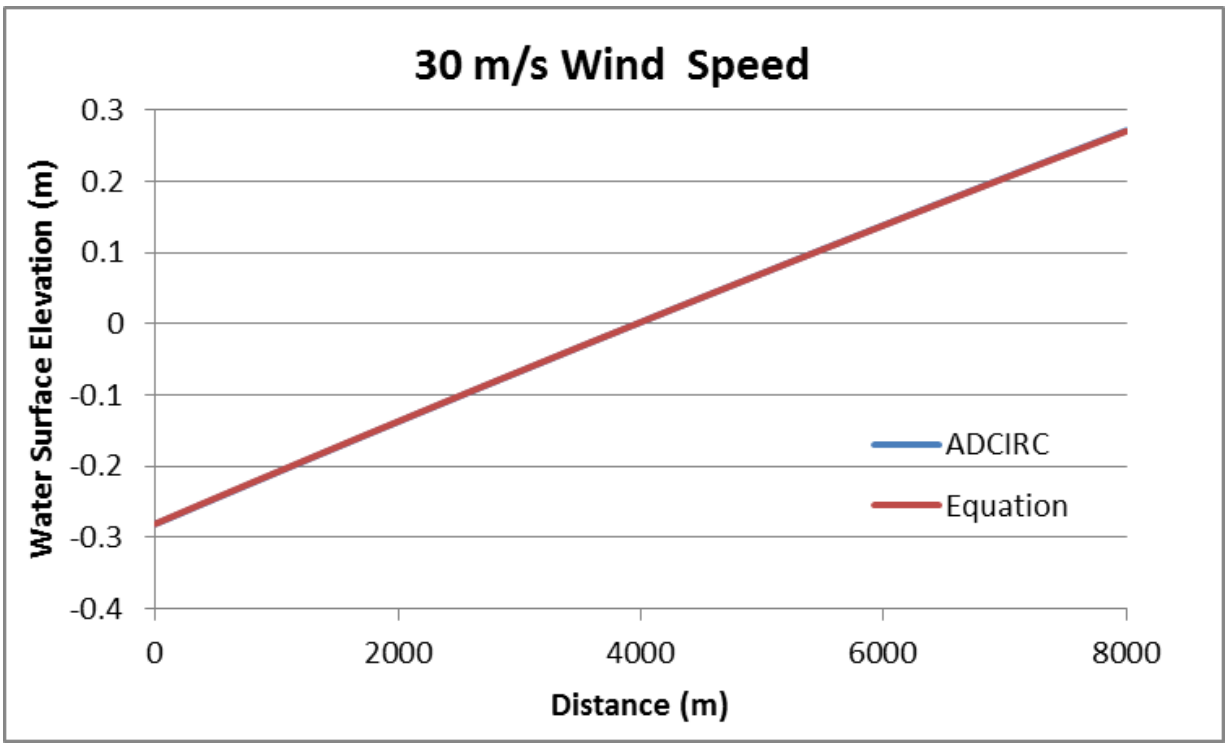


Figure 4-10. Water surface comparison plot for a rectangular basin with a 30 m/s wind speed and r = 0.05

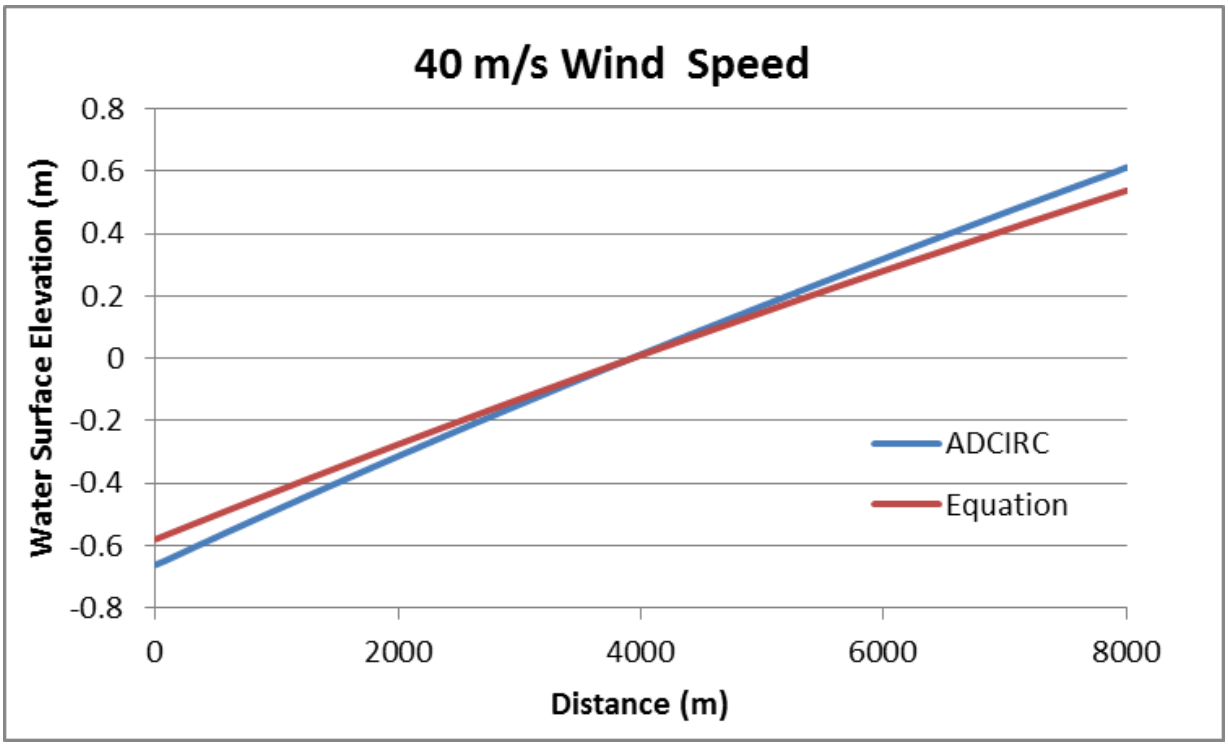


Figure 4-11. Water surface comparison plot for a rectangular basin with a 40 m/s wind speed and r = 0.1

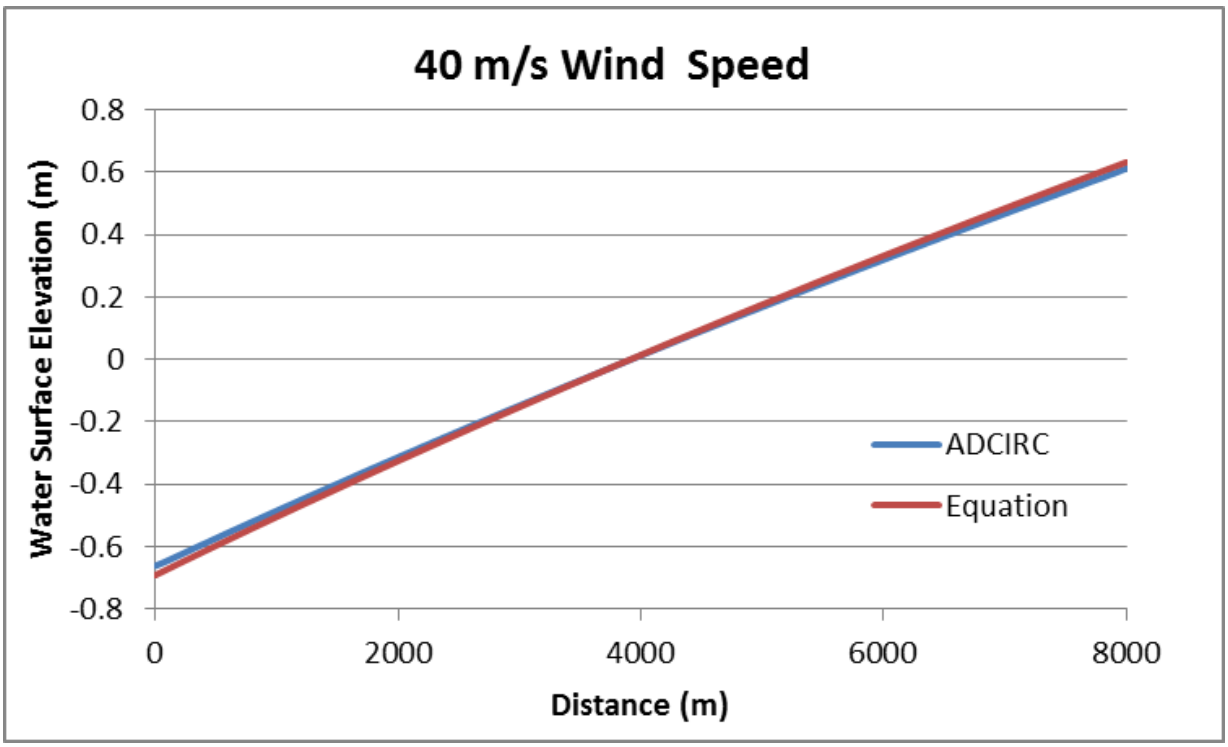


Figure 4-12. Water surface comparison plot for a rectangular basin with a 40 m/s wind speed and r = 0.3

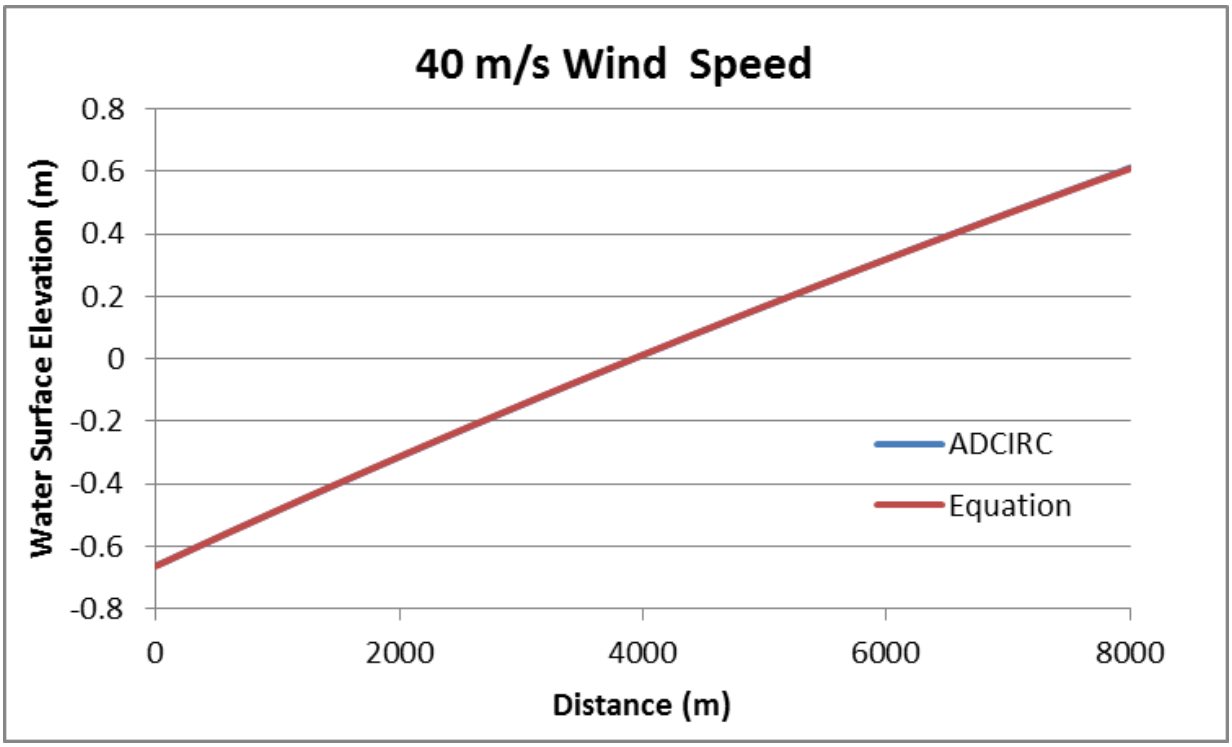


Figure 4-13. Water surface comparison plot for a rectangular basin with a 40 m/s wind speed and r = 0.25

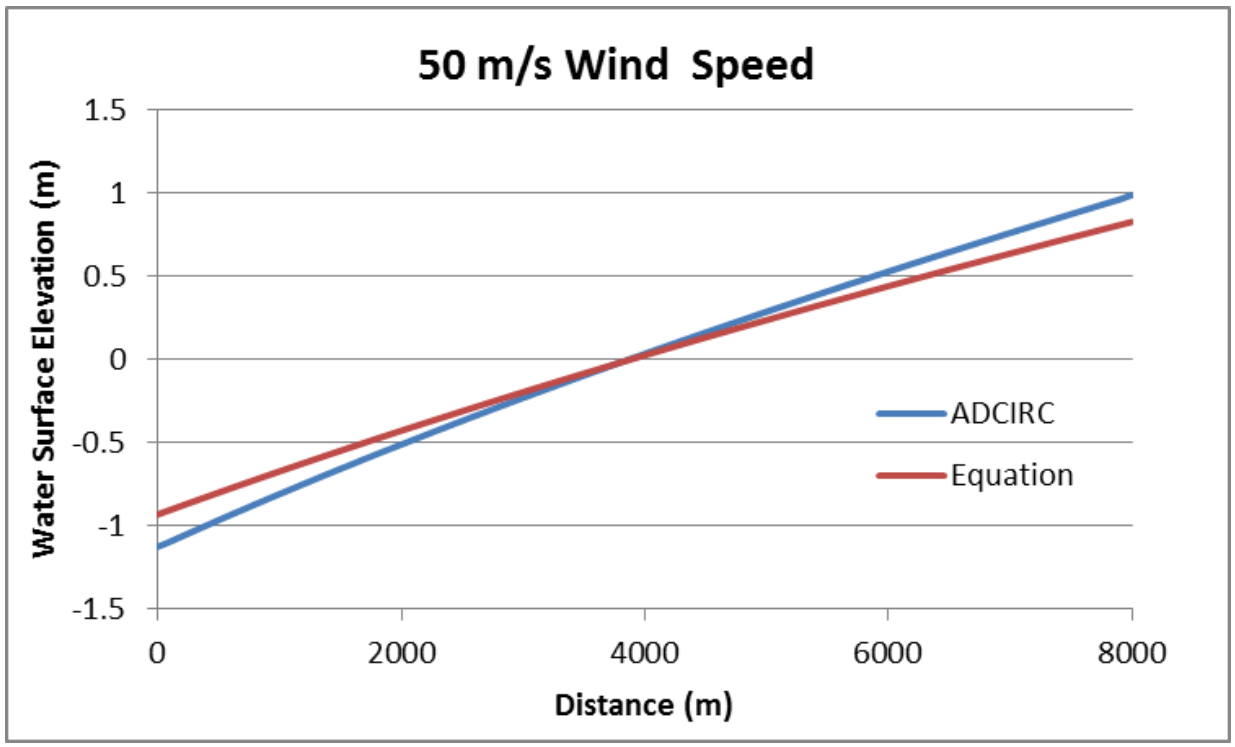


Figure 4-14. Water surface comparison plot for a rectangular basin with a 50 m/s wind speedand r = 0.1

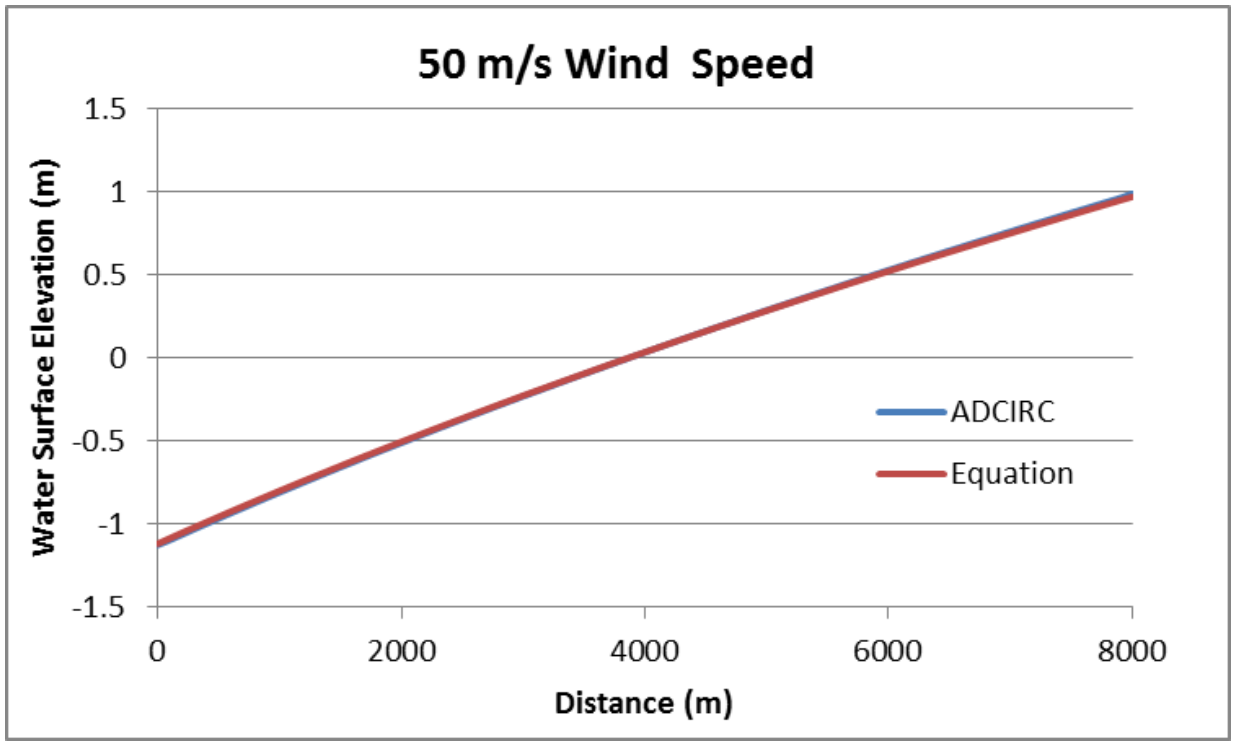


Figure 4-15. Water surface comparison plot for a rectangular basin with a 50 m/s wind speed and r = 0.3

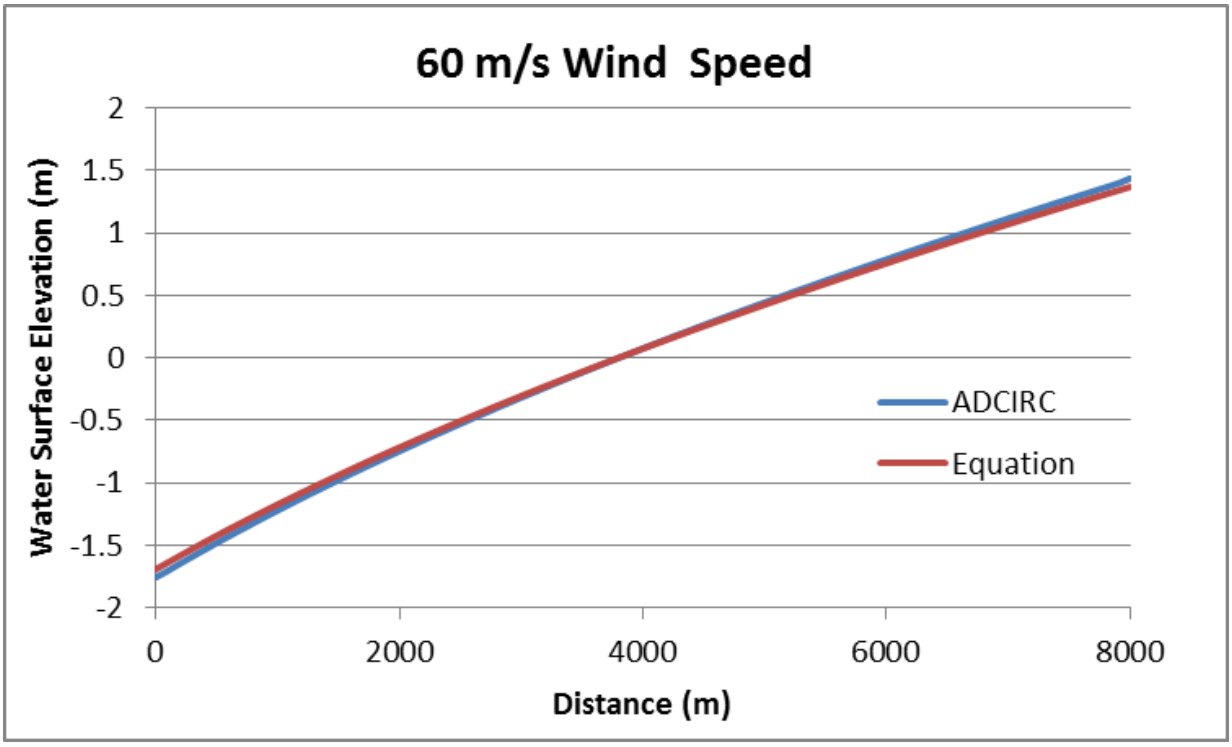


Figure 4-16. Water surface comparison plot for a rectangular basin with a 60 m/s wind speed and r = 0.3

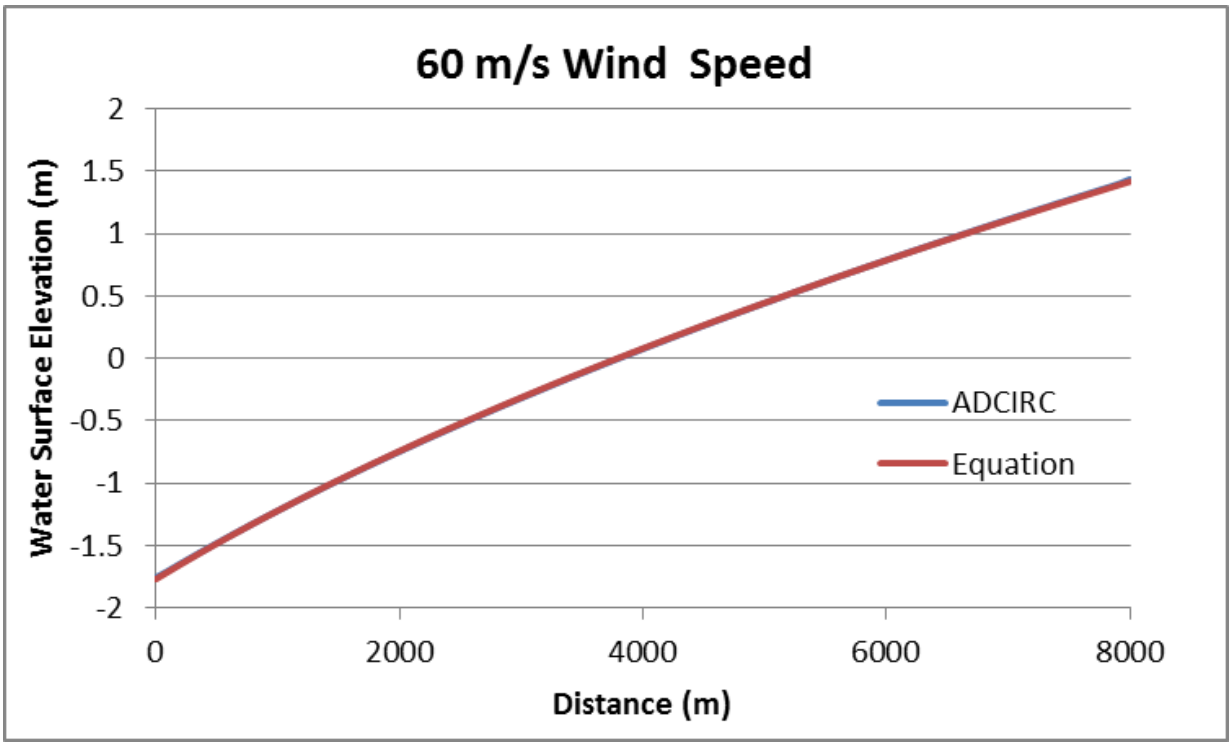


Figure 4-17. Water surface comparison plot for a rectangular basin with a 60 m/s wind speed and r = 0.35

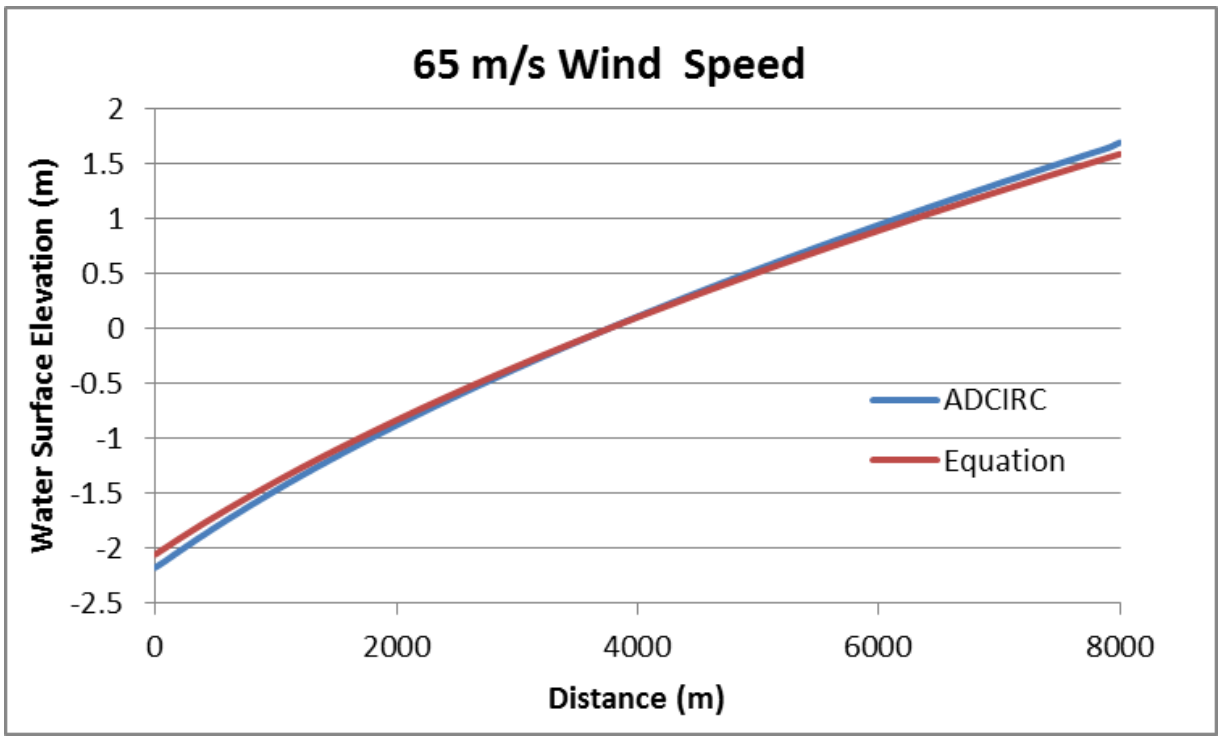


Figure 4-18. Water surface comparison plot for a rectangular basin with a 65 m/s wind speed and r = 0.3

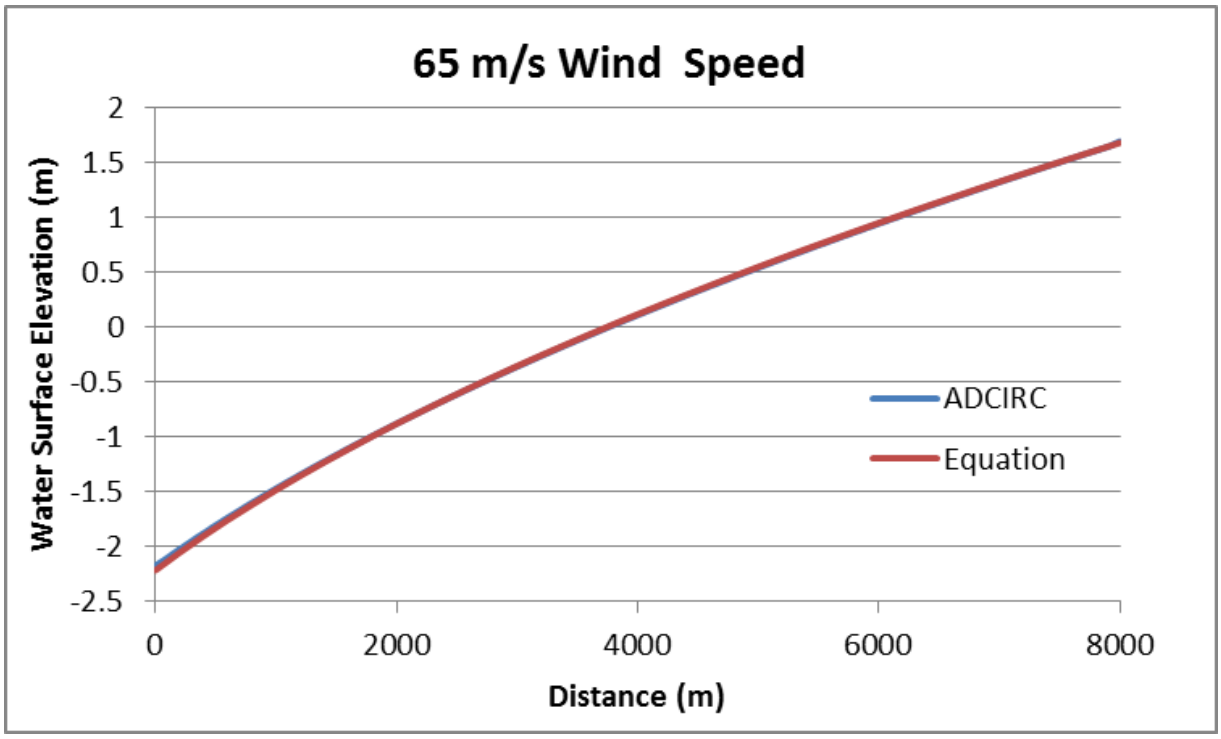


Figure 4-19. Comparison plot for a rectangular basin with a 65 m/s wind speed and r = 0.38

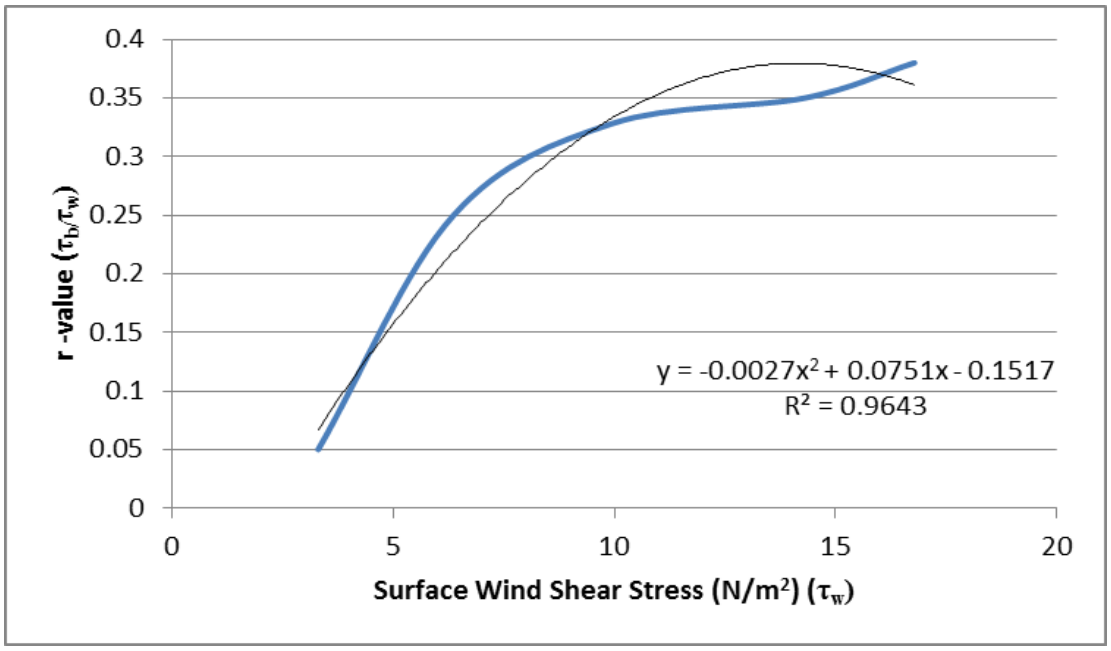


Figure 4-20. Plot of r-value versus surface wind shear stress with a polynomial curve fit

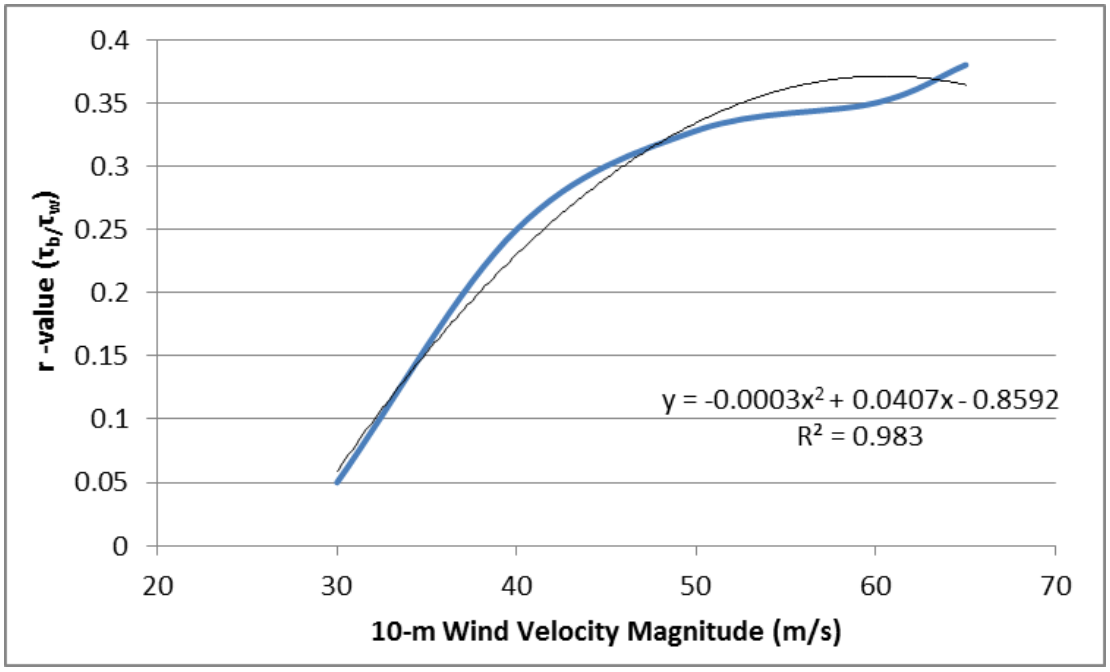


Figure 4-21. Plot of r-value versus 10-m wind speed with a polynomial curve fit

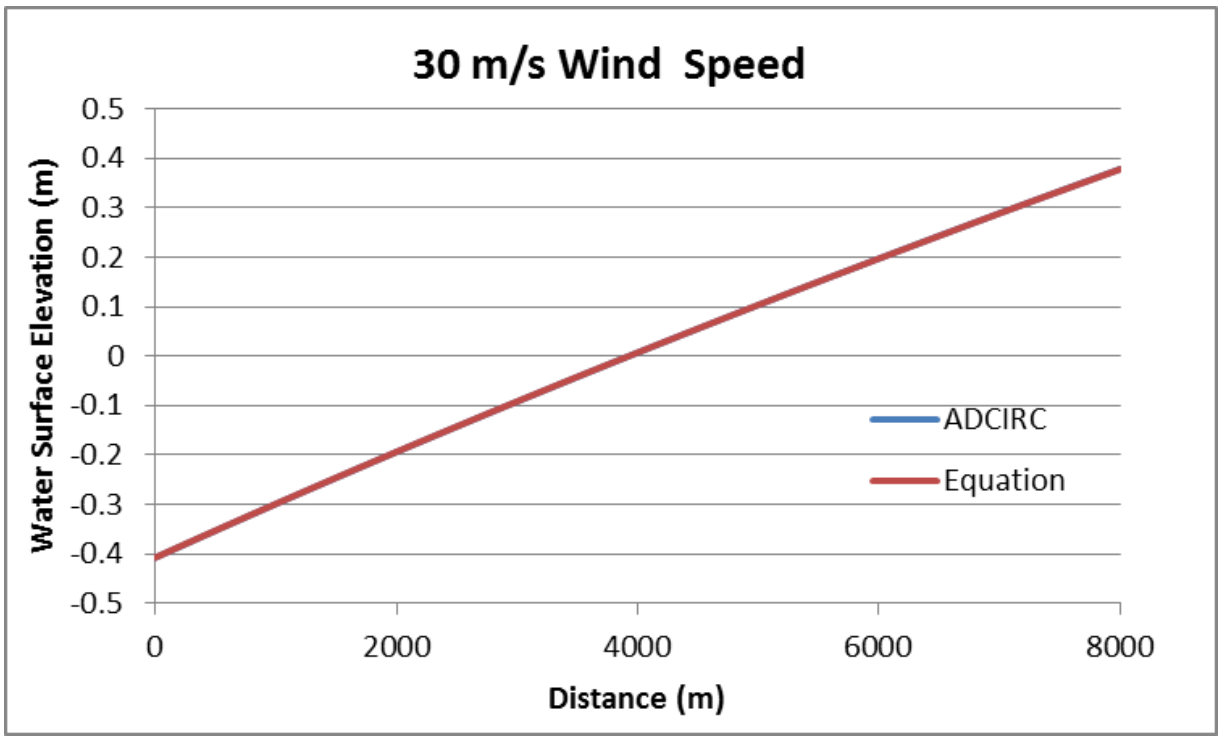


Figure 4-22. Water surface comparison plot for a 3.5-m deep rectangular basin with a 30 m/s wind speed and r = 0.045

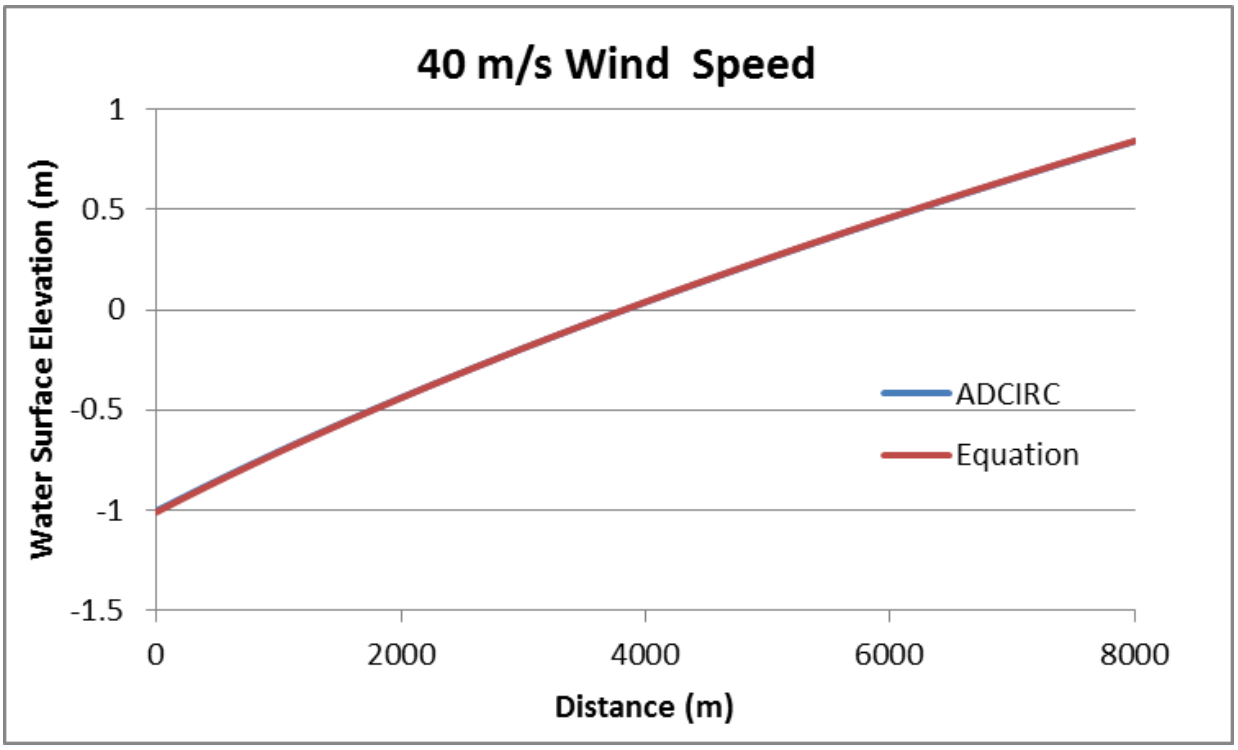


Figure 4-23. Water surface comparison plot for a 3.5-m deep rectangular basin with a 40 m/s wind speed and r = 0.25

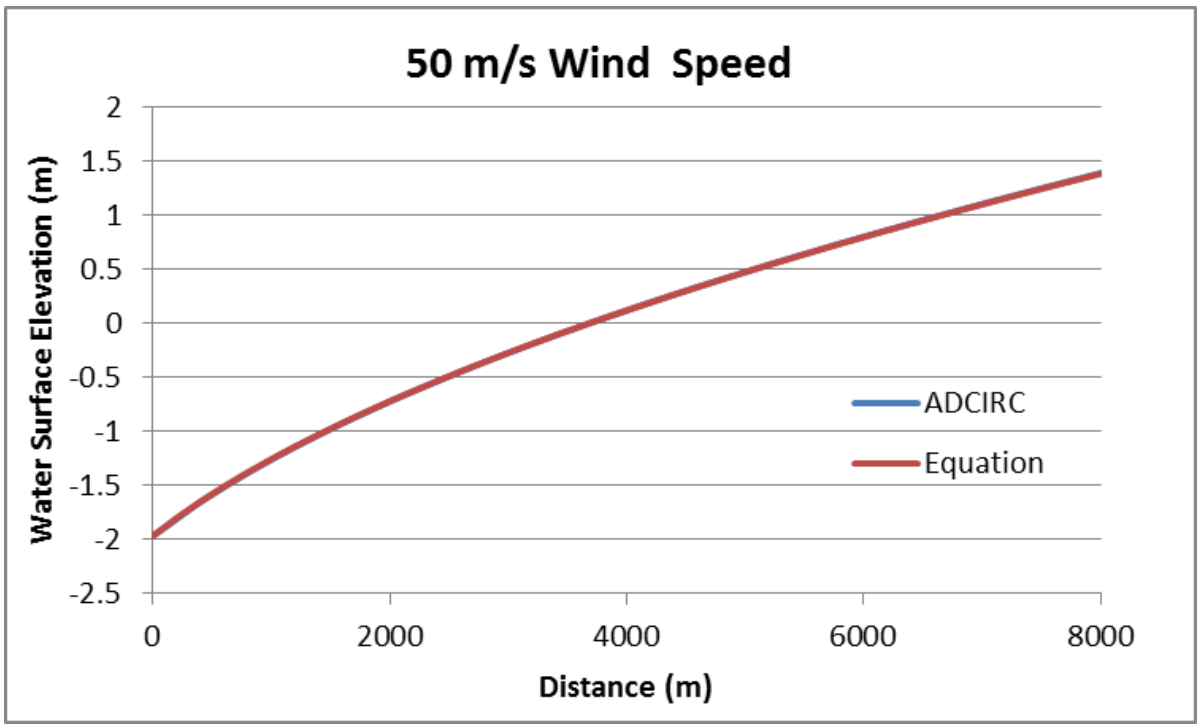


Figure 4-24. Water surface comparison plot for a 3.5-m deep rectangular basin with a 50 m/s wind speed and r = 0.36

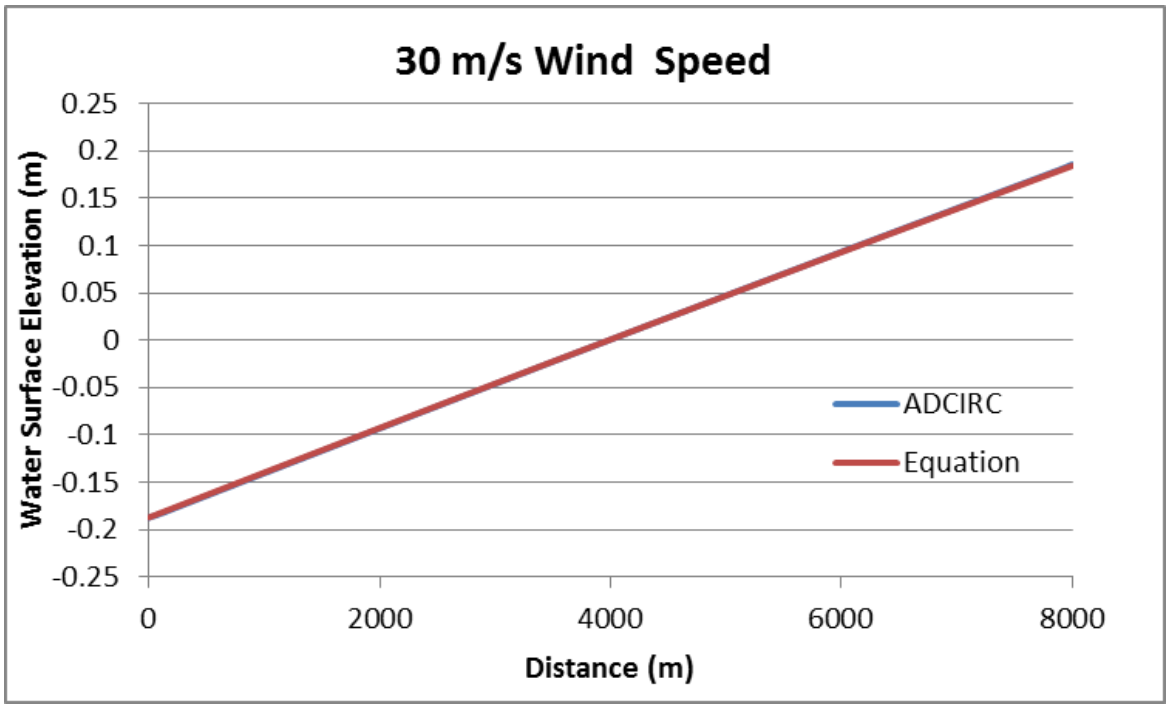


Figure 4-25. Water surface comparison plot for a 7.5-m deep rectangular basin with a 30 m/s wind speed and r = 0.063

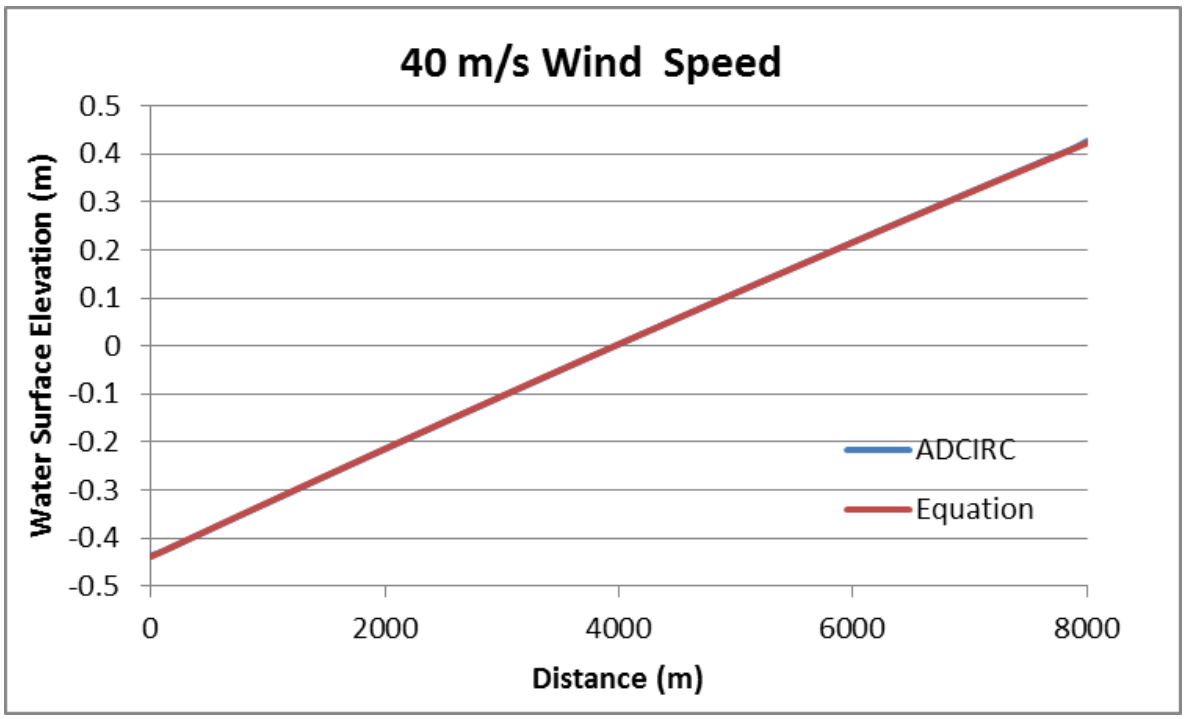


Figure 4-26. Water surface comparison plot for a 7.5-m deep rectangular basin with a 40 m/s wind speed and r = 0.275

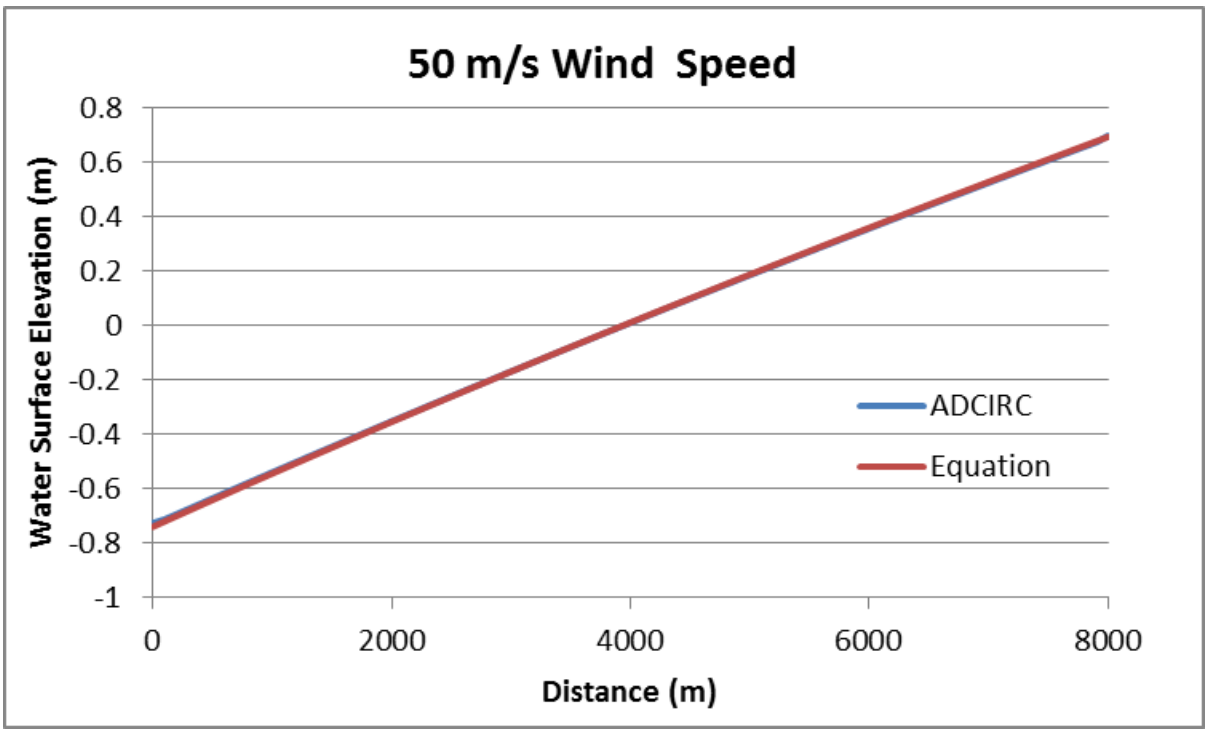


Figure 4-27. Water surface comparison plot for a 7.5-m deep rectangular basin with a 50 m/s wind speed and r = 0.355

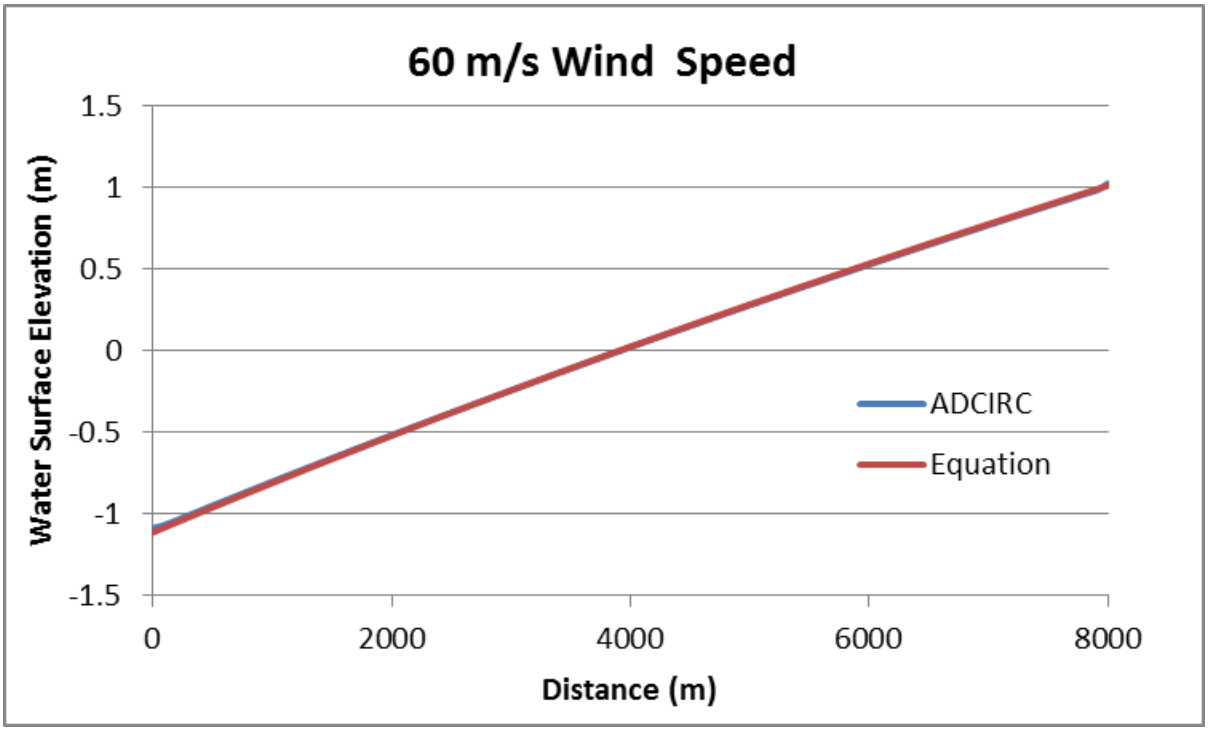


Figure 4-28. Water surface comparison plot for a 7.5-m deep rectangular basin with a 60 m/s wind speed and r = 0.39

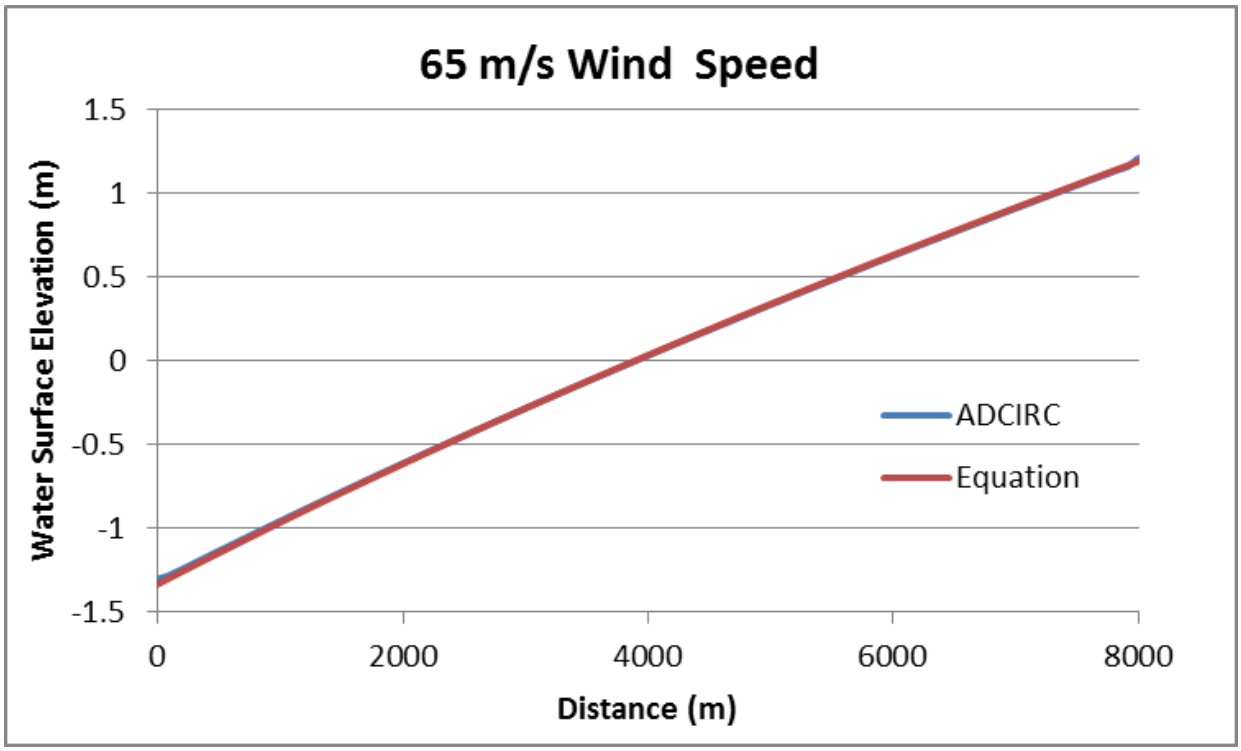


Figure 4-29. Water surface comparison plot for a 7.5-m deep rectangular basin with a 65 m/s wind speed and r = 0.4025

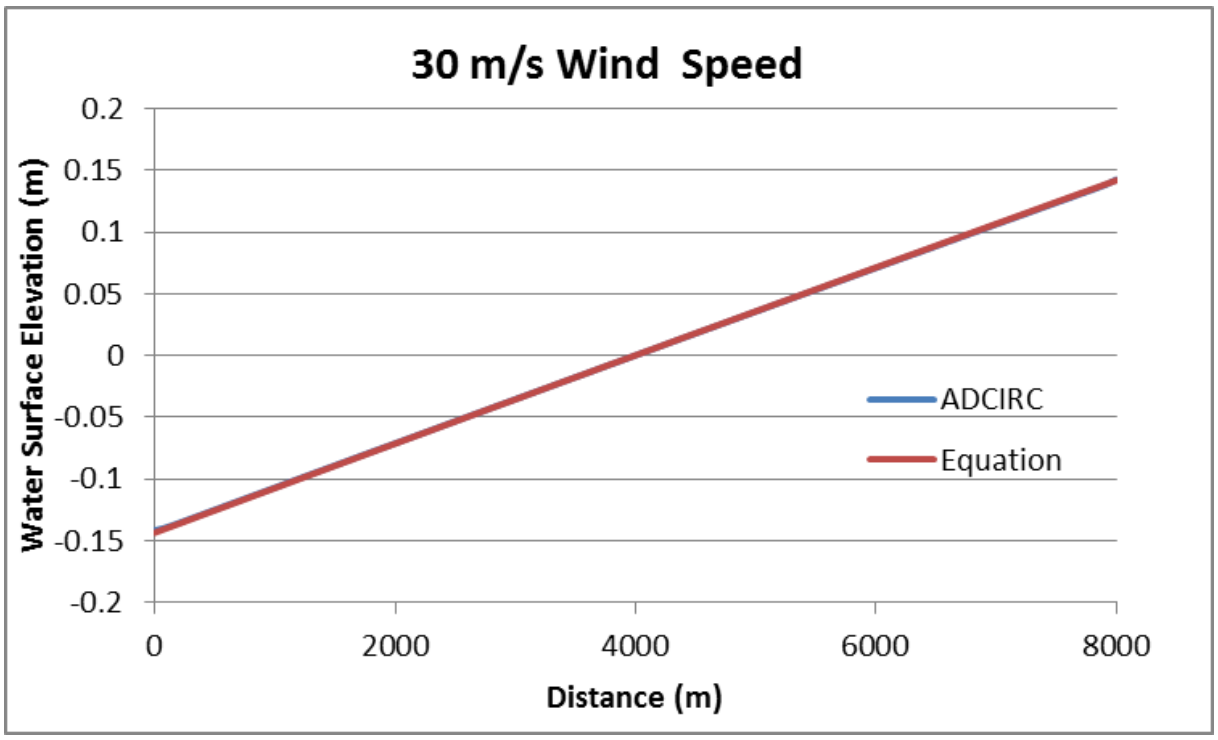


Figure 4-30. Water surface comparison plot for a 10-m deep rectangular basin with a 30 m/s wind speed and r = 0.09

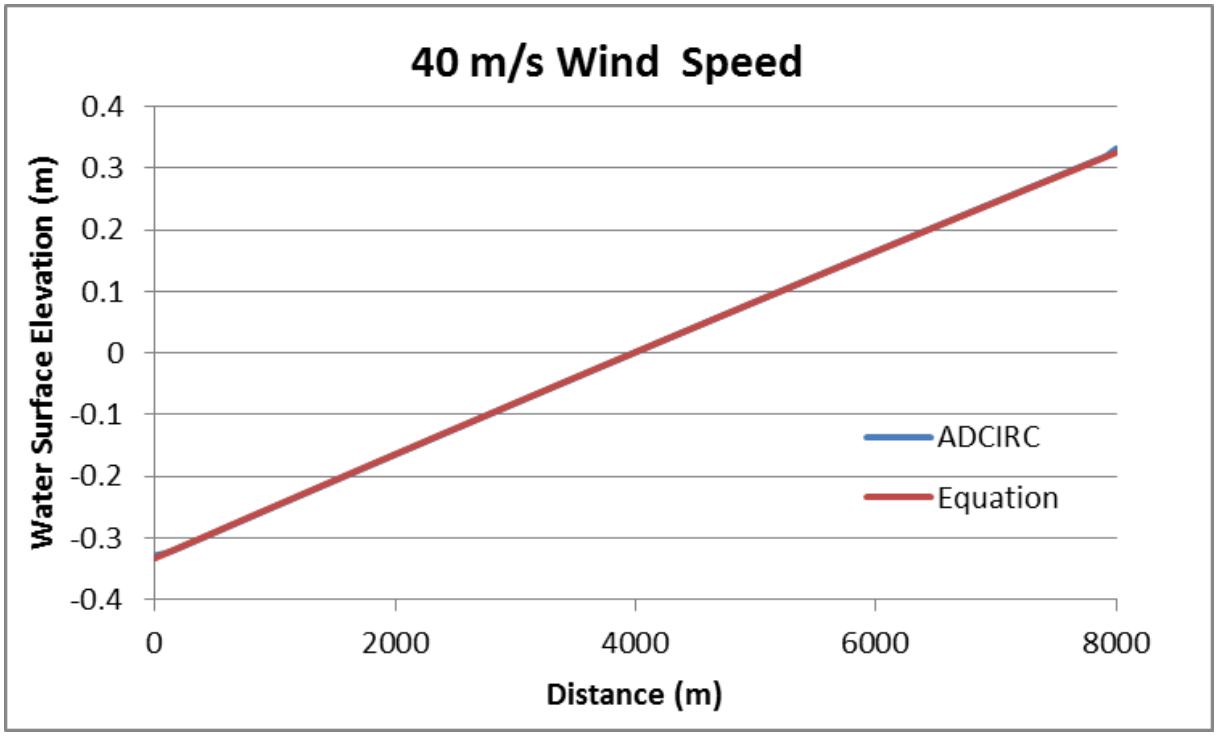


Figure 4-31. Water surface comparison plot for a 10-m deep rectangular basin with a 40 m/s wind speed and r = 0.30

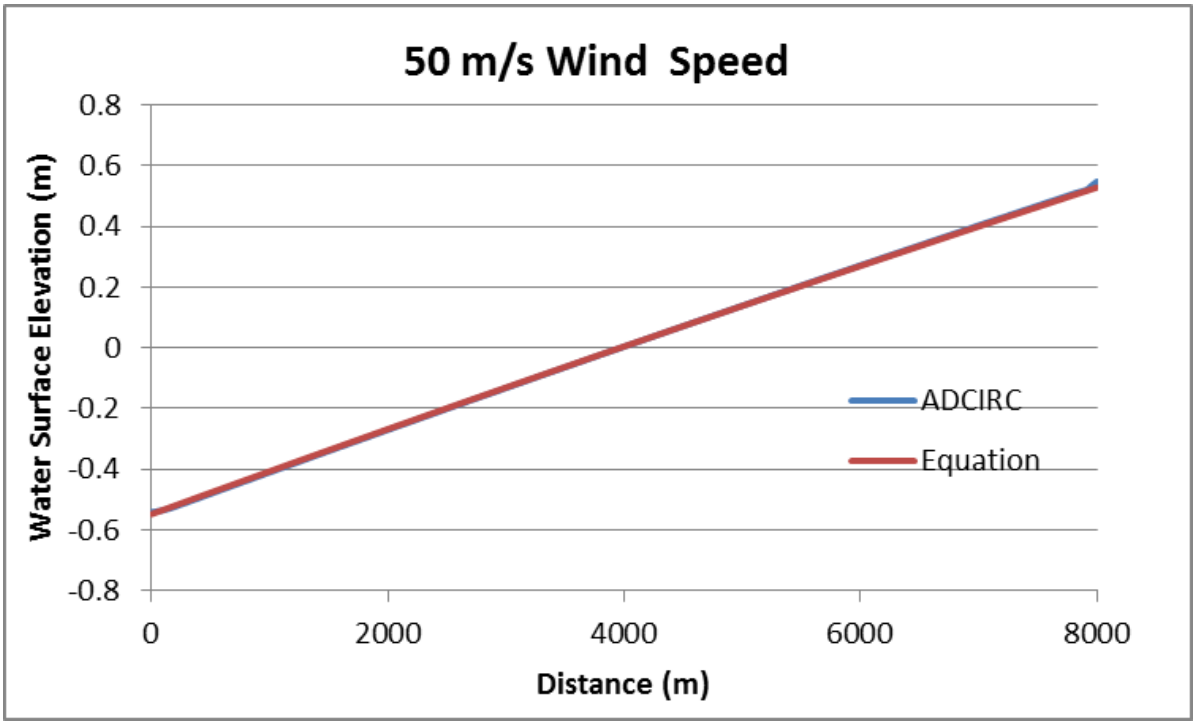


Figure 4-32. Water surface comparison plot for a 10-m deep rectangular basin with a 50 m/s wind speed and r = 0.36

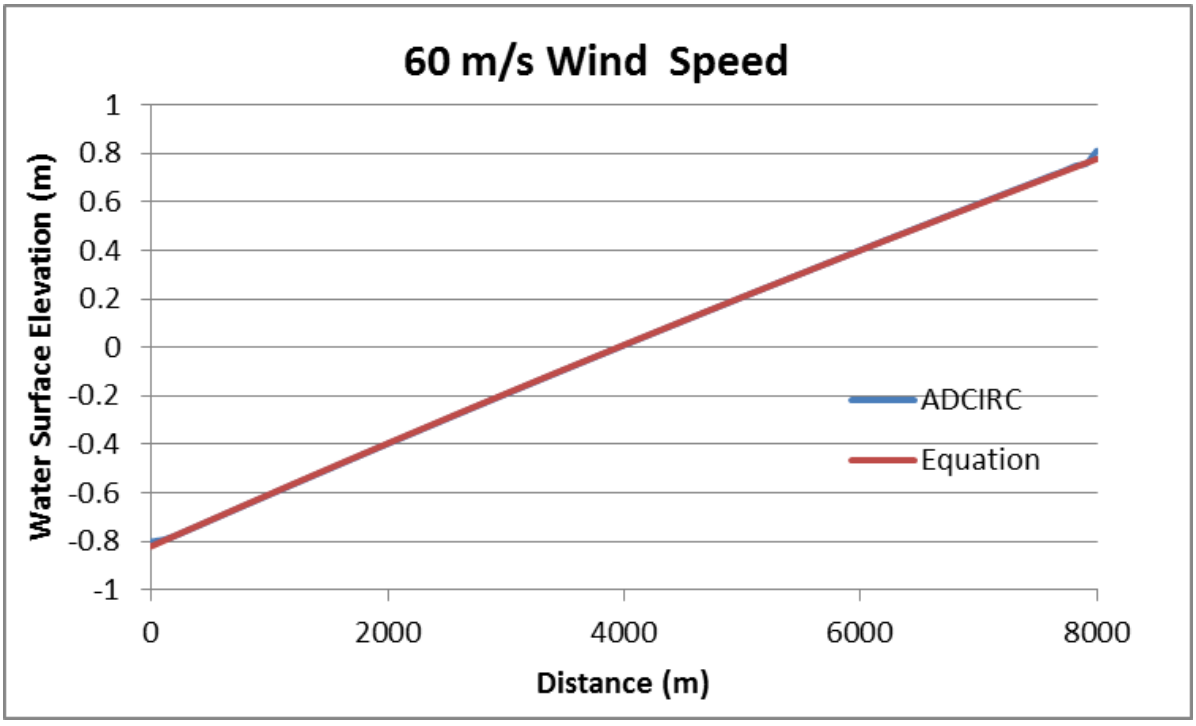


Figure 4-33. Water surface comparison plot for a 10-m deep rectangular basin with a 60 m/s wind speed and r = 0.40

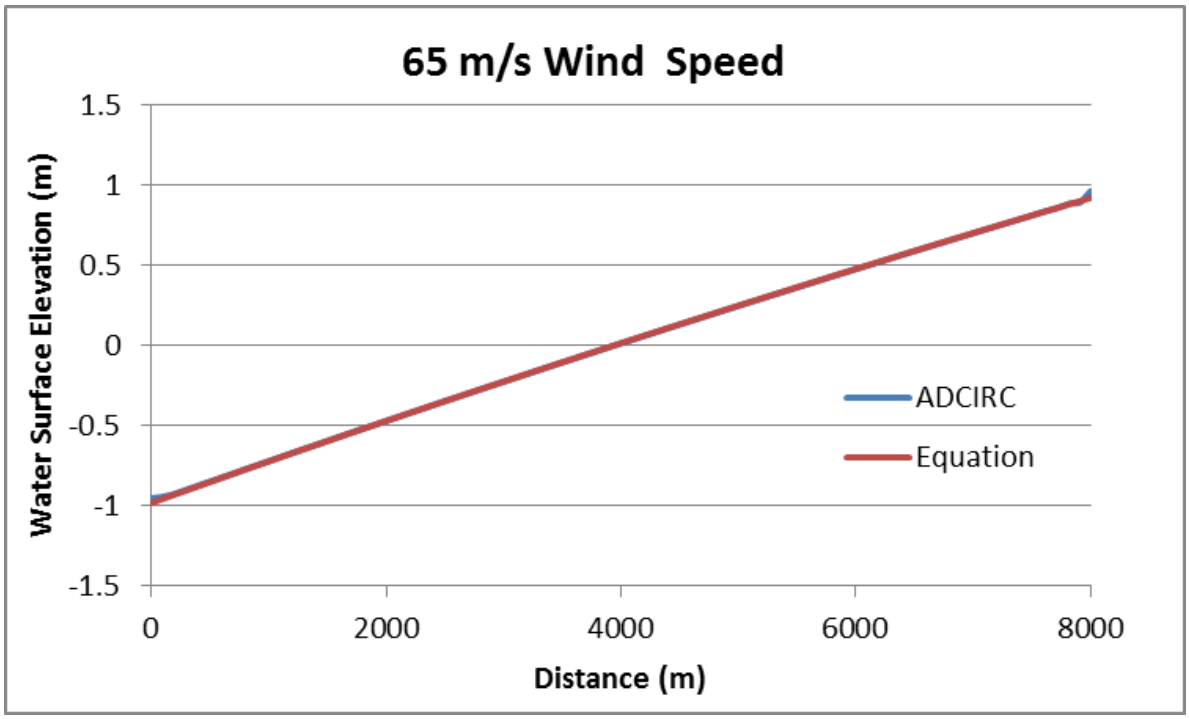


Figure 4-34. Water surface comparison plot for a 10-m deep rectangular basin with a 65 m/s wind speed and r = 0.42

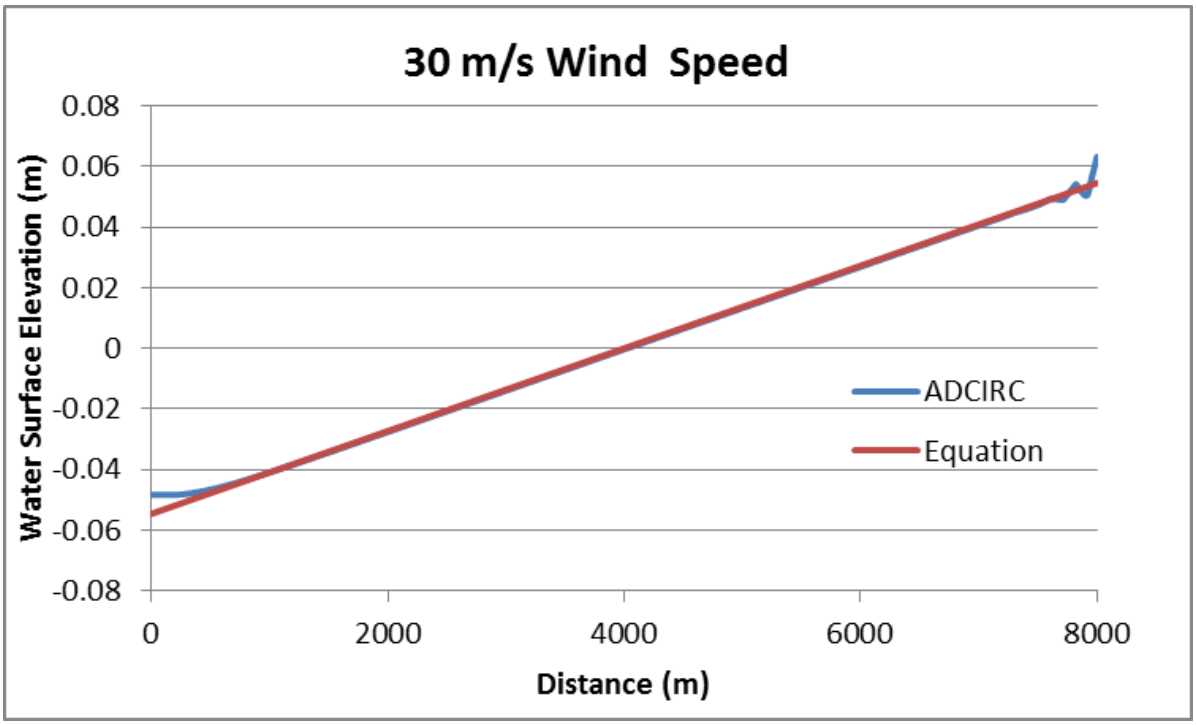


Figure 4-35. Water surface comparison plot for a 30-m deep rectangular basin with a 30 m/s wind speed and r = 0.25

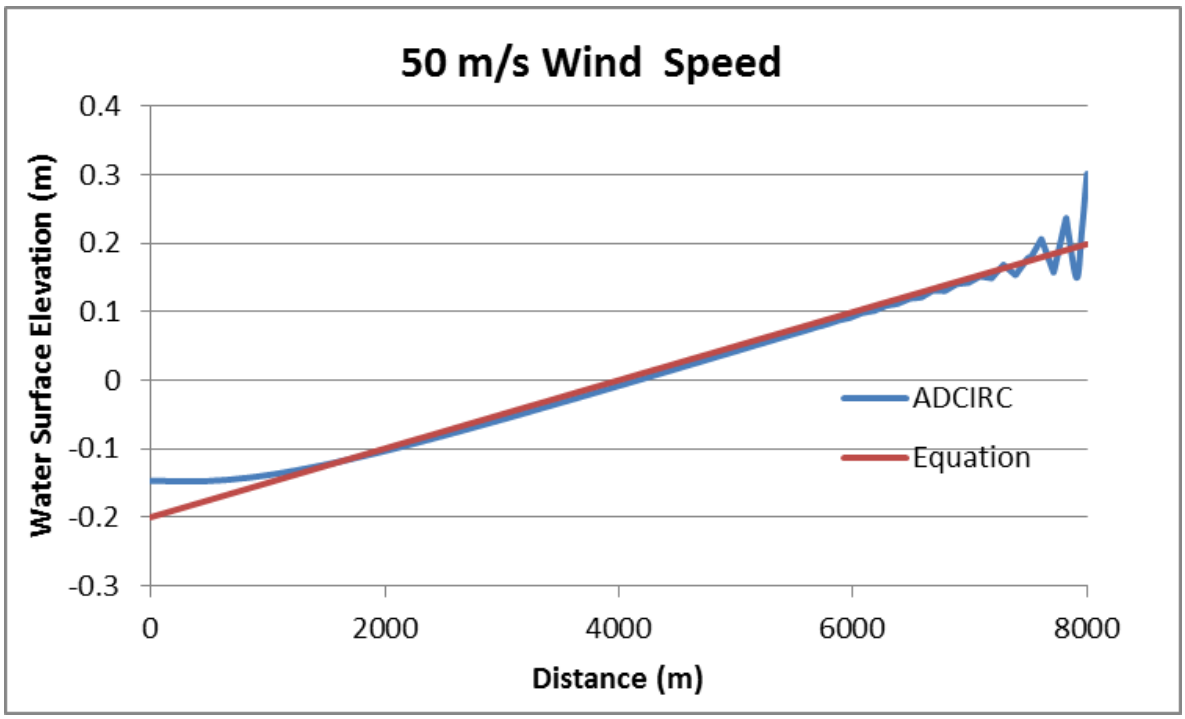


Figure 4-36. Water surface comparison plot for a 30-m deep rectangular basin with a 50 m/s wind speed and r = 0.51

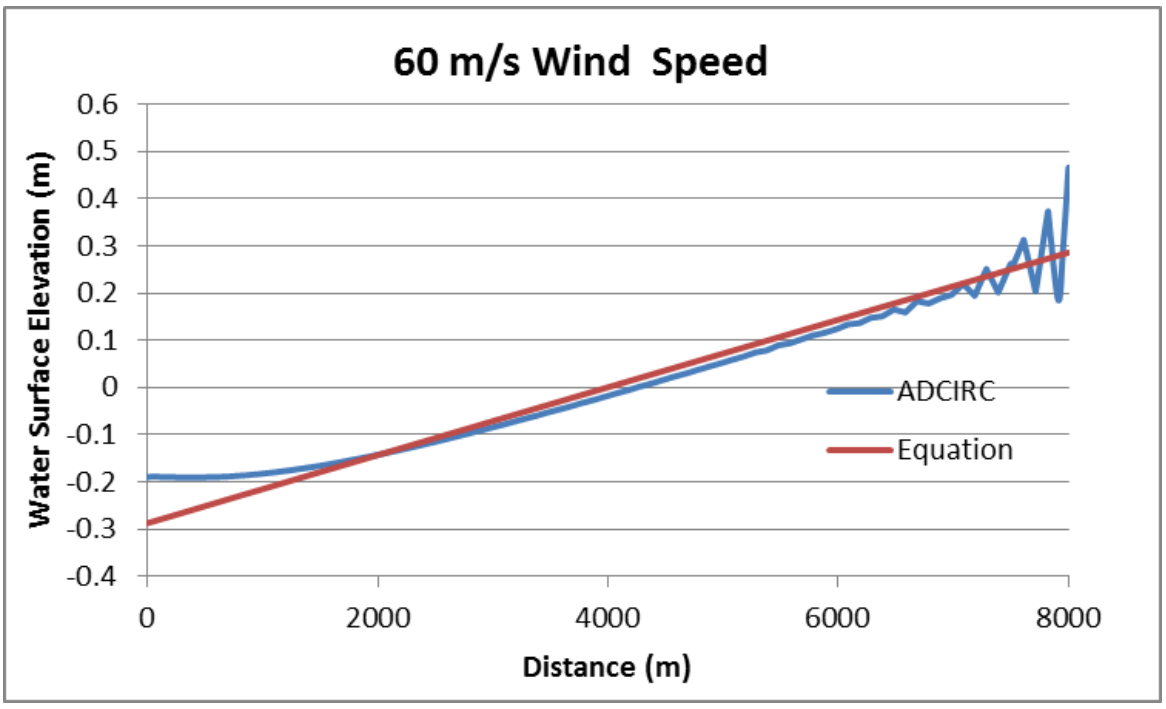


Figure 4-37. Water surface comparison plot for a 30-m deep rectangular basin with a 60 m/s wind speed and r = 0.51

Table 4-2. Summary of r-values for different water depths and wind shear stresses

| Values of r | | | | | |
|---|---|---|---|---|---|
| Wind Shear Stress ($N/m^2$) | Basin Depth 3.5 m | Basin Depth 5 m | Basin Depth 7.5 m | Basin Depth 10 m | Basin Depth 30 m |
| 3.2889 | 0.045 | 0.050 | 0.063 | 0.090 | 0.250 |
| 6.35535 | 0.250 | 0.250 | 0.275 | 0.300 | - |
| 9.93024 | 0.360 | 0.328 | 0.355 | 0.360 | 0.510 |
| 14.2995 | - | 0.350 | 0.390 | 0.400 | 0.510 |
| 16.7821 | - | 0.380 | 0.4025 | 0.420 | - |

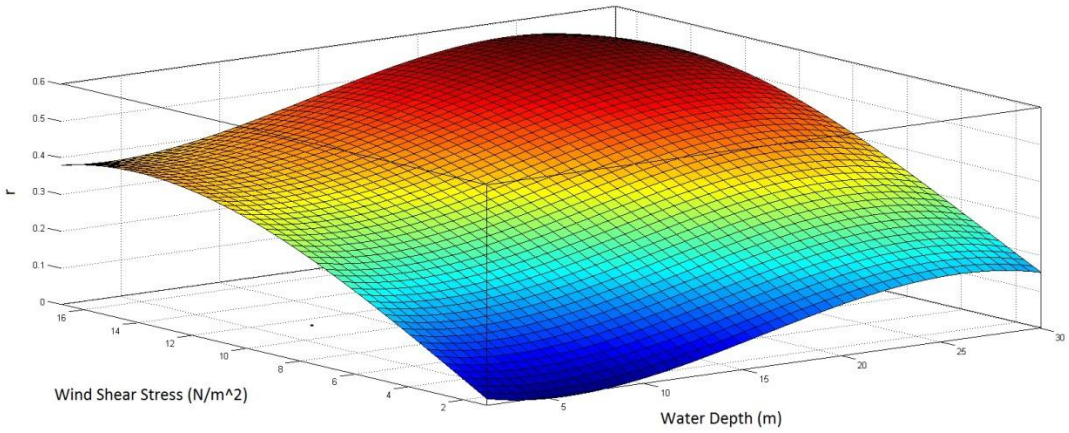


Figure 4-38. Best fit surface for r as a function of wind shear stress and basin depth

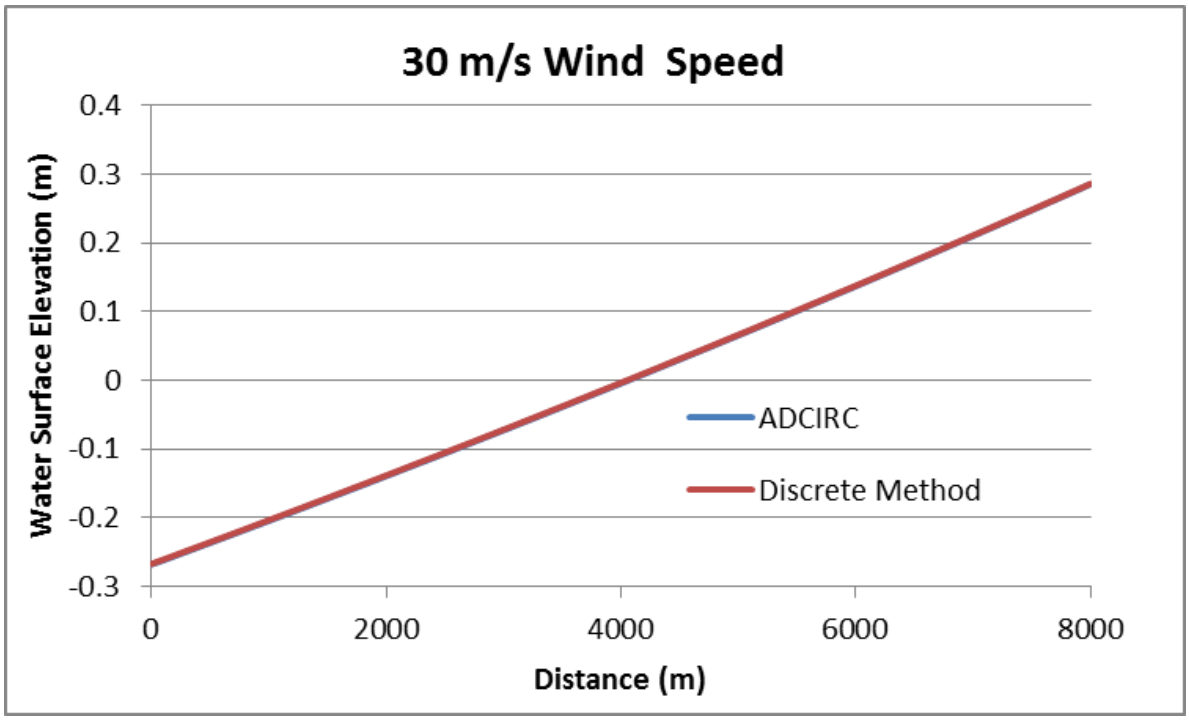


Figure 4-39. Water surface comparison plot for a rectangular basin with a 5-m mean depth and a 30-m/s wind speed

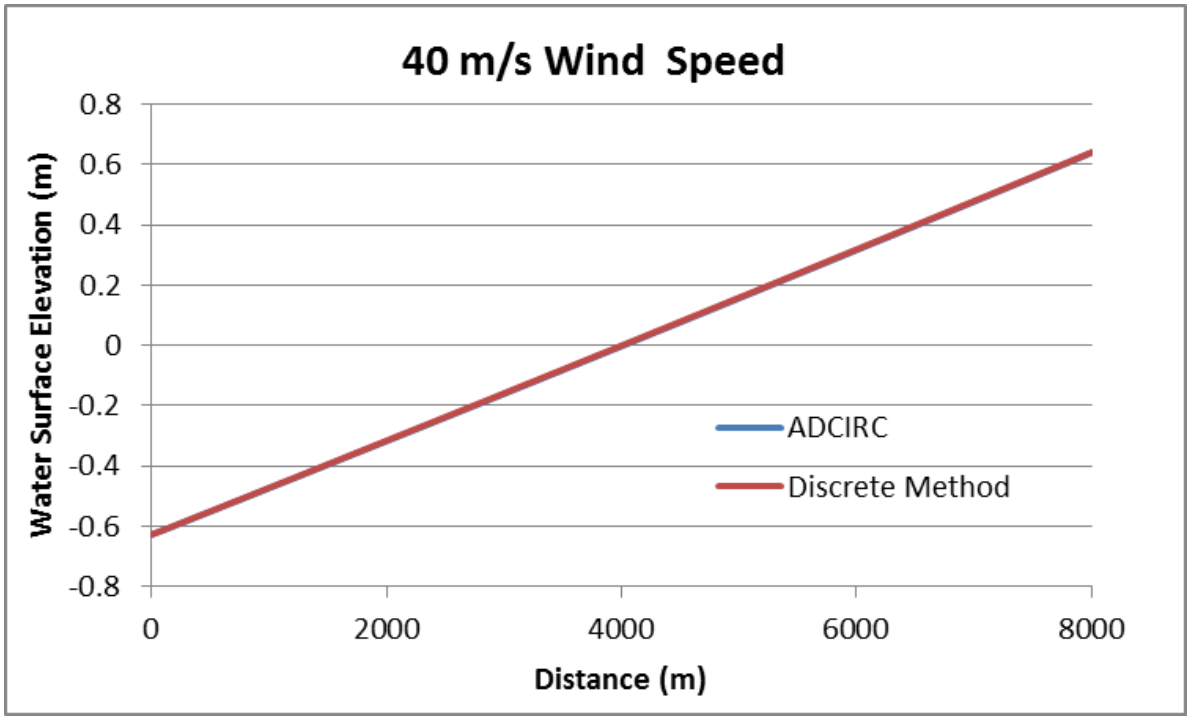


Figure 4-40. Water surface comparison plot for a rectangular basin with a 5-m mean depth and a 40-m/s wind speed

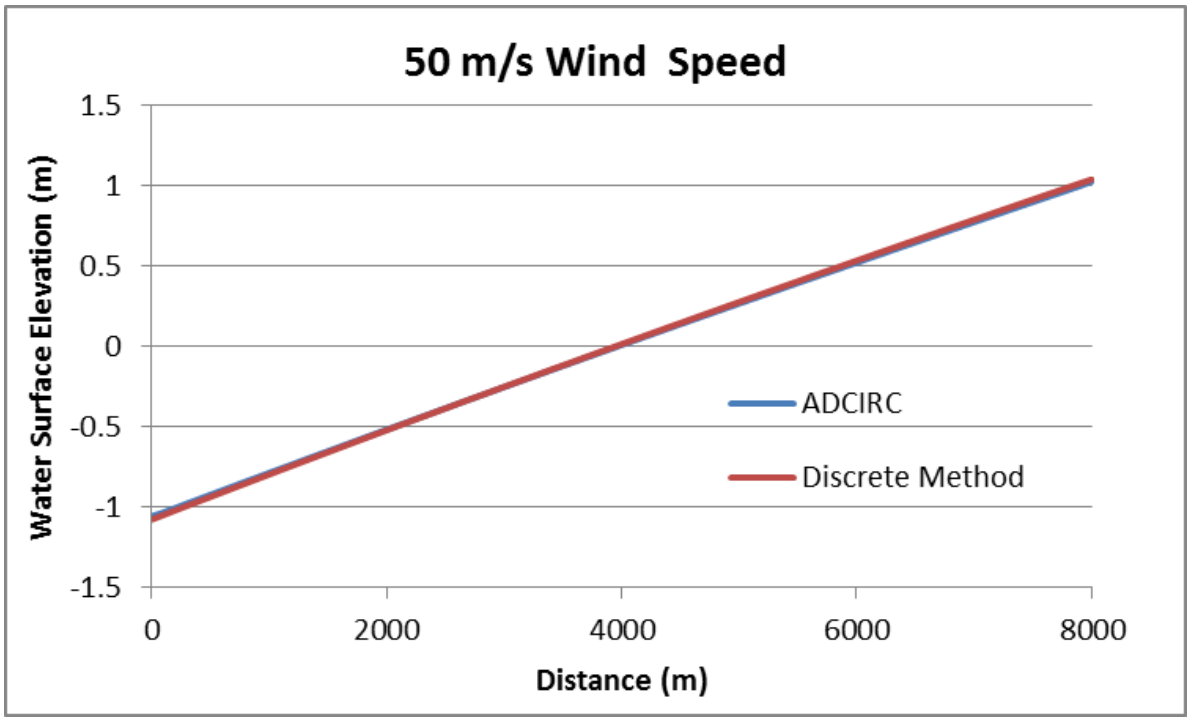


Figure 4-41. Water surface comparison plot for a rectangular basin with a 5-m mean depth and a 50-m/s wind speed

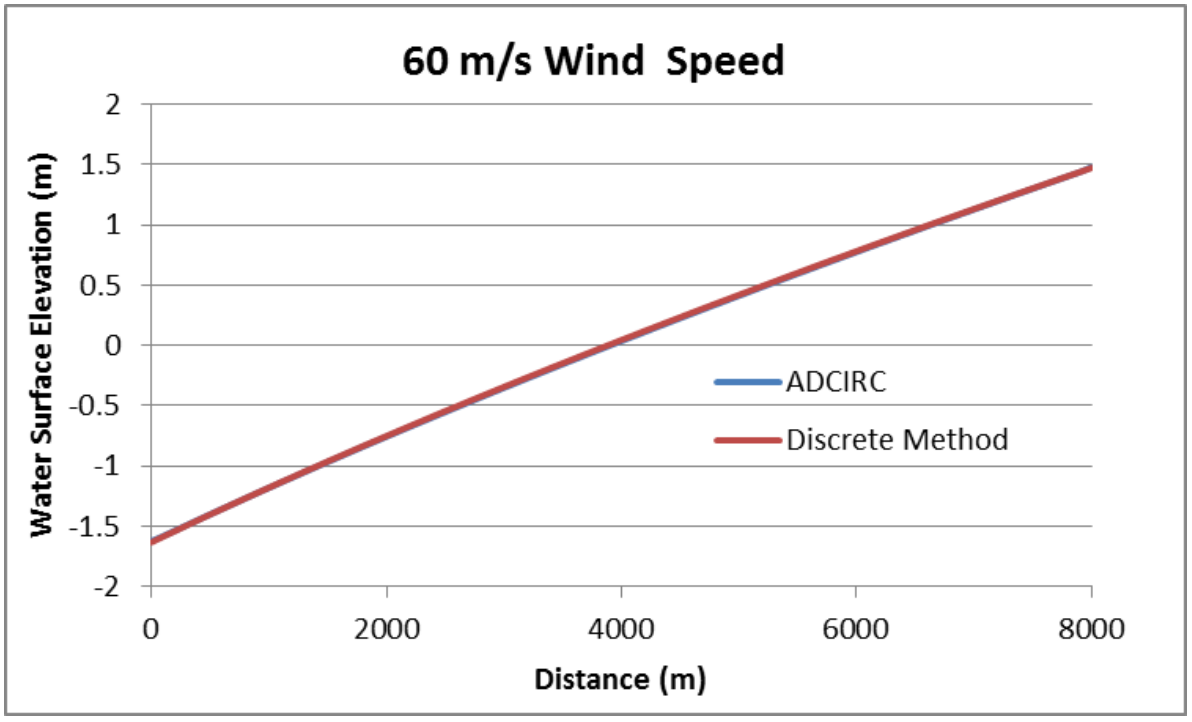


Figure 4-42. Water surface comparison plot for a rectangular basin with a 5-m mean depth and a 60-m/s wind speed

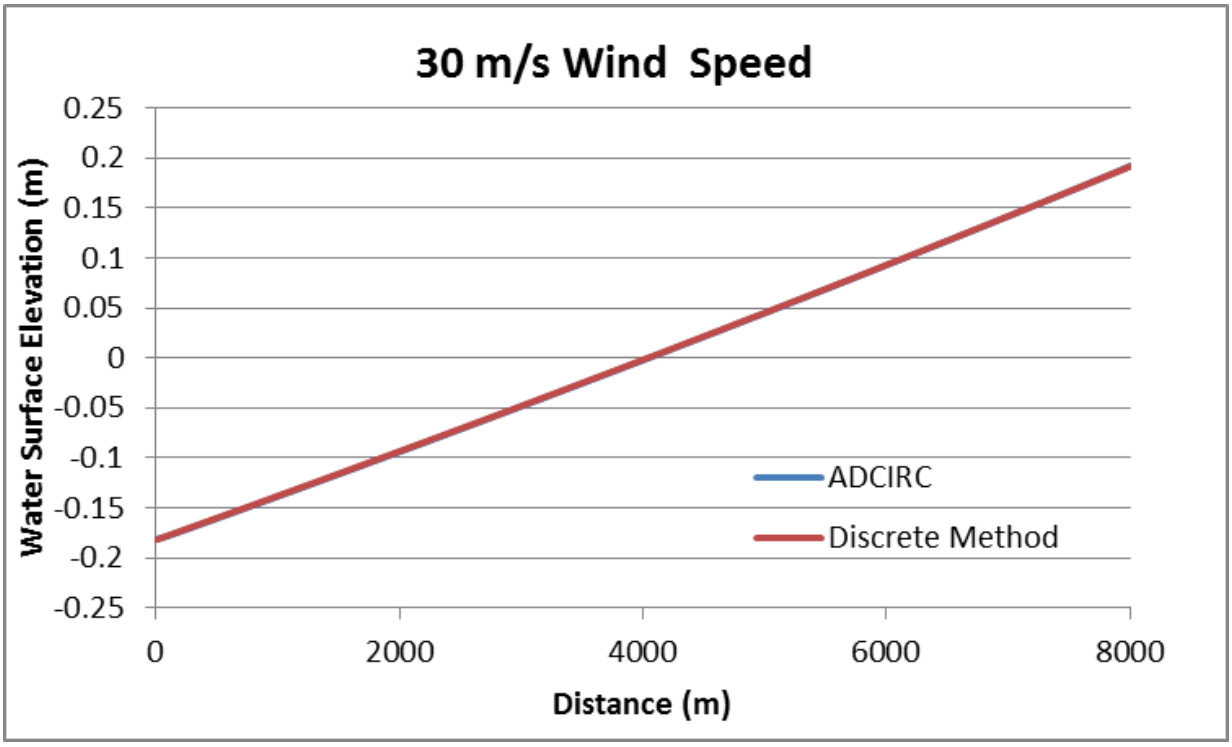


Figure 4-43. Water surface comparison plot for a rectangular basin with a 7.5-m mean depth and a 30-m/s wind speed

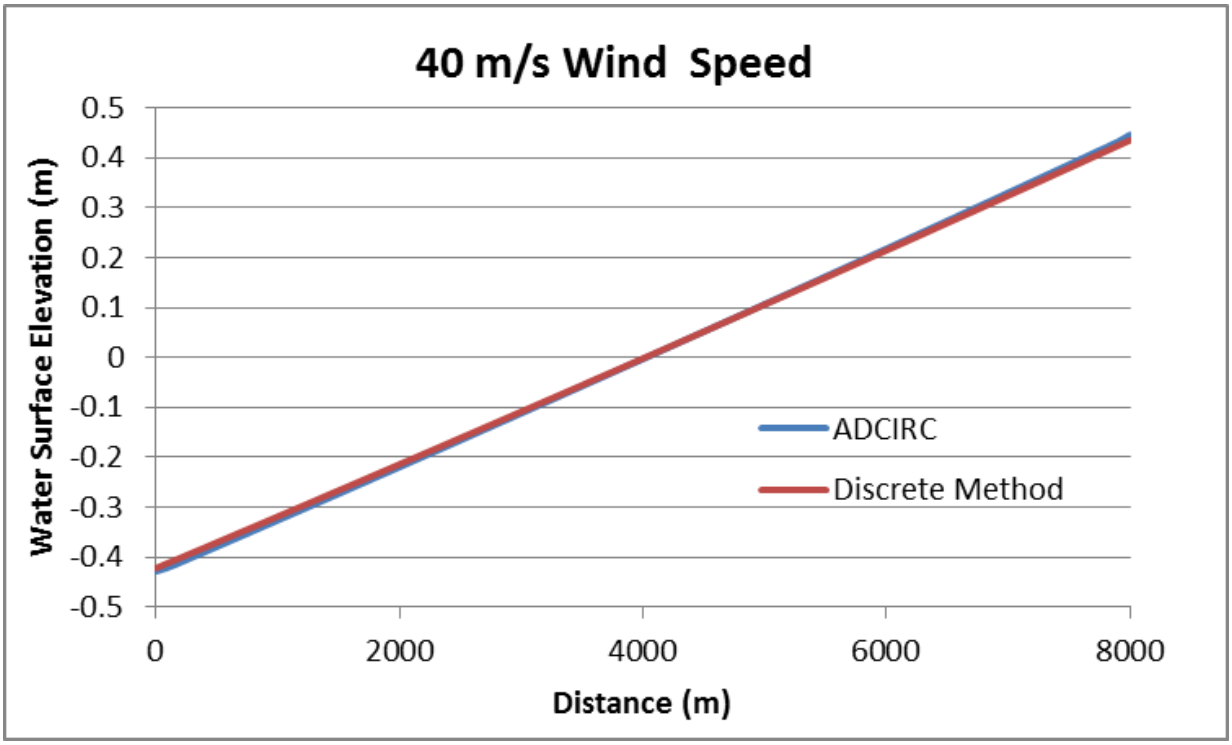


Figure 4-44. Water surface comparison plot for a rectangular basin with a 7.5-m mean depth and a 40-m/s wind speed

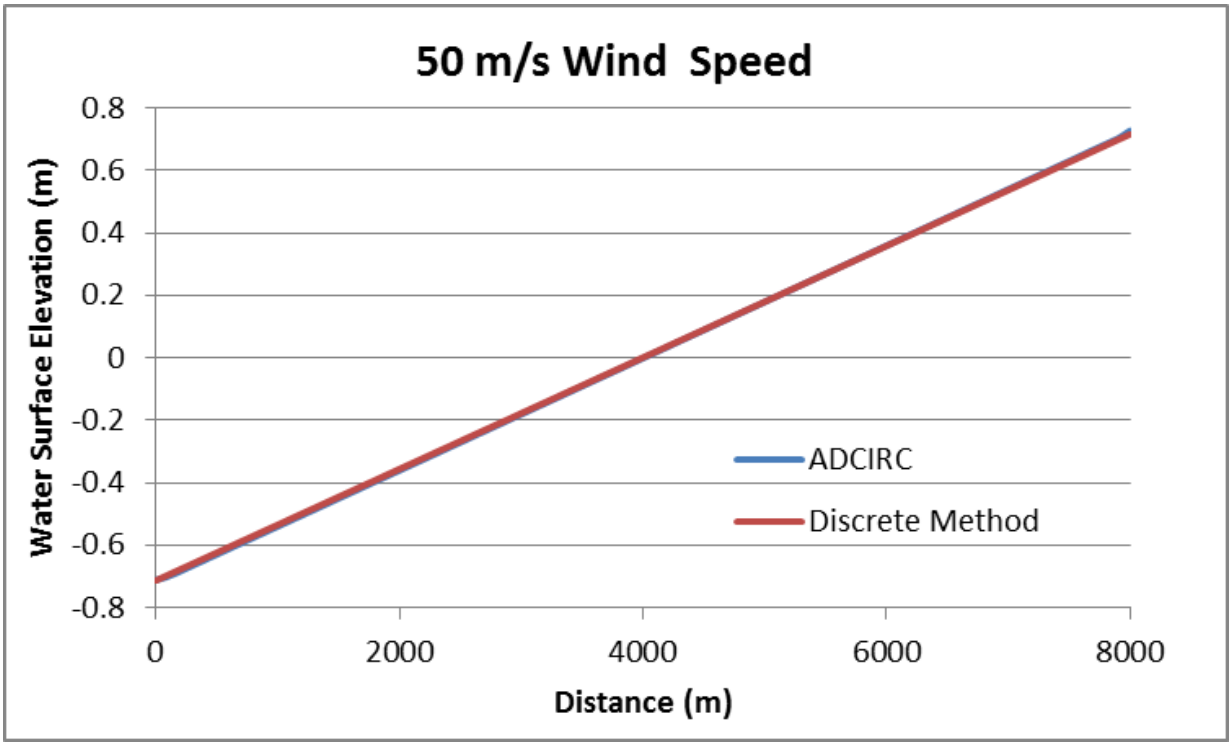


Figure 4-45. Water surface comparison plot for a rectangular basin with a 7.5-m mean depth and a 50-m/s wind speed

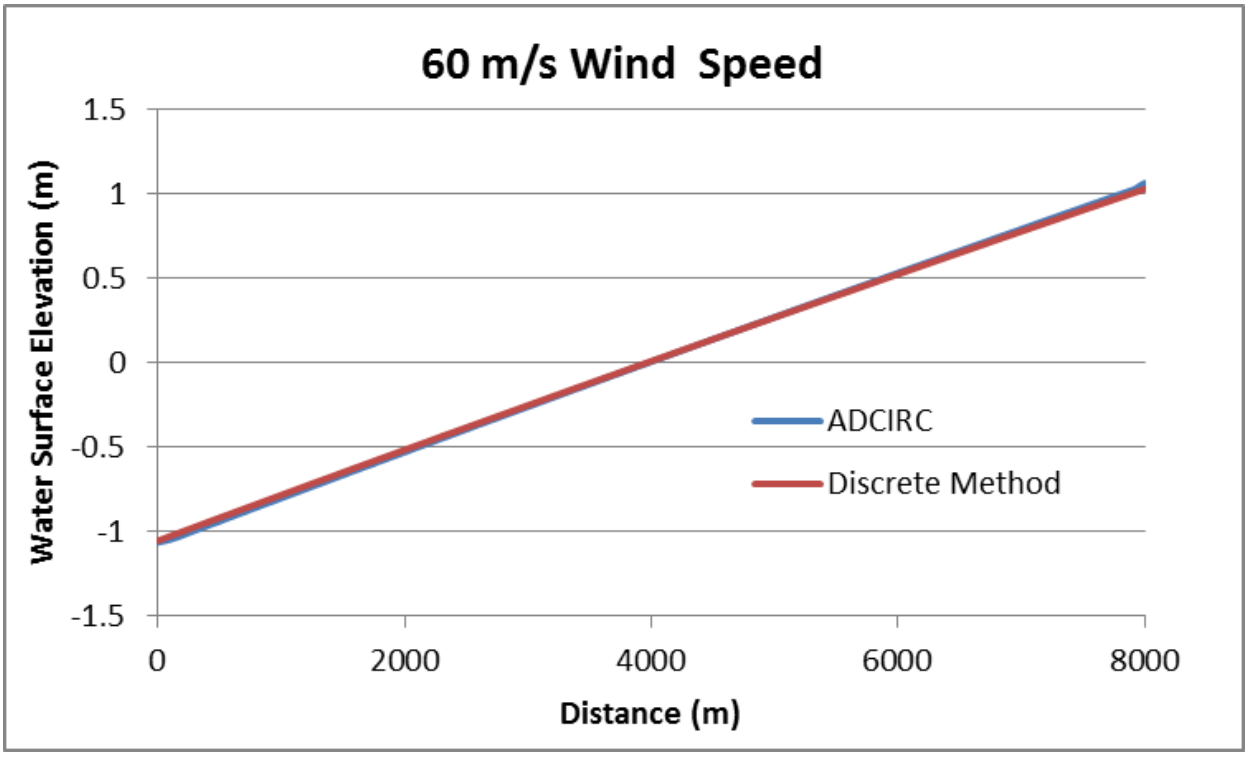


Figure 4-46. Water surface comparison plot for a rectangular basin with a 7.5-m mean depth and a 60-m/s wind speed

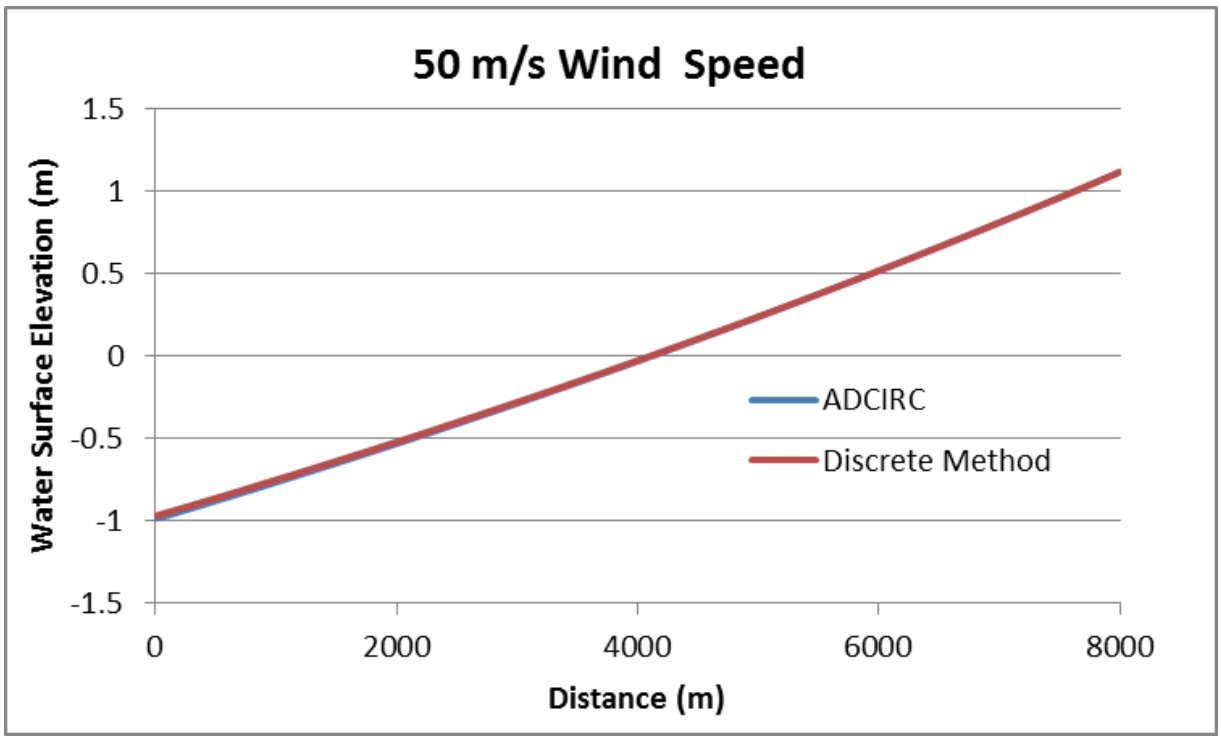


Figure 4-47. Water surface comparison for a basin with a bottom slope of 0.0005, mean depth of 5 m, and a 50-m/s wind speed

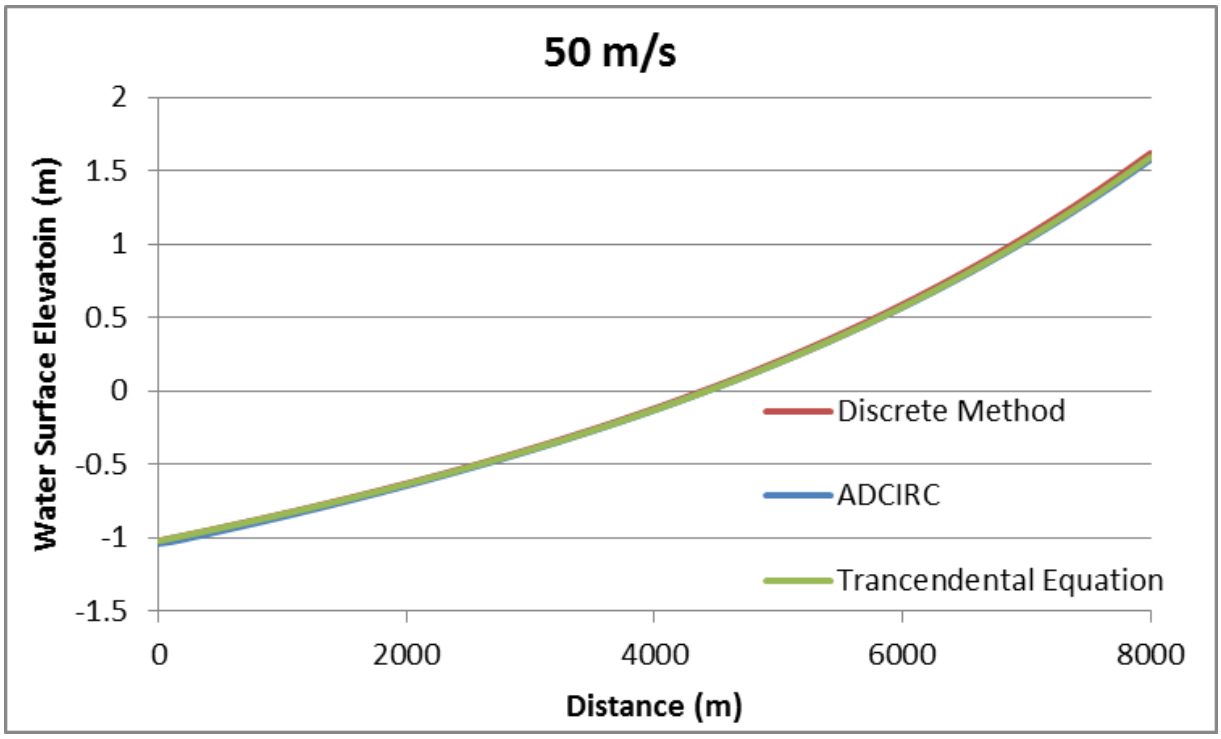


Figure 4-48. Water surface comparison for a basin with a bottom slope of 0.001, mean depth of 4.5 m, and a 50-m/s wind speed

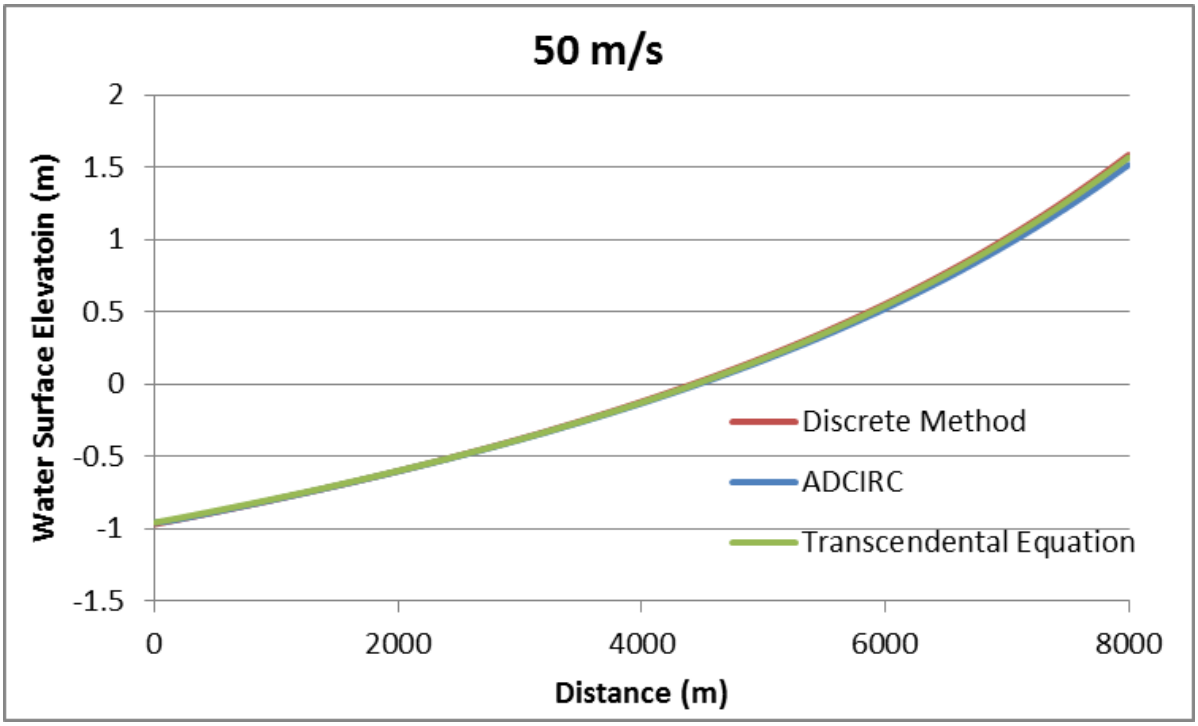


Figure 4-49. Water surface comparison for a basin with a bottom slope of 0.0011, mean depth of 4.9 m, and a 50-m/s wind speed

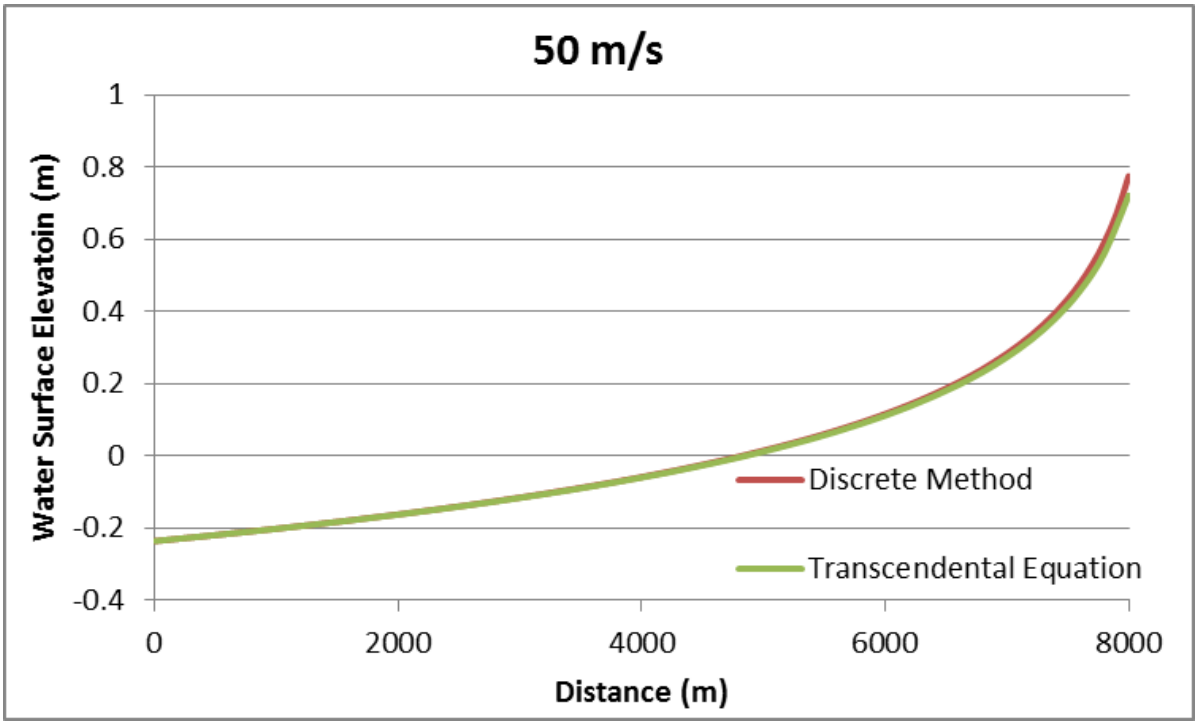


Figure 4-50. Water surface comparison for a basin with a bottom slope of 0.005, mean depth of 20.5 m, and a 50-m/s wind speed

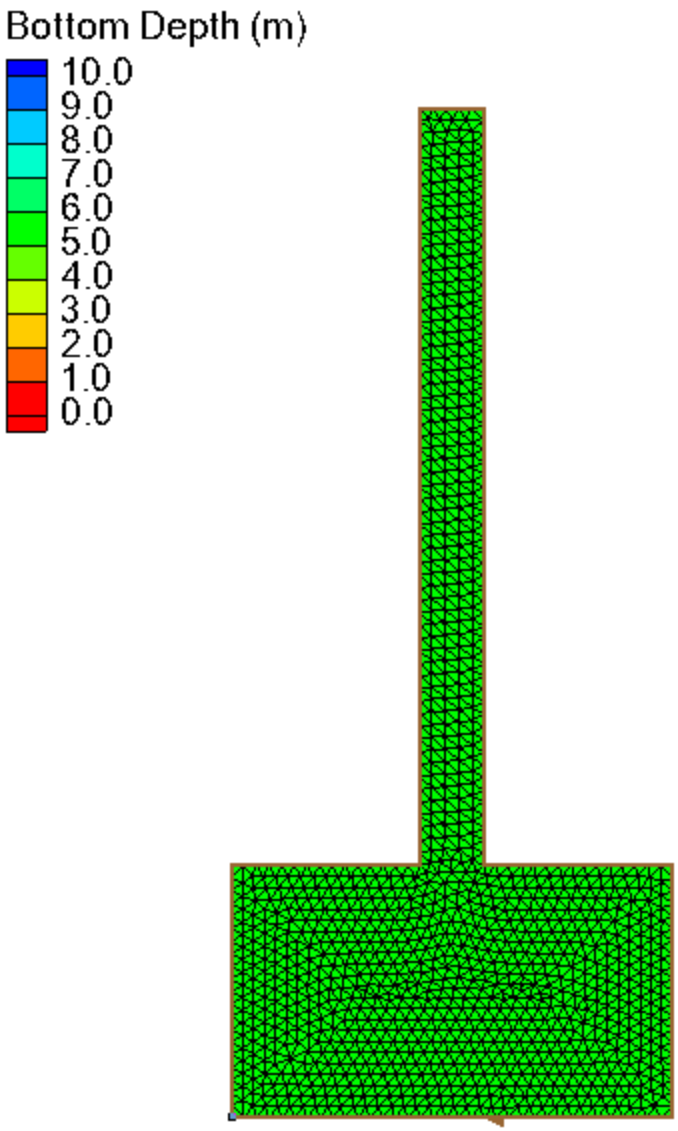


Figure 4-51. T-shaped basin complex ADCIRC model mesh geometry with a flat bottom

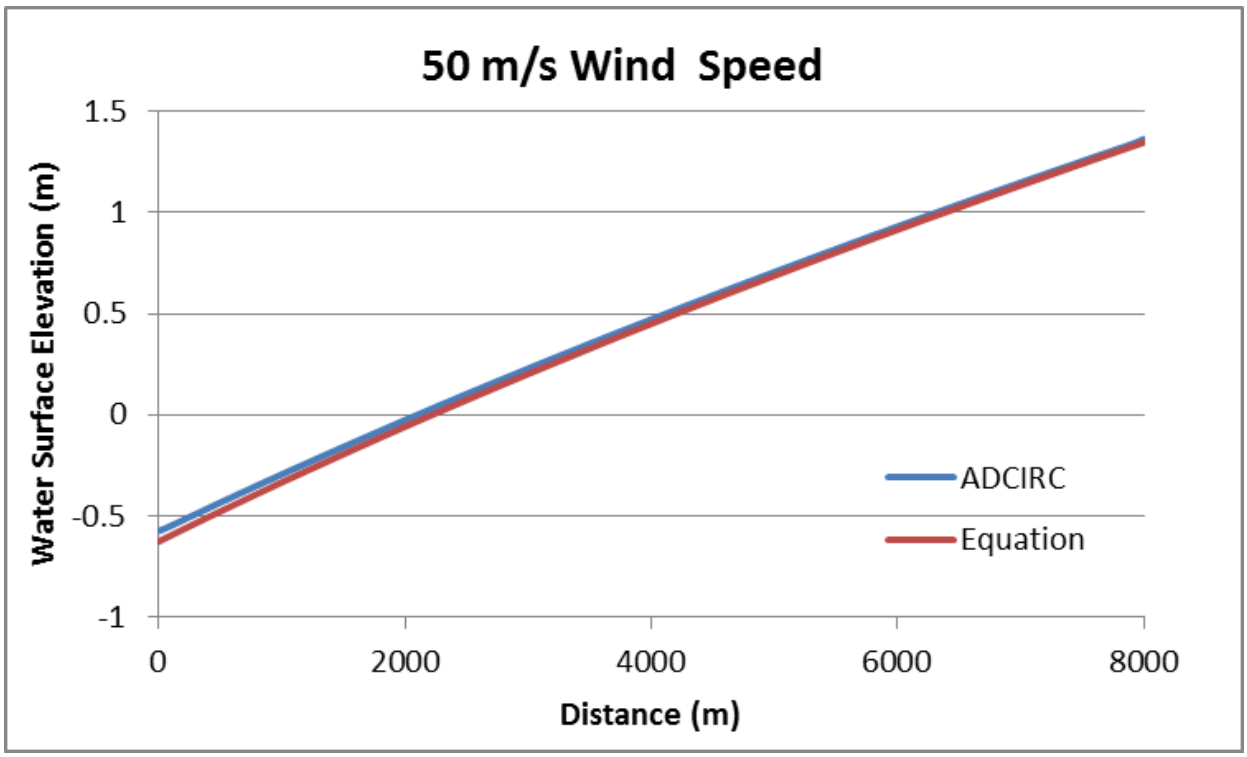


Figure 4-52. Water surface comparison plot for a T-basin with a 5-m depth and a 50 m/s wind speed

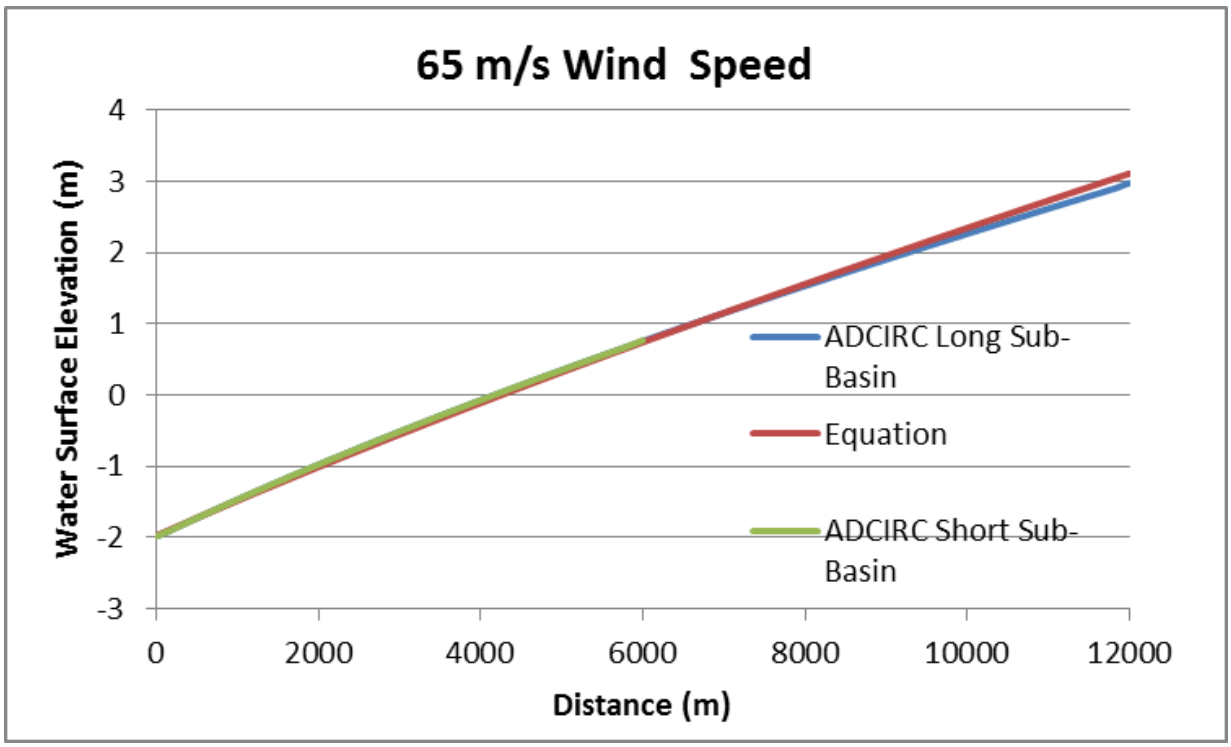


Figure 4-53. Water surface comparison plot for a 2-leg with a 5-m mean depth and a 65 m/s wind speed

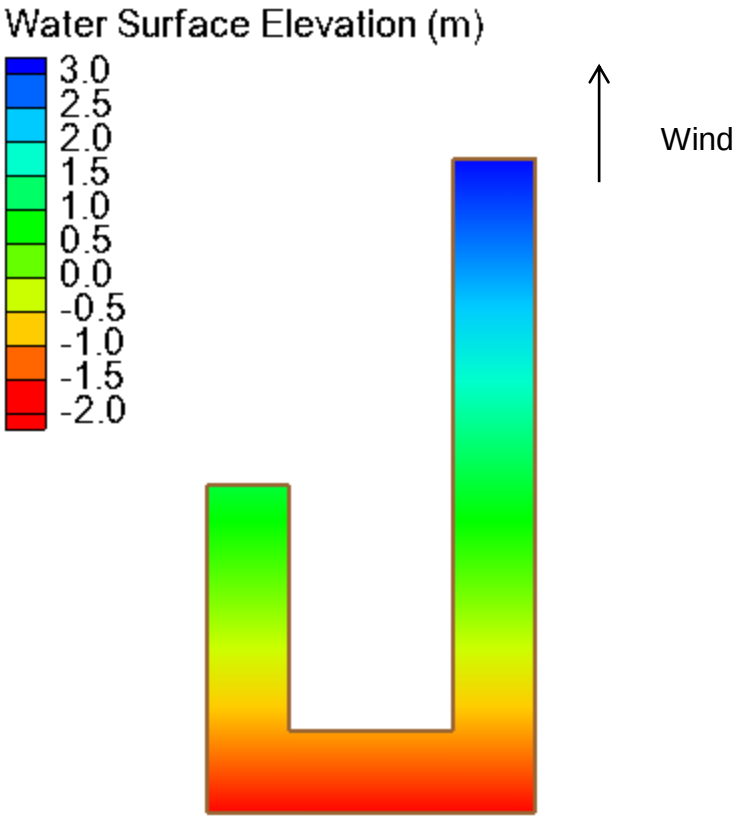


Figure 4-54. Water surface elevation contours for 65-m/s wind speed over a 2-leg basin

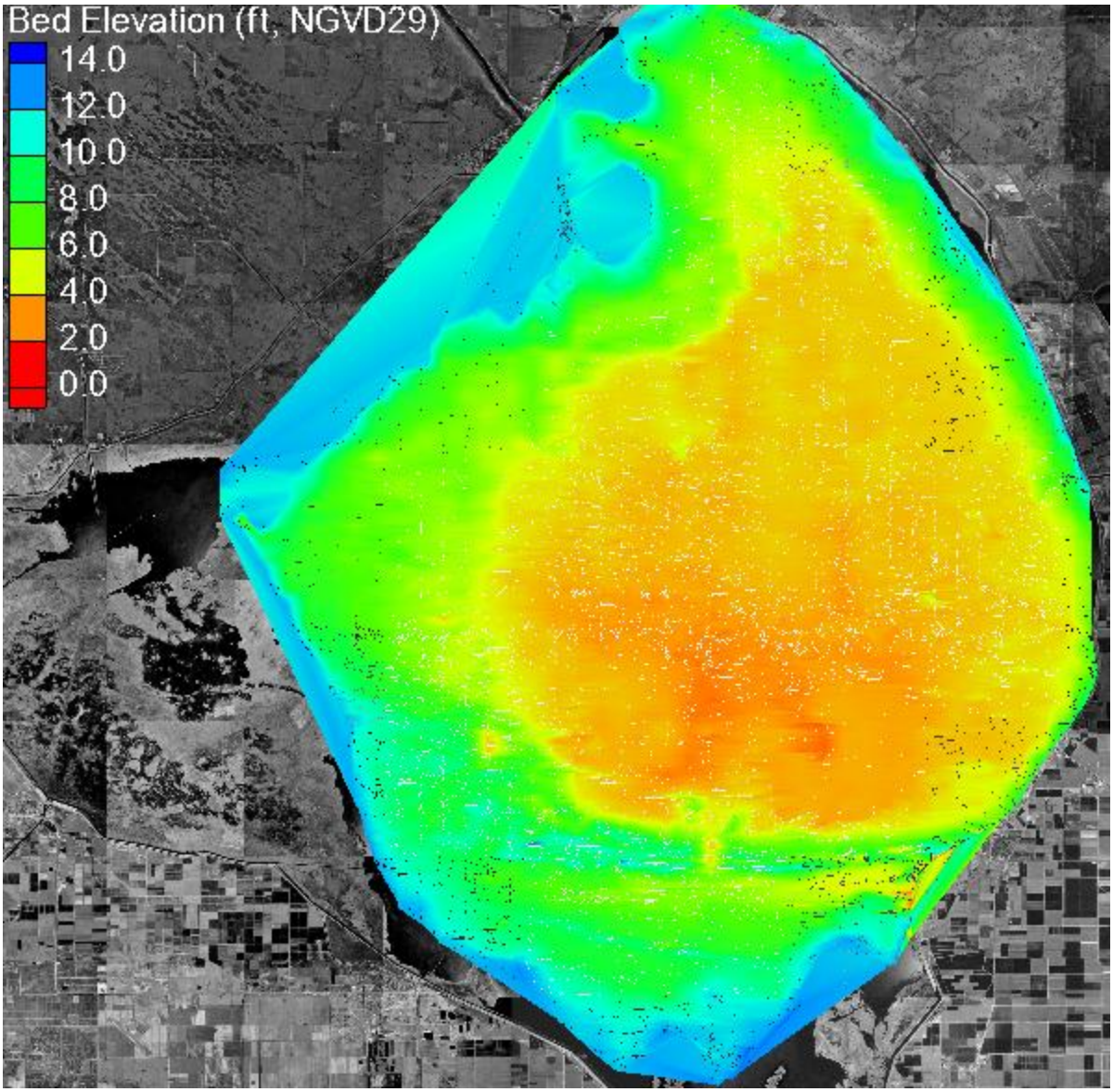


Figure 4-55. Bottom elevation contour plot for Lake Okeechobee

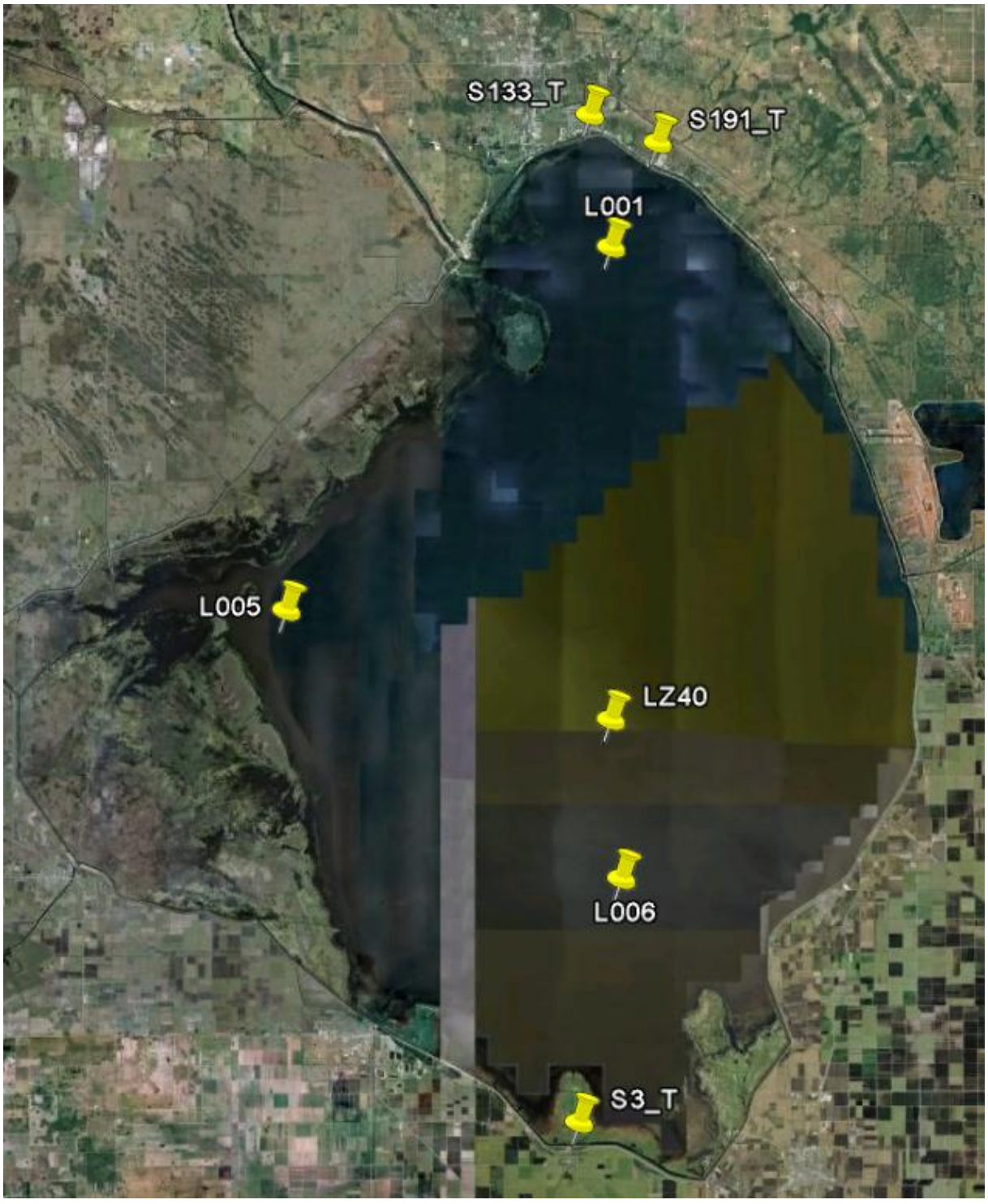


Figure 4-56. Location map for Lake Okeechobee water level gages

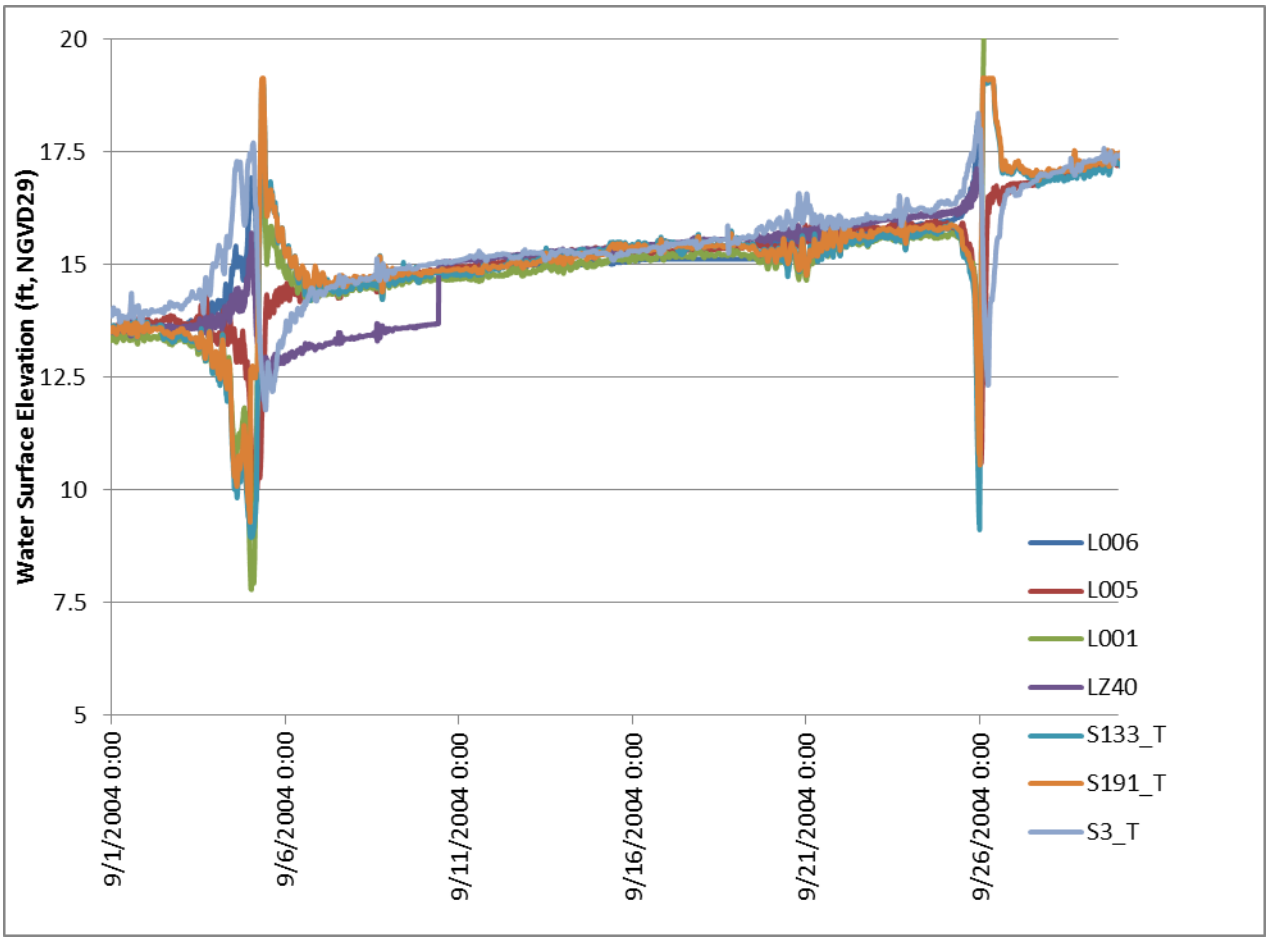


Figure 4-57. Time series plots of water level at seven gages on Lake Okeechobee during September 2004

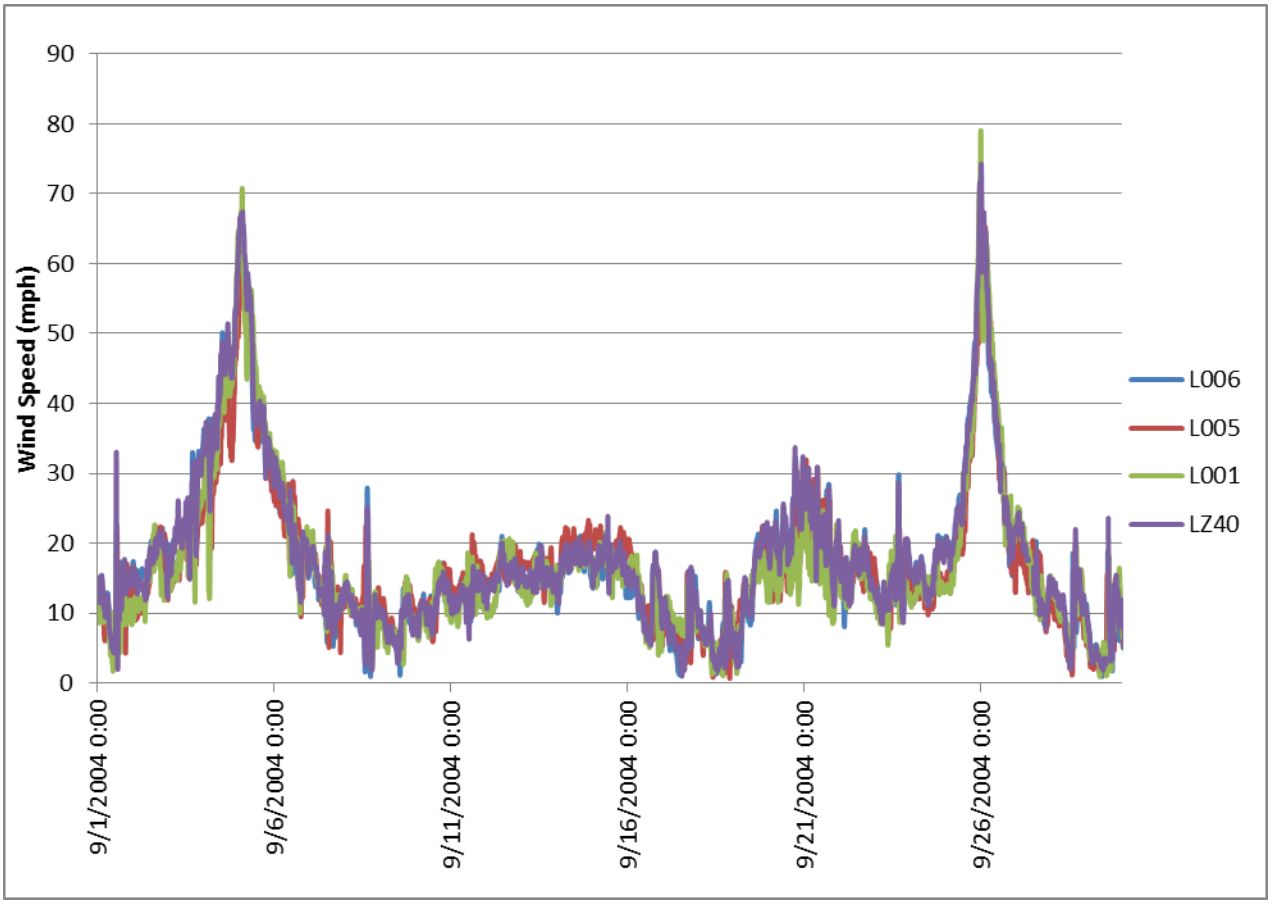


Figure 4-58. Wind speed measurements from four stations on Lake Okeechobee during September 2004

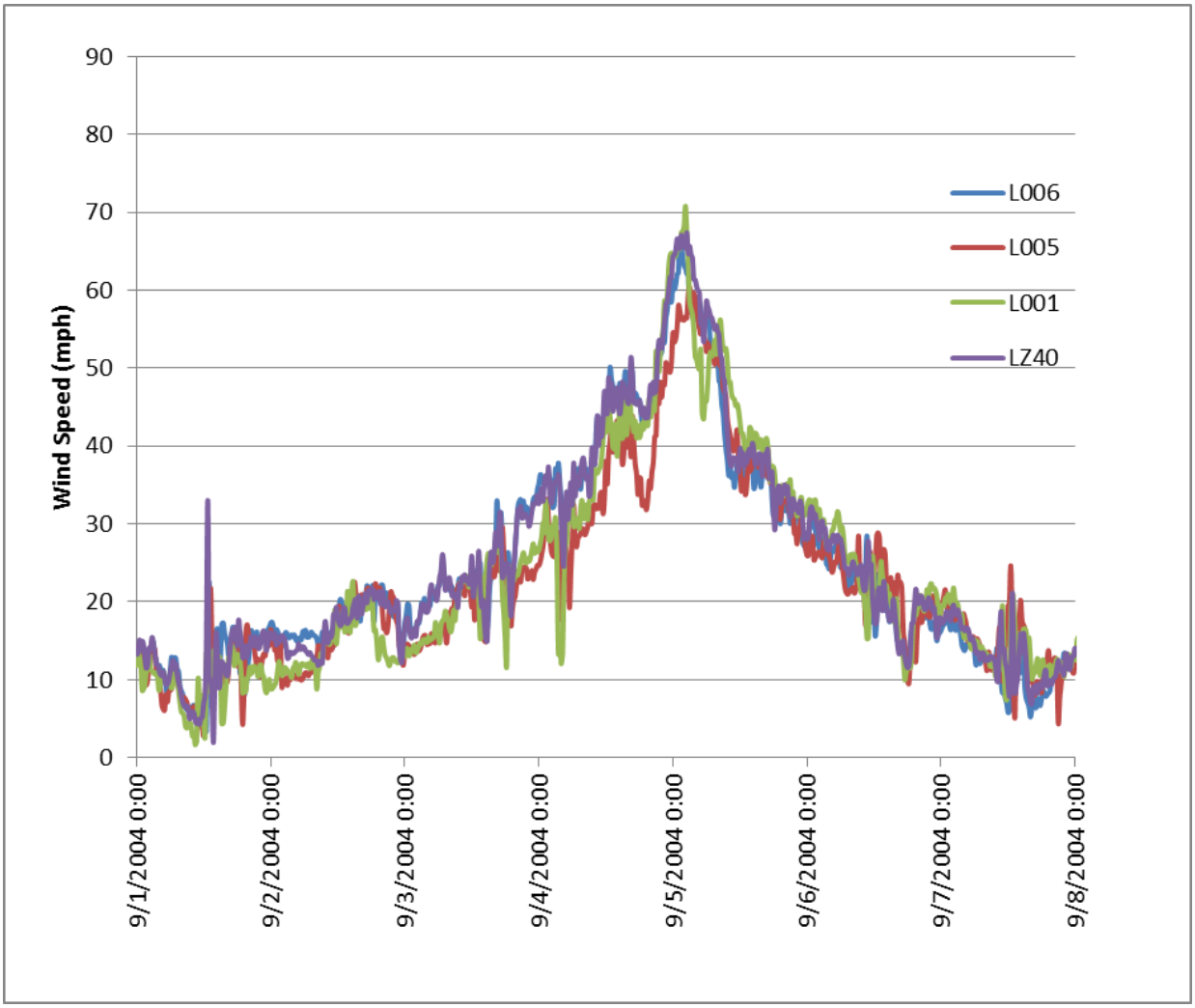


Figure 4-59. Wind speed measurements from four stations on Lake Okeechobee during Hurricane Frances

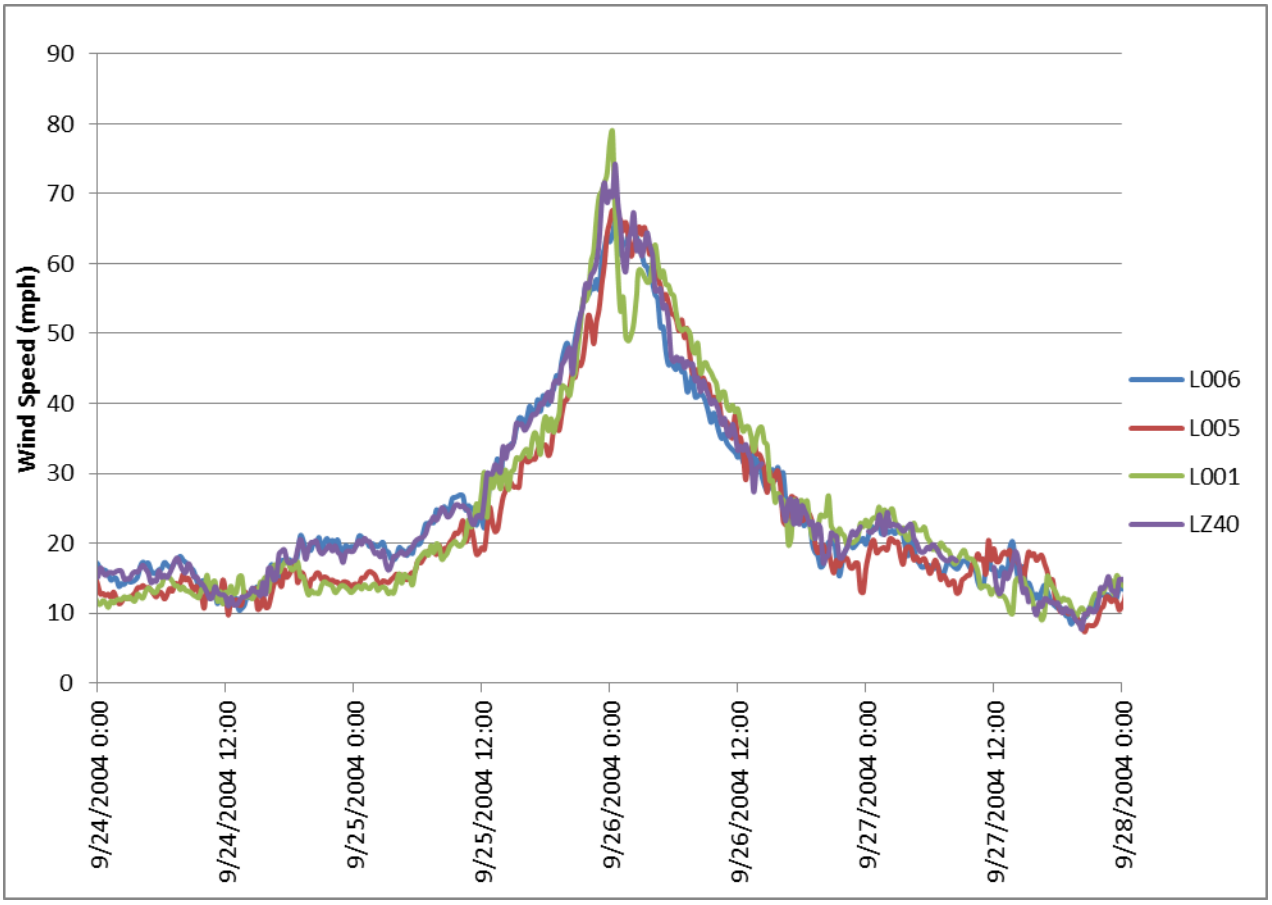


Figure 4-60. Wind speed measurements from four stations on Lake Okeechobee during Hurricane Jeanne

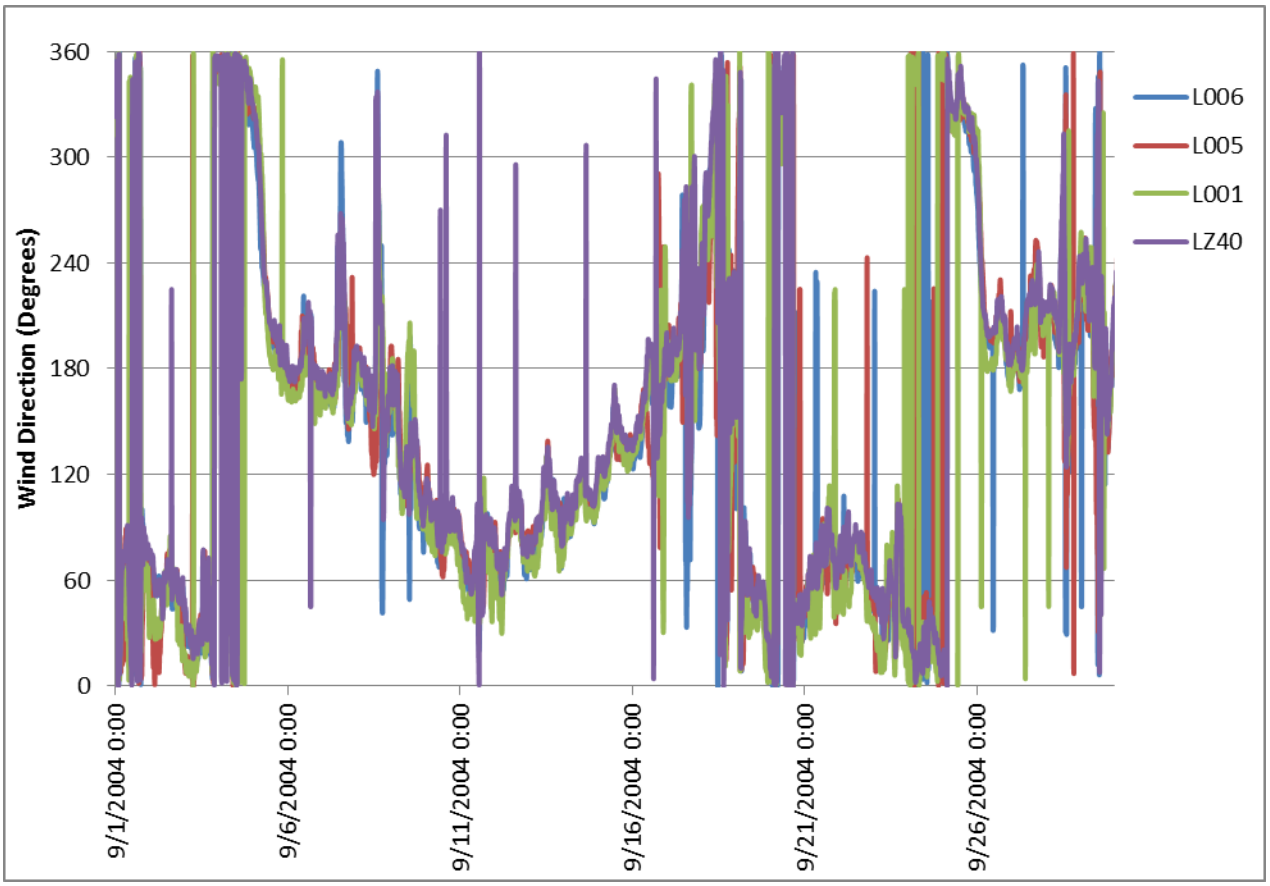


Figure 4-61. Wind direction (in degrees) measurements from four stations on Lake Okeechobee during September 2004

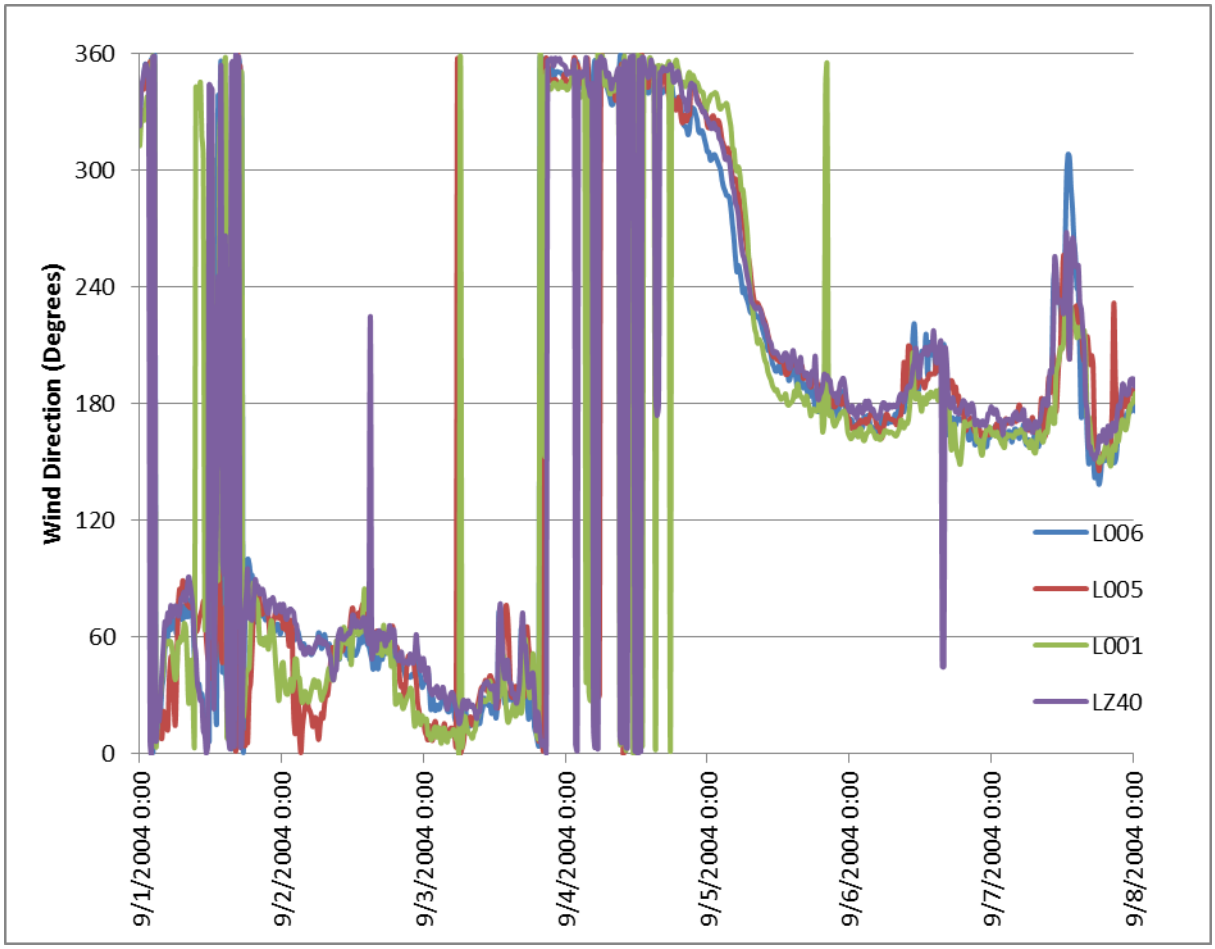


Figure 4-62. Wind direction (in degrees) measurements from four stations on Lake Okeechobee during Hurricane Frances

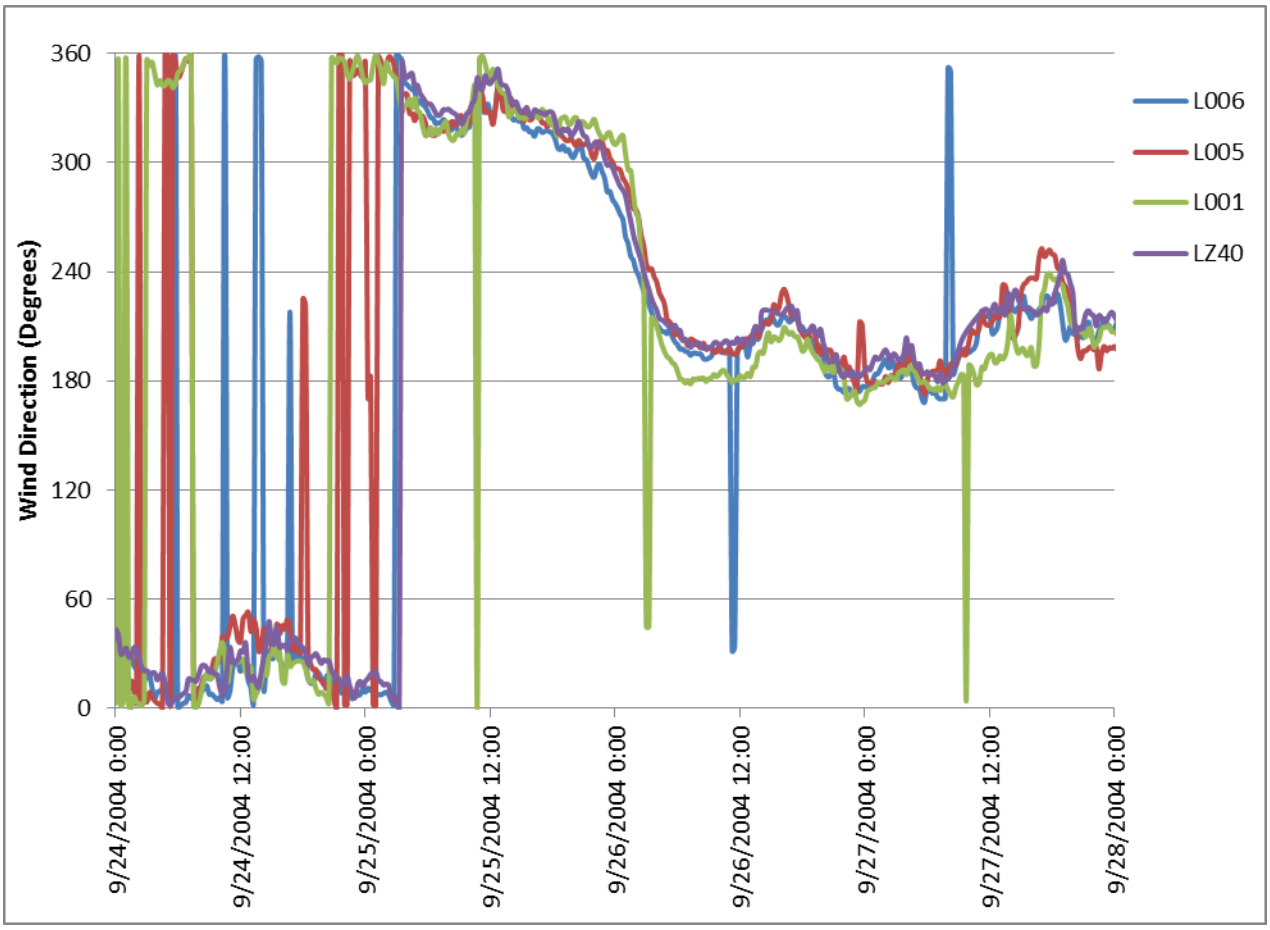


Figure 4-63. Wind direction (in degrees) measurements from four stations on Lake Okeechobee during Hurricane Jeanne

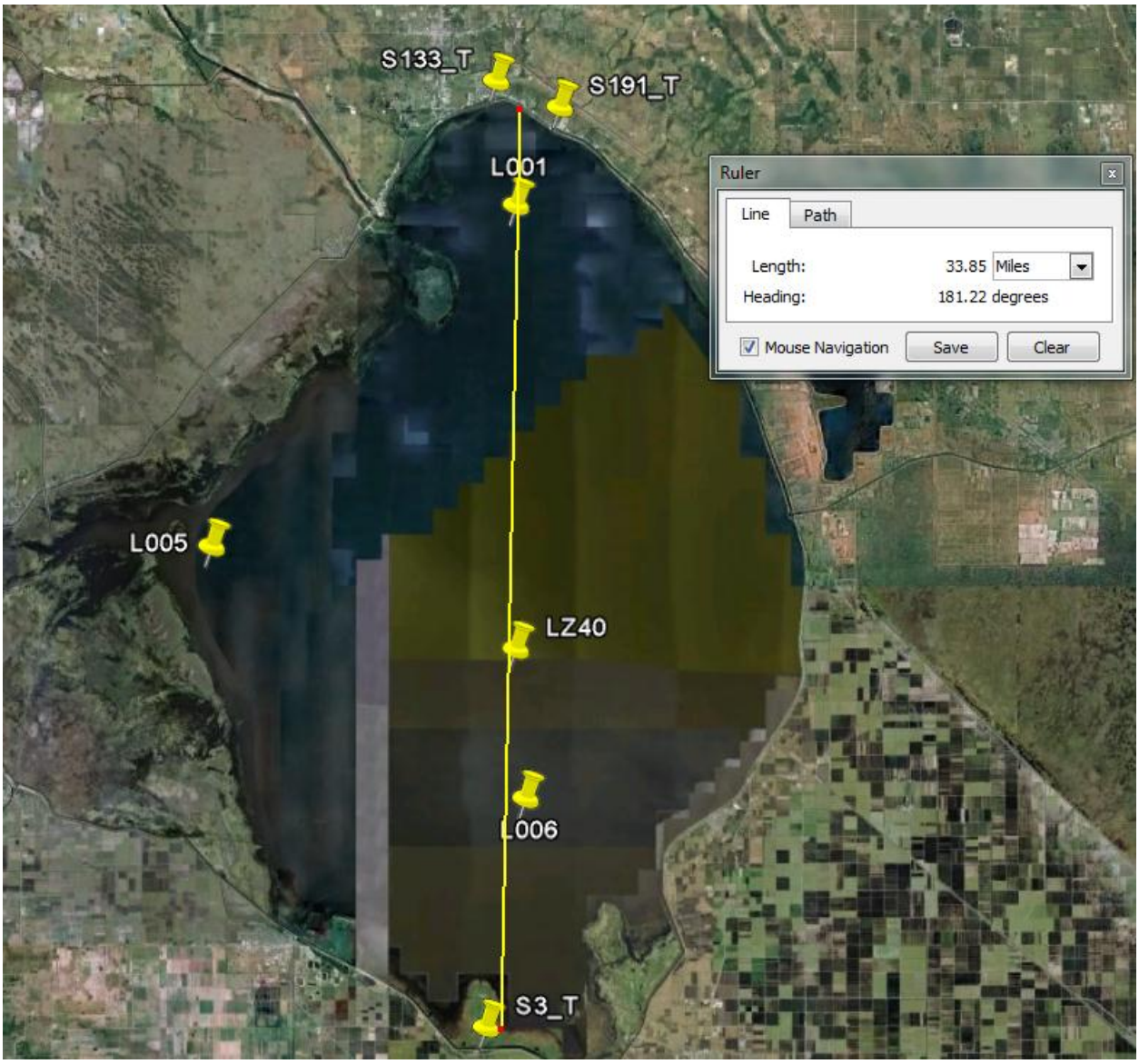


Figure 4-64. Local wind fetch for local wind set-up/set-down analyses for Lake Okeechobee

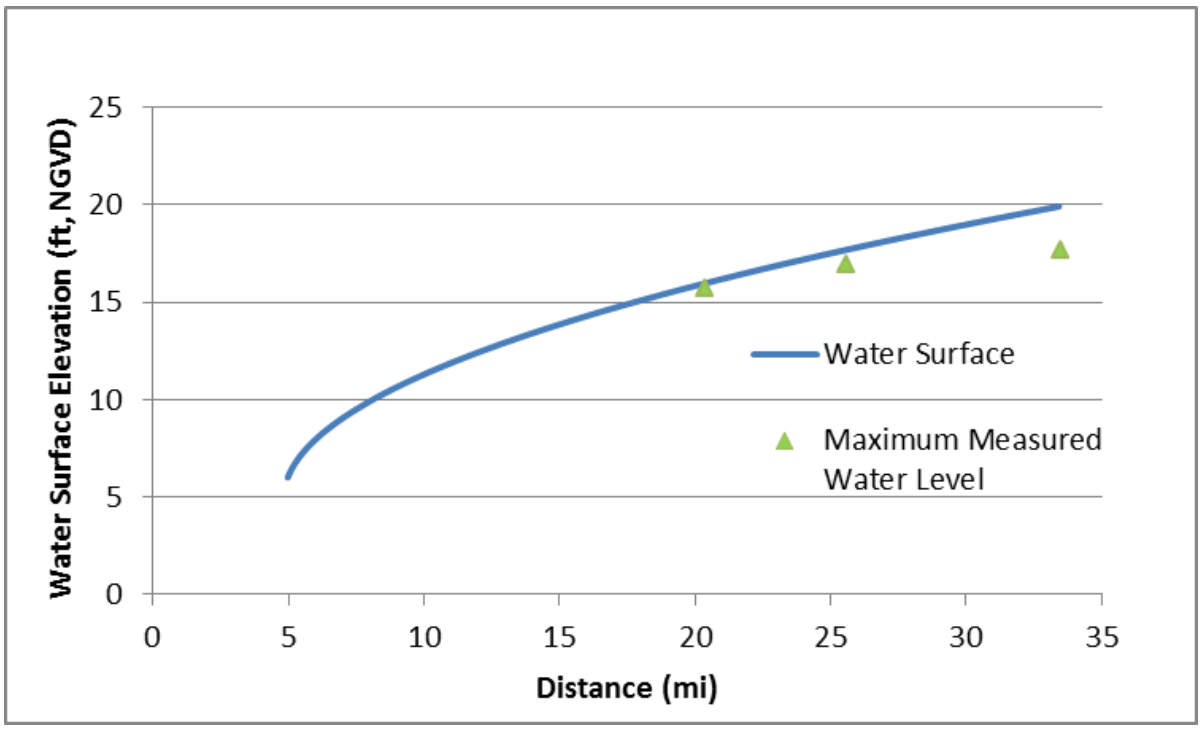


Figure 4-65. Water surface profile as calculated with horizontal bottom equation during Hurricane Frances

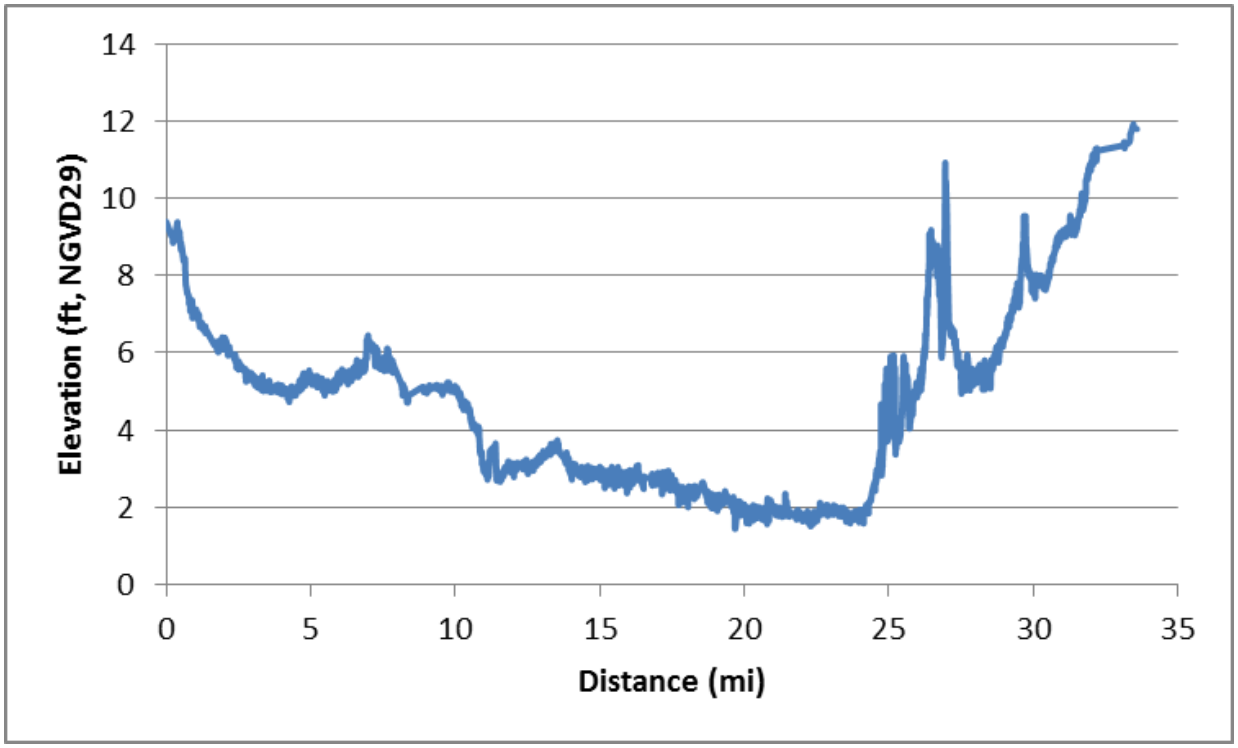


Figure 4-66. Bed elevation along the local wind fetch shown in Figure 4-64

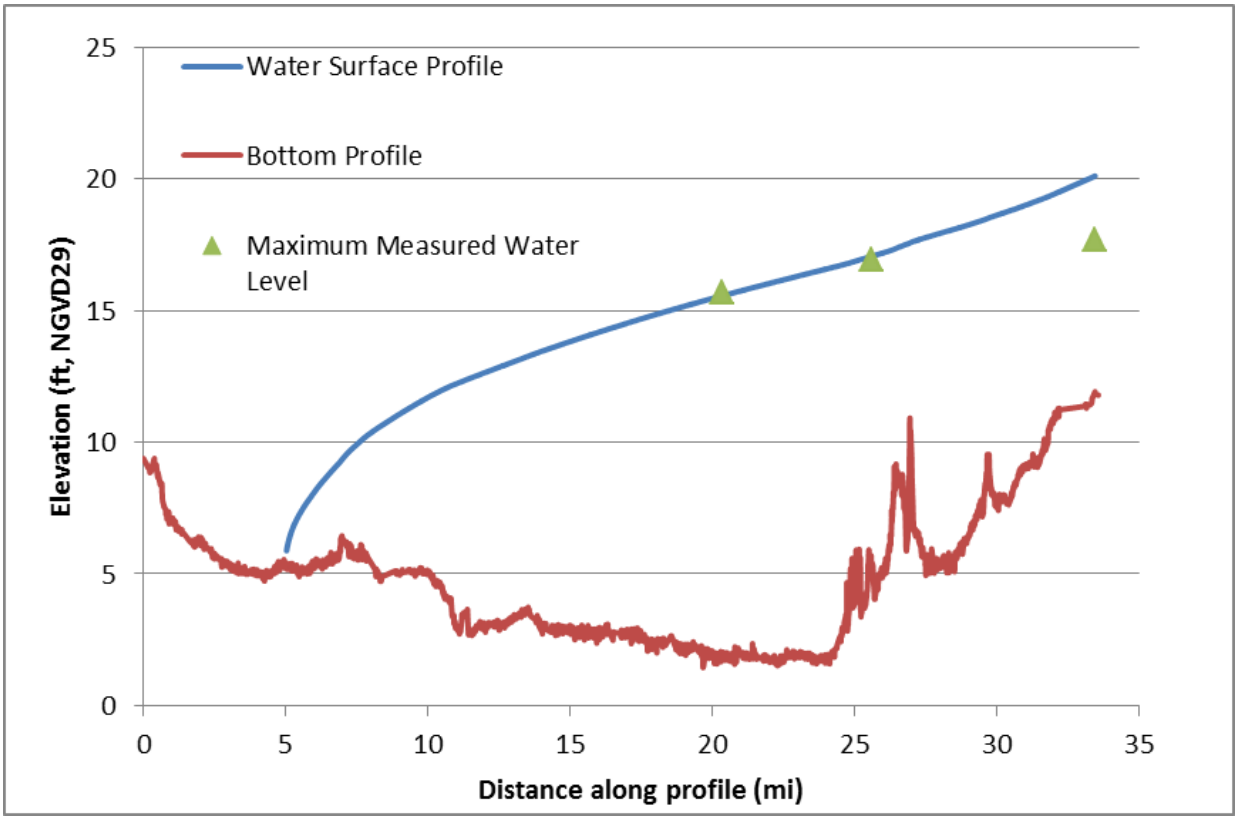


Figure 4-67. Water surface profile as calculated using the discrete method for a rectangular basin during Hurricane Frances

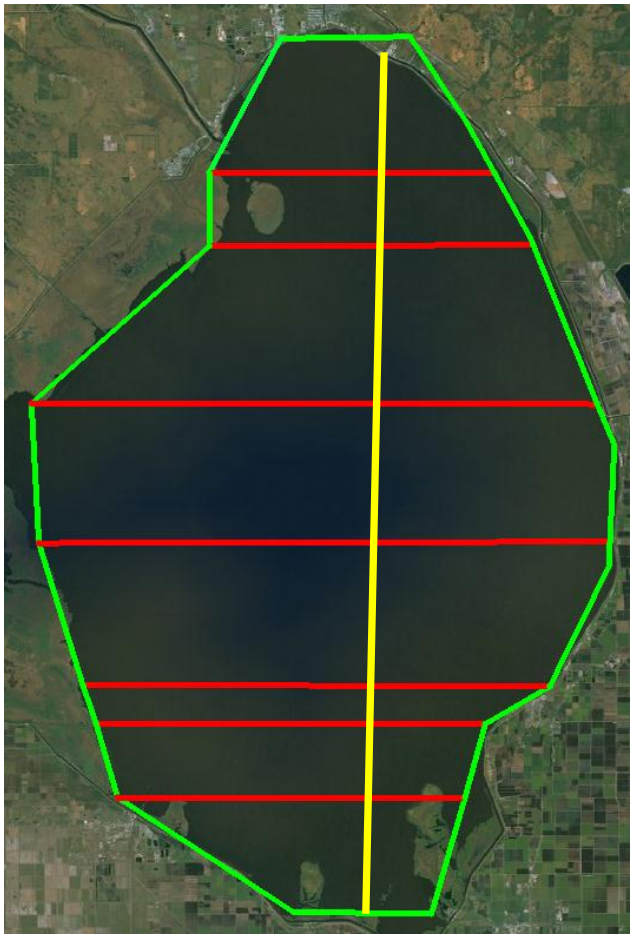

Figure 4-68. Map 1) showing approximate boundary, local wind fetch and cross-sections used for the Lake Okeechobee analyses.

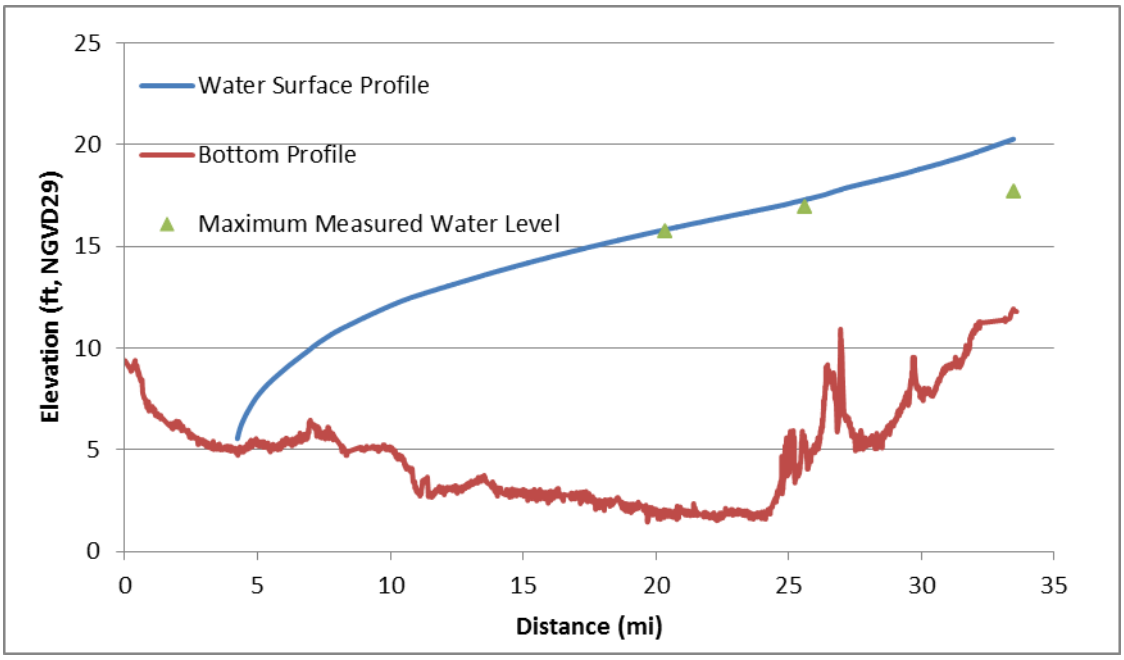


Figure 4-69. Water surface profile for Lake Okeechobee during Hurricane Frances as calculated using the discrete method for the complex basin geometry

Table 4-3. Summary of modeled versus measured water levels for Hurricane Frances

| Gage | Rectangular Horizontal (ft, NGVD) | Rectangular Discrete (ft, NGVD) | Complex Horizontal (ft, NGVD) | Complex Discrete (ft, NGVD) | Measured Water Level (ft, NGVD) |
|---|---|---|---|---|---|
| LZ40 | +16.0 | +15.6 | +16.2 | +15.8 | +15.7 |
| L006 | +17.7 | +17.1 | +17.9 | +17.25 | +16.9 |
| S-3_T | +19.9 | +20.1 | +20.1 | +20.2 | +17.7 |

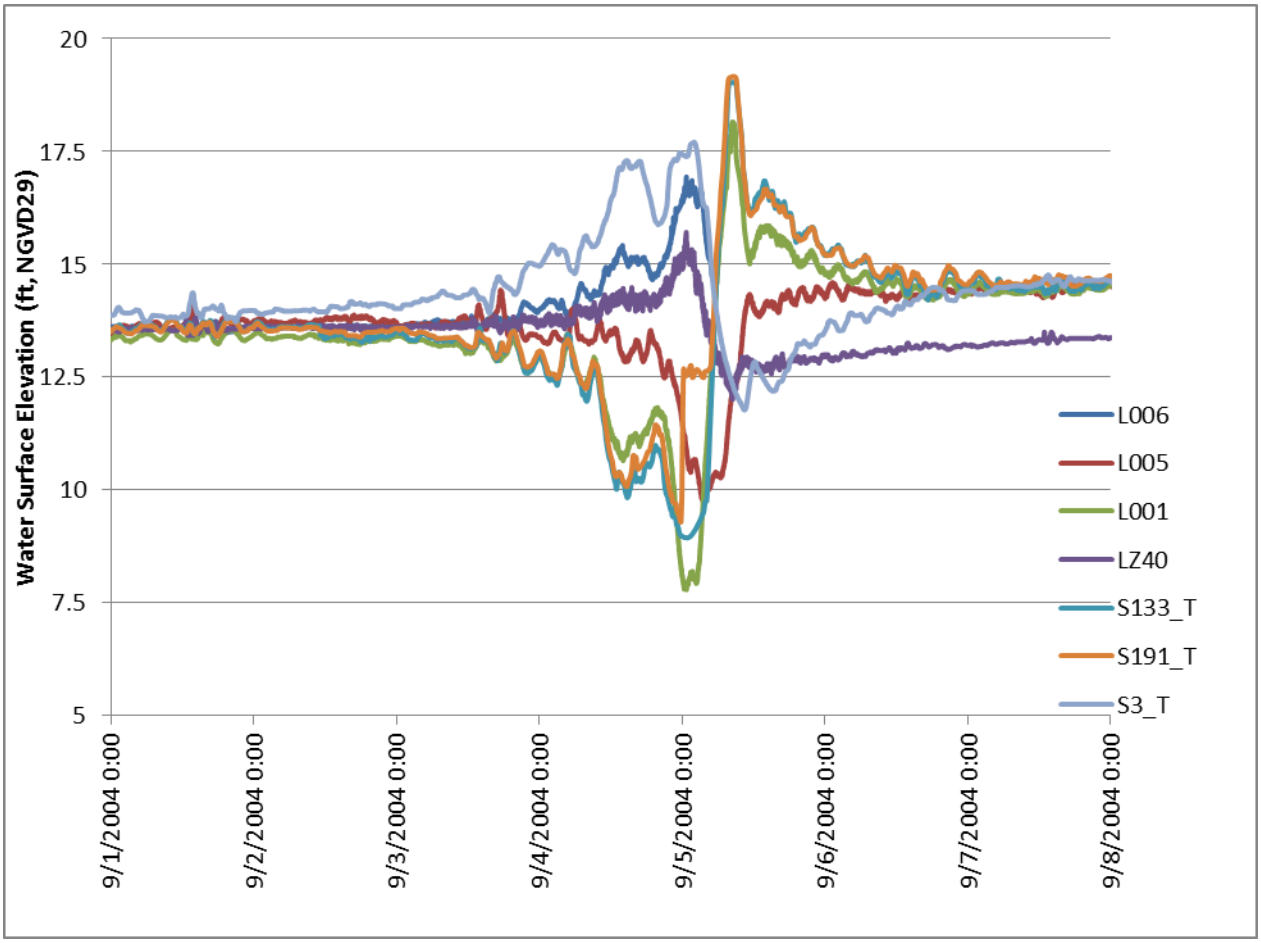


Figure 4-70. Time series plot of water elevations at each gage within Lake Okeechobee during Hurricane Frances

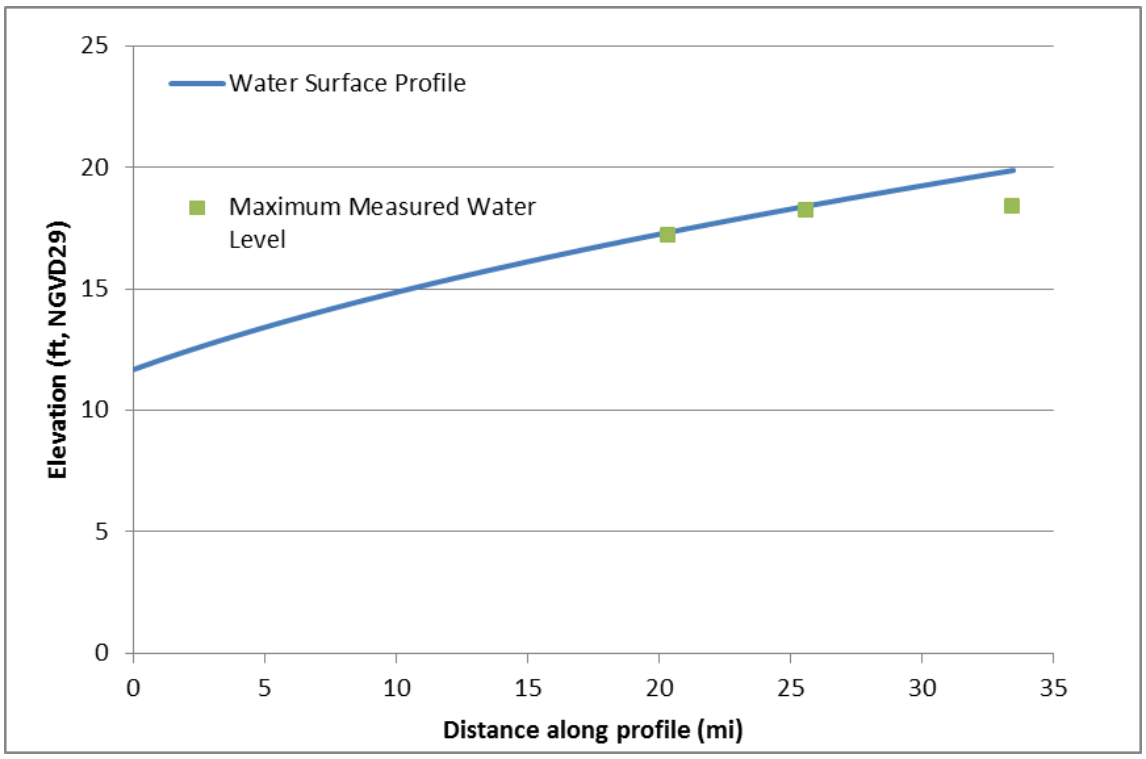


Figure 4-71. Water surface profile along the fetch in Lake Okeechobee as calculated with the horizontal bottom equation during Hurricane Jeanne

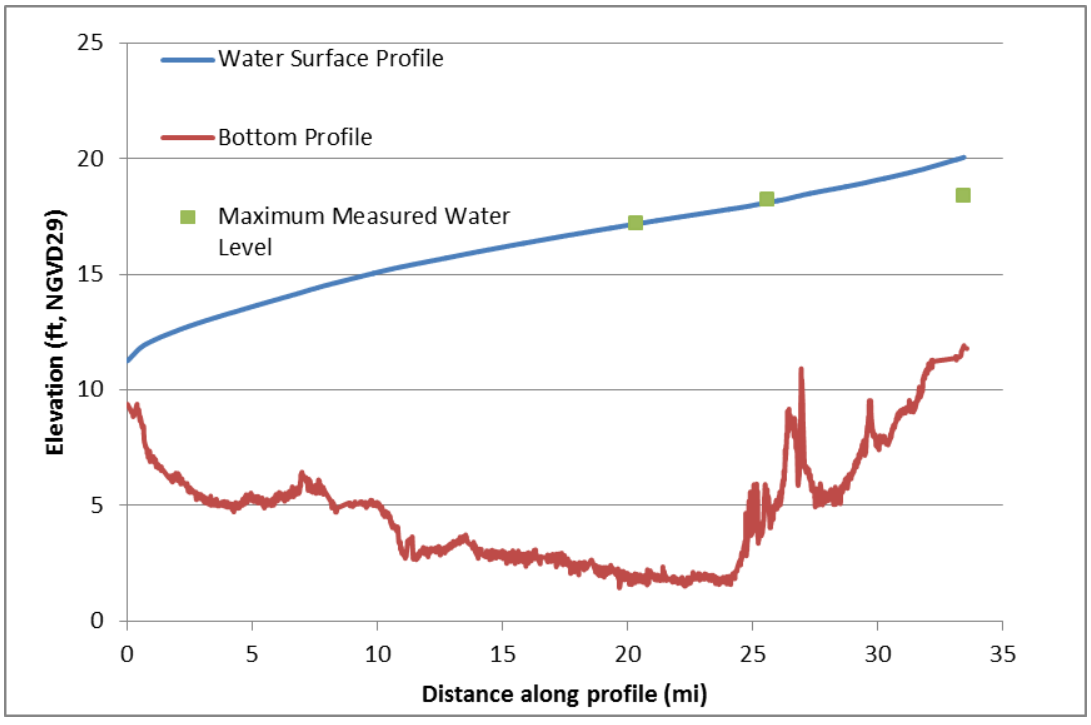


Figure 4-72. Water surface profile in Lake Okeechobee along the fetch as calculated with the discrete method for a rectangular basin during Hurricane Jeanne

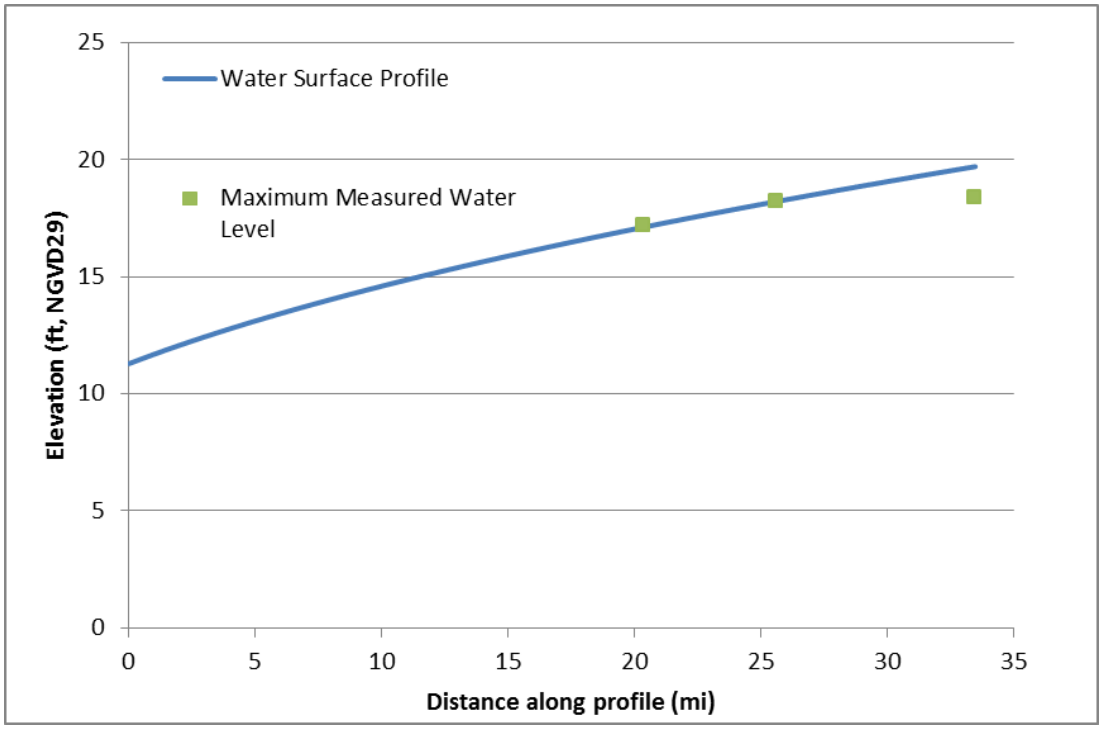


Figure 4-73. Water surface profile in Lake Okeechobee along the fetch as calculated with horizontal bottom equation for the complex basin geometry during Hurricane Jeanne

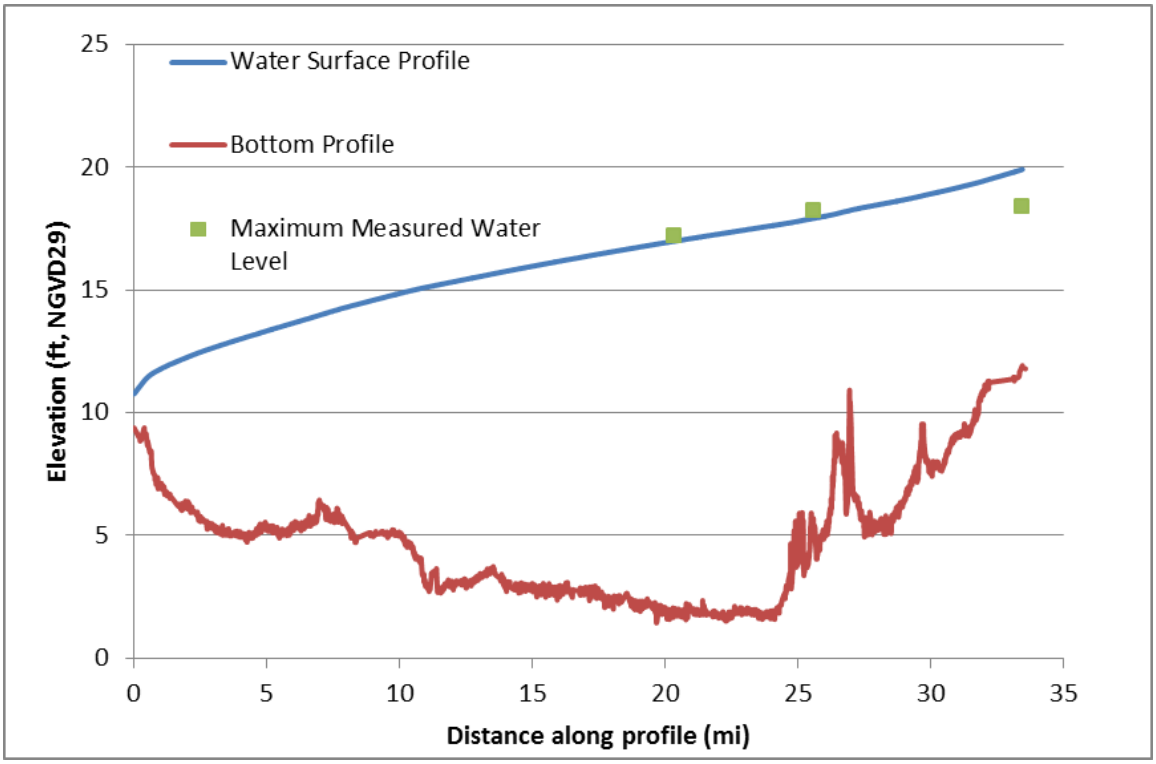


Figure 4-74. Water surface profile in Lake Okeechobee along the fetch transect as calculated with discrete method for a complex basin during Hurricane Jeanne

Table 4-4. Summary of modeled versus measured water elevations for Hurricane Jeanne

| Gage | Rectangular Horizontal (ft, NGVD29) | Rectangular Discrete (ft, NGVD29) | Complex Horizontal (ft, NGVD29) | Complex Discrete (ft, NGVD29) | Measured Water Level (ft, NGVD29) |
|---|---|---|---|---|---|
| LZ40 | +17.3 | +17.2 | +17.2 | +17.0 | +17.2 |
| L006 | +18.4 | +18.1 | +18.2 | +17.9 | +18.2 |
| S-3_T | +19.8 | +20.1 | +19.7 | +19.9 | +18.4 |

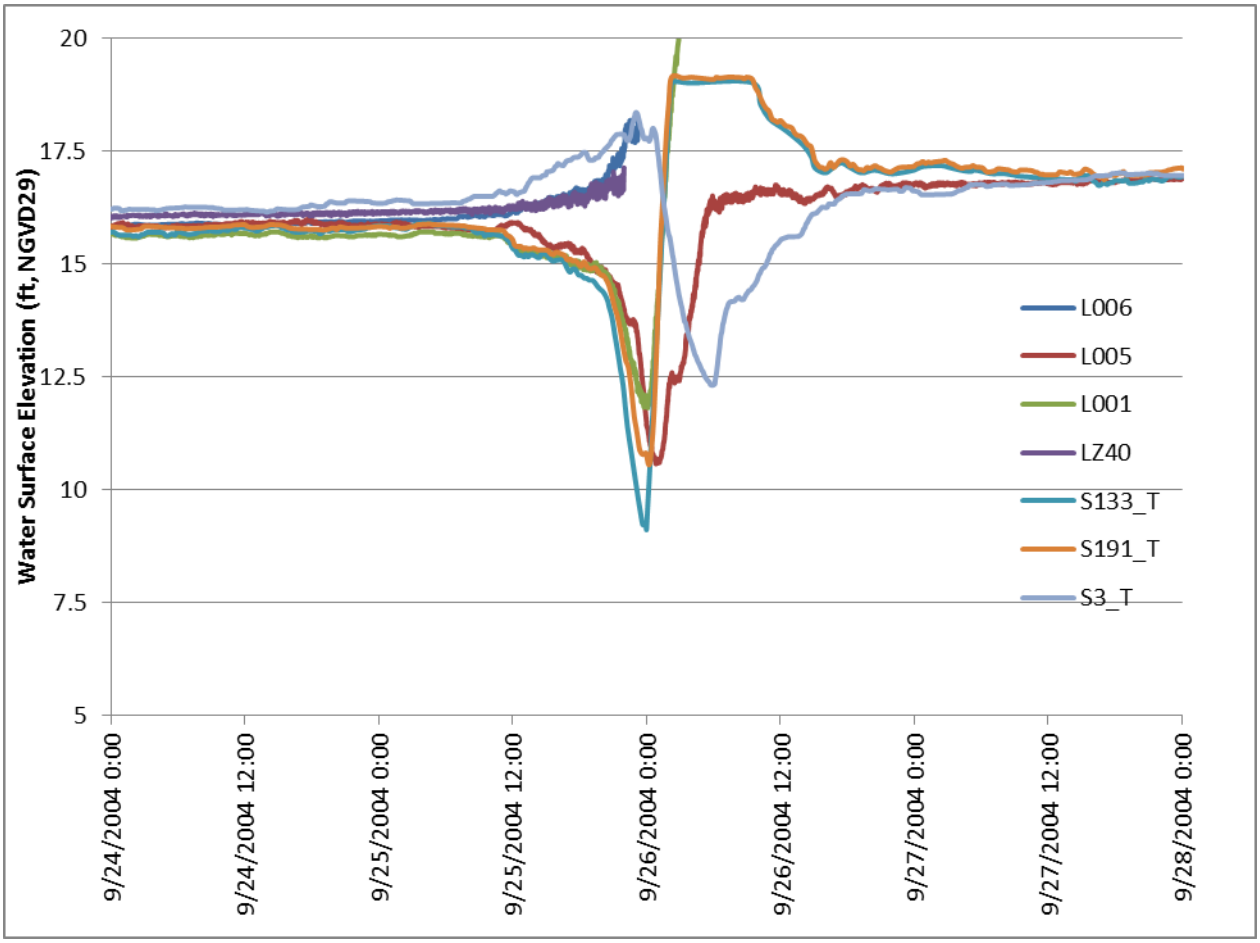


Figure 4-75. Time series plot of water elevations at each gage within Lake Okeechobee during Hurricane Jeanne

# CHAPTER 5
# CONCLUSIONS AND FUTURE RESEARCH

In this study, analytic models and methodologies for the estimation of local wind setup/set-down in bays, lakes, and estuaries were developed and validated. A number of idealized basin geometries and bathymetries were investigated along with a real basin. Previous work on this topic relates bed shear stress, $\tau_b$, to the wind shear stress at the water surface, $\tau_w$. During the course of this investigation it was determined that the ratio of bed to wind shear stress ($r = \tau_b/\tau_w$) varies with wind shear stress (wind speed) and water depth. Numerical experiments performed with a 3D hydraulics model (ADCIRC) provided the data for development of an empirical relationship between r and water depth, h, and surface wind stress, $\tau_w$. It was also found that for even small bed slopes, gravity plays an important role in predicting local wind generated setup/set-down. The analytic models performed well versus the 3D computer model for idealized basins and versus measurements for storm events at Lake Okeechobee in central Florida. The analytic model results for Lake Okeechobee do, however, over predict measurements at the extreme downwind end of the lake for both Hurricanes Frances and Jeanne. It is possible that the water level being measured at the downwind end of the lake is affected by one or more of the following factors: 1) restriction of flow to the gauge due to its location on a narrow canal not directly on the lake, 2) local lowering of water surface elevation due to large flows through the S-3 control structure (not accounted for in the model), and 3) inadequate duration of winds to achieve equilibrium local wind set-up conditions.

Future research needs include examining the impact of flow into and out of tidal inlets due to local wind setup/set-down in the bay on the setup/set-down. These flows

should not impact the shape of the bay water surface but rather the vertical position of the surface relative to the storm water level. A cursory review of methods for undertaking such a scenario is provided in the literature review contained in Chapter 2. Also, r obviously depends on bed roughness as well as water depth and surface wind stress. More work is needed to determine both the dependence of r on bed roughness and the sensitivity of setup/set-down to variations in roughness.

LIST OF REFERENCES

Andreas, A. L. [2009] "Relating the drag coefficient and the roughness length over the sea to the wavelength of the wave peaks," *Journal of Physical Oceanography* **39**, 3011-3020.

Beaches and Shores Resource Center [2010] "Florida storm surge research and reports," (Beaches and Shores Resource Center, Florida State University, http://beach10.beaches.fsu.edu/).

Chimney, M. J. [2005] "Surface seiche and wind set-up on Lake Okeechobee (Florida, USA) during Hurricanes Frances and Jeanne," *Lake and Reservoir Management* **21**, 465-473.

Dattatri, J., Shankar N., & Raman H. [1977] "Wind velocity distribution over wind-generated water waves." *Coastal Engineering* **1**, 243-260.

Dean, R. G., & Dalrymple, R. A. [2002] *Coastal Processes with Engineering Applications* (Cambridge University Press, New York, NY). pp. 78-86.

Harris, L. D. United States. [1963] *Technical Paper No. 48: Characteristics of the Hurricane Storm Surge*. (Government Printing Office, Washington, D.C.).

Ippen, A. T. [1966] *Estuary and Coastline Hydrodynamics* (McGraw-Hill, New York, NY).

Jones, I. S. F., & Yoshiaki, T. [2001] *Wind Stress over the Ocean* (Cambridge University Press, Cambridge, UK), pp. 1-81.

Leuttich, R. & Westerink, J. [2010]"ADCIRC user manual." (ADCIRC, http://adcirc.org/documentv49/ADCIRC_title_page.htm)

Luettich, R. & Westerink, J. [2004] "ADCIRC theory and formulation." (ADCIRC, http://adcirc.org/adcirc_theory_2004_12_08.pdf).

Seabergh, W. C., & Kraus, N. C. [1997] *Coastal Engineering Technical Note: PC Program for Coastal Inlet Stability Analysis Using Escoffier Method*. (US Army Corps of Engineers Waterways Experiment Station, Vicksburg, MS).

United States Army Corps of Engineers [2002] Hydrodynamics of tidal inlets. Coastal Engineering Manual, Part 2, Chapter 6. (Coastal and Hydraulics Laboratory, Vicksburg, MS).

United States Army Corps of Engineers [1977] Shore Protection Manual, 3rd Ed. Vol I. (Coastal Engineering Research Center, Alexandria, VA).

Walton, T. L. & Dean R. G. [2009] "Influence of discrete step size on wind setup component of storm surge." *Coastal Engineering* **56**, 1005-1008.

Weaver, R. J. & Slinn D. N. [2010] "Influence of bathymetric fluctuations on coastal storm surge." *Coastal Engineering* **57**, 62-70.

# BIOGRAPHICAL SKETCH

Jacob McBee graduated with his Bachelor of Science in Civil Engineering with a specialization in structural engineering at the University of Florida in 2007. During his undergraduate studies, he was selected to participate in the University Scholars Program, and researched over-saturation of signalized traffic intersections under Mr. Bill Sampson, the director of McTrans. As an undergraduate, Mr. McBee worked as an intern for Ocean Engineering Associates, Inc., where his interest in coastal engineering flourished. Upon graduation in 2007, Mr. McBee transitioned to a full-time engineer position at OEA. Mr. McBee enjoys the OEA's wide array of challenging and diverse projects. In December 2010, Mr. McBee's graduate studies at the University of Florida culminated in a degree of Master of Science.